Posterior Meta-Replay for Continual Learning

Christian Henning *1 Maria R. Cervera *1 Francesco D'Angelo 1 Johannes von Oswald 1 Regina Traber 1 Benjamin Ehret 1 Seijin Kobayashi 1 João Sacramento 1 Benjamin F. Grewe 1

Abstract

Continual Learning (CL) algorithms have recently received a lot of attention as they attempt to overcome the need to train with an i.i.d. sample from some unknown target data distribution. Building on prior work, we study principled ways to tackle the CL problem by adopting a Bayesian perspective and focus on continually learning a task-specific posterior distribution via a shared meta-model, a task-conditioned hypernetwork. This approach, which we term Posterior-replay CL, is in sharp contrast to most Bayesian CL approaches that focus on the recursive update of a single posterior distribution. The benefits of our approach are (1) an increased flexibility to model solutions in weight space and therewith less susceptibility to task dissimilarity, (2) access to principled task-specific predictive uncertainty estimates, that can be used to infer task identity during test time and to detect task boundaries during training, and (3) the ability to revisit and update task-specific posteriors in a principled manner without requiring access to past data. The proposed framework is versatile, which we demonstrate using simple posterior approximations (such as Gaussians) as well as powerful, implicit distributions modelled via a neural network. We illustrate the conceptual advance of our framework on low-dimensional problems and show performance gains on computer vision benchmarks.

1. Introduction

Most modern machine learning (ML) algorithms rely on the assumption that samples are independent and identically distributed (i.i.d.). In such case, a sample can be written as $\mathcal{D} \overset{i.i.d.}{\sim} p(\mathbf{X}, \mathbf{Y}) = p(\mathbf{X})p(\mathbf{Y} \mid \mathbf{X})$, where the marginal $p(\mathbf{X})$ denotes a distribution over an input random variable \mathbf{X} (such as natural images in pixel space) and the condi-

Preliminary work. Under review.

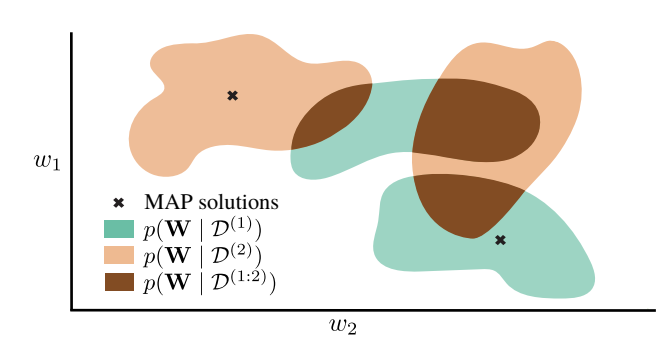


Figure 1. The proposed posterior-replay framework is able to learn task-specific posterior distributions $p(\mathbf{W} \mid \mathcal{D}^{(t)})$ via a single shared meta-model. Therefore, it does not explicitly depend on whether tasks share admissible solutions. In contrast, prior-focused methods attempt to learn a single posterior $p(\mathbf{W} \mid \mathcal{D}^{(1:T)})$ and thus require the existence of trade-off solutions in weight space. Deterministic task-specific solutions (e.g., MAP), on the other hand, capture a single weight configuration per task. Shaded areas indicate the high density regions of the different posteriors.

tional $p(\mathbf{Y} \mid \mathbf{X})$ refers to a target predictive distribution (such as object labels). Crucially, when the i.i.d. assumption is violated, standard ML algorithms suffer from catastrophic forgetting (Kirkpatrick et al., 2017). This poses a serious problem because not only is the i.i.d. assumption in strong disagreement with how data is perceived by agents in natural environments, but it also hinders the ability of trained systems to obtain new skills or improve on existing ones without retraining on all data.

A variety of continual learning (CL) algorithms have been developed to deploy ML to scenarios with less restrictive data gathering and data access demands (for a review refer to Parisi et al. (2019)). The majority of the CL literature focuses on continually learning a sequence of tasks $\mathcal{D}^{(1)},\dots,\mathcal{D}^{(T)}$, with $\mathcal{D}^{(t)}\stackrel{i.i.d.}{\sim}p^{(t)}(\mathbf{X})p^{(t)}(\mathbf{Y}\mid\mathbf{X})$ for t=1..T. Because only access to the current task is granted, successful training has to occur without an i.i.d. training sample from the overall joint, e.g., $\mathcal{D}^{(1:T)}\stackrel{i.i.d.}{\sim}\frac{1}{T}\sum_{t=1}^{T}p^{(t)}(\mathbf{X})p^{(t)}(\mathbf{Y}\mid\mathbf{X})$. Adopting a Bayesian perspective to find principled solutions to this problem has a multitude of benefits. First and foremost, all i.i.d. data assumptions can be dropped in a mathematically sound way. For instance, individual tasks can be learned via an online recursive update of the posterior (e.g., Zeno et al. (2018)).

^{*}Equal contribution ¹Institute of Neuroinformatics, University of Zürich and ETH Zürich, Zürich, Switzerland. Correspondence to: Christian Henning <henningc@ethz.ch>.

Second, tasks can be revisited at any point and updated using new data without requiring access to past data. Third, principled uncertainty estimates that capture both data and model uncertainty are accessible. This is relevant for intelligent systems deployed in safety-critical applications (Kendall & Gal, 2017).

Building upon these benefits, we focus on comparing two principled Bayesian approaches to CL: (1) prior-focused CL (**PF-CL**) (Farquhar & Gal, 2018b), where a combined posterior distribution $p(\mathbf{W} \mid \mathcal{D}^{(1:T)}) \propto p(\mathbf{W} \mid \mathcal{D}^{(1:T-1)})p(\mathcal{D}^{(T)} \mid \mathbf{W})$ is obtained via a recursive Bayesian update, and (2) our proposed posterior-replay CL framework (**PR-CL**), where a task-specific posterior $p(\mathbf{W} \mid \mathcal{D}^{(t)})$ for t=1..T is learned via a single shared meta-model. Although none of these two approaches mathematically require i.i.d. samples within individual tasks (see Sec. 3 for details), here we apply this restriction in order to simplify our empirical evaluation and to ensure comparability to related work.

We illustrate the conceptual difference between PF-CL and PR-CL in Fig. 1. PF-CL relies on the existence of highperforming solutions in the overlap of all task-specific posteriors. In practice, this overlap is further contracted by applying coarse posterior approximations such as meanfield Gaussians, as done in EWC (Kirkpatrick et al., 2017) and VCL (Nguyen et al., 2018), cf. SM Fig. S1. The need to find viable trade-off solutions between all tasks is a severe practical limitation for intelligent systems that learn a diverse set of skills, each of which may require a very different solution. Our proposed PR-CL framework overcomes this limitation by continually learning task-specific posteriors within a single shared meta-model that uses task-specific low-dimensional embedding vectors to encode distributions. The CL problem is therewith shifted to the meta-model, where it can be simplified and forgetting can be prevented using a simple regularizer (cf. von Oswald et al. (2020)). Importantly, we restrict our empirical evaluation of computer vision benchmarks to settings where, despite the use of auxiliary networks, the number of trainable parameters in our framework is lower than in comparison baselines.

Another advantage of the Bayesian treatment is the explicit handling of knowledge transfer, a CL desideratum, via the prior. While pure PF-CL methods allow little flexibility due to the mathematically prescribed nature of the prior, PR-CL methods can utilize an arbitrary prior distribution per task, for instance, a combination of an uninformed prior with posteriors from a subset of already learned tasks that are considered similar.

Despite the advantages of using task-specific solutions, a challenge arises during inference, since task-identity has to be known in order to choose the correct posterior. This is also the case for PF-CL approaches, which in practice em-

ploy a set of task-specific parameters besides the shared ones (e.g., by using a multihead network). We investigate how this problem can be tackled by selecting the task-embedding that yields the lowest predictive uncertainty, effectively resorting to out-of-distribution (OOD) detection (Louizos & Welling, 2017; Ritter et al., 2018).

With recent advances in approximate inference (Wilson & Izmailov, 2020), the benefits of a Bayesian approach to learning are progressively within reach. Here we contribute to the development of Bayesian approaches to tackle CL in the following ways:

- We propose the posterior-replay CL framework, which overcomes the need to find trade-off solutions across several tasks by continually learning task-specific posterior distributions within a single shared meta-model.
- We demonstrate the flexibility of this framework by considering a diverse set of posterior approximations, ranging from mean-field Gaussians to complex implicit distributions parametrized by an auxiliary network.
- We study task identity inference based on predictive uncertainty of individual samples whenever input distributions between tasks are sufficiently distinct.
- We explore a more flexible approach for prior-focused CL which makes use of an auxiliary network to parametrize implicit distributions.
- We show that predictive uncertainty obtained through the presence of task-specific parameters (e.g., multihead CL) can noticeably improve performance of prior-focused CL when used for task inference.
- We provide extensive empirical evaluation of the advantages of our framework on low-dimensional problems and in a set of computer vision benchmarks.

2. Related Work

Continual learning. CL algorithms attempt to mitigate catastrophic interference while facilitating transfer of skills whenever possible. They can be coarsely categorized as (1) regularization-methods that put constraints on weight updates, (2) replay-methods that mimic pseudo-i.i.d. training by rehearsing stored or generated data and (3) dynamic architectures which can grow to allocate capacity for new knowledge (Parisi et al., 2019). Most related to our work is the study from von Oswald et al. (2020) that introduces taskconditioned hypernetworks for CL, and already considers task inference via predictive uncertainty in the deterministic case. Our framework can be seen as a probabilistic extension of their deterministic setup, which provides single task-specific solutions via a shared meta-model (cf. Sec. 3). Wortsman et al. (2020) also studies task inference based on predictive uncertainty in a deterministic setup, using a

learned binary mask per task that modulates a random base network.

A variety of methods tackling CL have been derived from a Bayesian perspective. A prominent example are *prior-focused* methods (Farquhar & Gal, 2018b), which incorporate knowledge from past data via the prior and, in contrast to our work, aim to find a shared posterior for all data. Examples include (Online) EWC (Kirkpatrick et al., 2017; Schwarz et al., 2018) and VCL (Nguyen et al., 2018). Other methods like CN-DPM (Lee et al., 2020) use Bayes' rule for task inference on the joint $p(\mathbf{X}, C)$, where C is a discrete condition such as the task identity. An evident downside of CN-DPM is the need for a separate generative and discriminative model per condition. More generally, such an approach requires meaningful density estimation in the input space, a requirement that is challenging for modern ML problems (Nalisnick et al., 2019).

Other Bayesian CL approaches consider instead taskspecific parameter posterior distributions. CBLN, for instance, (Li et al., 2020) learns a separate Gaussian posterior approximation per task and later tries to merge similar posteriors in the induced Gaussian mixture model. Task inference is also done via predictive uncertainty although, for a more reliable estimation, all experiments consider batches of 200 samples that are assumed to belong to the same task. Tuor et al. (2021) also learn a separate approximate posterior per task and use predictive uncertainty for task-boundary detection and task inference. In contrast to these approaches, we learn all task-specific posteriors via a single shared metamodel and remain agnostic to the approximate inference method being used. A conceptually related approach is MERLIN (Joseph & Balasubramanian, 2020), which learns task-specific weight distributions by training an ensemble of models per task that is used as training set for a taskconditional variational autoencoder. Importantly, MERLIN requires a fine-tuning stage at inference, such that every model drawn is fine-tuned on stored coresets, i.e., a small set of samples withheld throughout training. Task-agnostic inference is achieved using an unjustified aggregated prior and fine-tuning the drawn models using coresets from all tasks. By contrast, our PR-CL approach learns the parameters of an approximate Bayesian posterior $p(\mathbf{W} \mid \mathcal{D}^{(t)})$ per task t, and no fine-tuning of drawn models is required.

Bayesian neural networks. Neural networks are expressive enough to fit almost any data (Zhang et al., 2017). Given that they are often employed in an overparametrized regime, it seems implausible to assume that a single model \mathbf{w} that matches the underlying ground truth $p(\mathbf{Y} \mid \mathbf{w}, \mathbf{X}) \approx p(\mathbf{Y} \mid \mathbf{X})$ with high fidelity can be identified from limited data. Based on this insight, Bayesian statistics considers a distribution over models rather than committing to a single one. This distribution is called the *posterior parameter distribution* $p(\mathbf{W} \mid \mathcal{D}) \propto p(\mathcal{D} \mid \mathbf{W}) p(\mathbf{W})$ which weights

models based on their ability to fit the data (via the likelihood $p(\mathcal{D} \mid \mathbf{W})$) by considering only plausible models according to prior knowledge $p(\mathbf{W})$. Predictions can be made within this framework via marginalization over models (for an introduction see MacKay (2003)). Bayesian neural networks (BNN) apply this formalism and, for practical reasons, only the network's parameters \mathbf{w} undergo a Bayesian treatment while hyperparameters like architecture are chosen deterministically (MacKay, 1992).

While a single model may only capture aleatoric uncertainty (i.e., the uncertainty intrinsic to the data $p(\mathbf{Y} \mid \mathbf{X})$), a Bayesian treatment allows to also capture epistemic uncertainty, i.e., the uncertainty in choosing the model parameters or simply model uncertainty. This proper treatment of uncertainty is of utmost importance for safety-critical applications, where intelligent systems are expected to know what they don't know. However, due to the complexity of modelling high-dimensional distributions at the scale of modern deep learning, BNNs still face severe scalability issues (Snoek et al., 2019). Here, we employ several approximations to the posterior based on variational inference (Blei et al. (2017)) that have been developed by prior work, ranging from simple and scalable methods with a Gaussian variational family like Bayes-by-Backprop (BbB, Blundell et al. (2015)) to complex but rich variational families like Adversarial Variational Bayes (Mescheder et al., 2017). For more details see Sec. 3 and SM C.

3. Methods

In this section we briefly describe our framework (Fig. 2) as well as the algorithms used for training. We start by introducing task-conditioned hypernetworks as a way to provide task-specific solutions in a deterministic setting. We then describe how this approach can be extended to a probabilistic setting using variational inference (VI, cf. SM C.1). We consider both simple, explicit posterior approximations, and complex ones parametrized by an auxiliary network. Then, we explain how predictive uncertainty, that naturally arises from a probabilistic view of learning, can be used to infer task identity for both PR-CL methods, and PF-CL methods that use a multi-head output. Finally, we outline how coresets can be used in our framework to improve task inference.

Task-conditioned hypernetworks. Hypernetworks are neural networks that generate the weights \mathbf{w} of a main network \mathbf{M} , which processes inputs as $\hat{\mathbf{y}} = f_{\mathbf{M}}(\mathbf{x}, \mathbf{w})$ (Schmidhuber, 1992; Ha et al., 2017). In the context of CL, hypernetworks have been used as meta-models that generate task-specific weight configurations for a target network according to $\mathbf{w}^{(t)} = f_{\mathbf{TC}}(\mathbf{e}^{(t)}, \boldsymbol{\psi})$ (von Oswald et al. (2020), **PR-Dirac**). Providing task embeddings $\mathbf{e}^{(t)}$ as inputs renders the computation of this hypernetwork (**TC**) task-conditional.

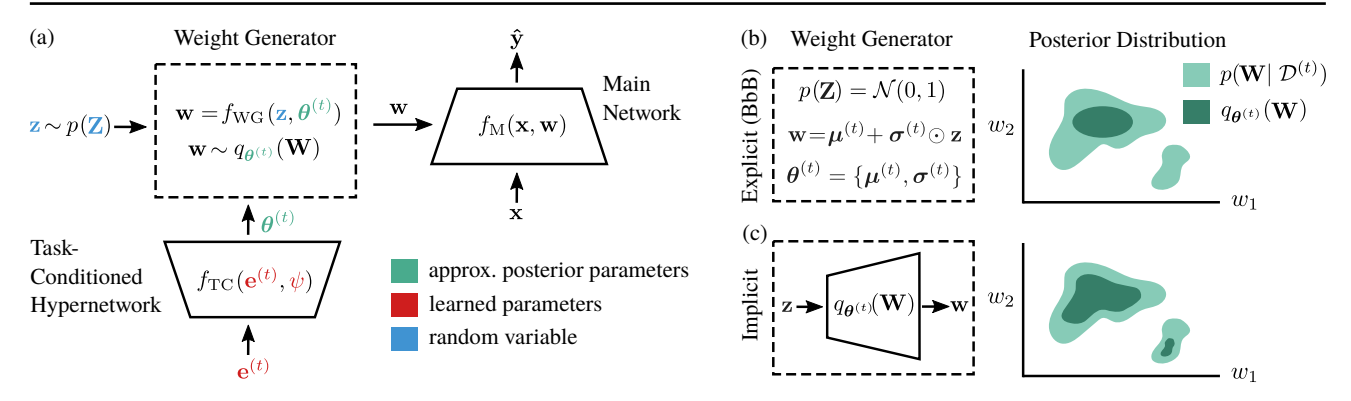


Figure 2. The proposed posterior-replay CL approach. (a) The architecture consists of a main network $f_{\rm M}$ that processes inputs ${\bf x}$ and generates predictions $\hat{{\bf y}}$ according to a set of weights ${\bf w}$ generated by a weight generator (WG). The WG is a deterministic function $f_{\rm WG}({\bf z}, {\boldsymbol \theta}^{(t)})$ that effectively transforms a noise distribution $p({\bf Z})$ into a distribution over main network weights, where ${\boldsymbol \theta}^{(t)}$ are the parameters of the approximate posterior $q_{{\boldsymbol \theta}^{(t)}}({\bf W})$. Crucially, ${\boldsymbol \theta}^{(t)}$ are task-specific, and generated by a task-conditioned (TC) hypernetwork, which receives task embeddings ${\bf e}^{(t)}$ as input. These embeddings, as well as the parameters ${\boldsymbol \psi}$ of the TC are learned continually via a simple meta-replay regularizer (cf. Eq. 1). (b) We refer to the approximate posteriors as explicit if the function $f_{\rm WG}$ is predefined. One such example is Bayes-by-Backprop (BbB), where the reparametrization trick allows to transform Gaussian noise into weight samples. (c) For more complex posterior approximations we resort to implicit distributions. These are parametrized by an auxiliary hypernetwork, that receives its task-conditioned parameters from the TC, which now plays the role of a hyper-hypernetwork. This setting allows obtaining more flexible posterior approximations which can, for example, capture multi-modality.

The embeddings as well as the parameters ψ of the hypernetwork are learned continually, and a *meta-replay* regularizer ensures that the output of the hypernetwork for previously learned tasks does not change, preventing forgetting at the meta level. When learning task t the loss thus becomes:

$$\mathcal{L}^{(t)}(\boldsymbol{\psi}, \mathcal{E}, \mathcal{D}^{(t)}) = \mathcal{L}_{\text{task}}(\boldsymbol{\psi}, \mathbf{e}^{(t)}, \mathcal{D}^{(t)})$$
$$+ \beta \sum_{t' < t} \|f_{\text{TC}}(\mathbf{e}^{(t', *)}, \boldsymbol{\psi}^*) - f_{\text{TC}}(\mathbf{e}^{(t')}, \boldsymbol{\psi})\|^2 \quad (1)$$

where $\mathcal{E} = \{\mathbf{e}^{(t')}\}_{t'=1}^t$ is the set of task embeddings up to the current task, β is the strength of the meta-replay regularizer, $\{\psi^*\} \cup \{\mathbf{e}^{(t',*)}\}_{t' < t}$ is a checkpoint of the hypernetwork parameters before learning task t and $\mathcal{L}_{\text{task}}$ is the task-specific loss that we want to minimize (e.g. crossentropy). Importantly, the loss on task t only depends on the corresponding dataset $\mathcal{D}^{(t)}$, and knowledge transfer across tasks is possible because task-specific models are generated through a shared meta-model. Hypernetworks can be designed to have less parameters than their output size, i.e., $\dim(\psi) + \sum_t \dim(\mathbf{e}^{(t)}) < \dim(\mathbf{w})$. We enforce this constraint in all our experiments, except when studying conceptual ideas on low-dimensional problems. Please refer to SM C.2 for details.

Posterior-replay with explicit parametric distributions.

We start by considering simple approximations $q_{\theta^{(t)}}(\mathbf{W})$ which can be sampled from according to a predefined function. We refer to these as *explicit* distributions (Fig. 2a and Fig. 2b). **PR-BbB** refers to finding a mean-field Gaussian approximation via the BbB algorithm (SM C.3.1, Blundell et al. (2015)). In this case, $\theta^{(t)}$ corresponds to the set of

means and variances that define a Gaussian for each weight, which are directly generated by the TC.¹ Because all of the mass of a high-dimensional, isotropic Gaussian distributions concentrates in a thin hyper-annulus, Farquhar et al. (2020) propose the use of a corrective normalization as a means to reduce variance (SM C.3.2). Within our posterior-replay framework, we refer to this approach as **PR-Radial**. Interestingly, for families of posterior approximations that possess an analytic expression for a divergence measure (e.g., Gaussian distributions), one can replace the isotropic output regularization in Eq. 1 with one that has explicit meaning in distribution and not just parameter space (SM C.2).

Posterior-replay with implicit distributions. Since the expressivity of explicit distributions is limited, we also explore the more diverse variational family of *implicit* distributions (Goodfellow et al., 2014; Huszár, 2017). We parameterize these with an auxiliary weight generator network (**WG**), and therefore the parameters $\theta^{(t)}$ of the approximate posterior depend on the chosen WG architecture. Overall, we have a hierarchy of three networks: a TC network generates task-specific parameters $\theta^{(t)}$ for the approximate posterior, which is defined through an arbitrary base distribution $p(\mathbf{Z})$ and the WG hypernetwork, which in turn generates weights w for a main network M that processes the actual inputs of the dataset $\mathcal{D}^{(t)}$. Interestingly, here the TC plays the role of a hyper-hypernetwork as it generates the weights of another hypernetwork (Fig. 2a and Fig. 2c). As a consequence, the CL problem is shifted to the

¹As the outputs of the TC system are real-valued, variances are squashed by a softplus nonlinearity.

TC hyper-hypernetwork, and catastrophic forgetting can be prevented via Eq. 1.

Note, that variational inference commonly resorts to optimizing an objective consisting of a data-dependent term and a prior-matching term $KL(q_{\theta}(\mathbf{W}) || p(\mathbf{W}))$. Since we do not have analytic access to the density nor the entropy of $q_{\boldsymbol{\theta}^{(t)}}(\mathbf{W})$, the use of implicit distributions as approximate posteriors introduces a problem when trying to optimize this prior-matching term, which can be written as an expectation over the log density ratio $\log q_{\theta^{(t)}}(\mathbf{W}) - \log p(\mathbf{W})$. One approach to overcome the problem is adversarial variational Bayes (AVB, SM C.4.1, Mescheder et al. (2017)), which introduces an auxiliary network to approximate the log density ratio inside the *prior-matching term*. While powerful on low-dimensional problems, this approach relies on minimax optimization and suffers from serious scalability issues in our experiments. As alternative, the spectral Stein gradient estimator (SSGE, SM C.4.2, Shi et al. (2018)) is based on the insight that direct access to the log-density is not required, but only to its gradient with respect to W, for which the authors develop a sample-based estimator. When used in the context of our posterior-replay framework we refer to these methods as PR-AVB and PR-SSGE.

Another issue introduced by the use of implicit distributions is the fact that the support of $q_{\theta^{(t)}}(\mathbf{W})$ is limited to a low-dimensional manifold when using an inflating architecture for WG, which causes the *prior-matching term* to be ill-defined. To overcome this, we investigate the use of small noise perturbations to the outputs of the WG (SM C.4). As an alternative to the aforementioned methods to estimate the optimization objective, normalizing flows (Papamakarios et al., 2019) can be utilized as WG architectures to gain analytic access to $q_{\theta^{(t)}}(\mathbf{W})$ at the cost of architectural constraints such as invertibility.

Task inference. Every system with task-specific solutions requires knowledge about which task is being solved. In our framework, this amounts to selecting the correct task embedding to condition the WG. Although auxiliary systems can be used to infer task identity (He et al., 2019; von Oswald et al., 2020), here we exploit predictive uncertainty, assuming task identity can be inferred from the input alone.

Recall that in a Bayesian framework predictions on unseen inputs $\tilde{\mathbf{x}}$ are made via the posterior predictive distribution $p(\mathbf{y} \mid \mathcal{D}^{(t)}; \tilde{\mathbf{x}}) = \int_{\mathbf{W}} p(\mathbf{y} \mid \mathbf{W}; \tilde{\mathbf{x}}) p(\mathbf{W} \mid \mathcal{D}^{(t)}) \, d\mathbf{W}$, which we approximate via a Monte-Carlo estimate. For a task inference approach based on predictive uncertainty to work, the properties of the input data distribution $p^{(t)}(x)$ need to be reflected in the uncertainty measure, i.e., uncertainty needs to be low for in-distribution data and high for out-of-distribution (OOD) data. This property is not a given, especially since $p(\mathbf{y} \mid \mathcal{D}^{(t)}; \tilde{\mathbf{x}})$ reflects both aleatoric and epistemic uncertainty, and behavior of aleatoric un-

certainty OOD is hard to foresee, since it is only calibrated in-distribution. In our case, epistemic uncertainty stems from the fact that the posterior parameter distribution $p(\mathbf{W}|\mathcal{D}^{(t)})$ in conjunction with the network architecture induces a distribution over functions. If this distribution captures a rich enough set of functions, a diversity of predictions on OOD data can be expected even if those functions agree in-distribution.

Here, we explore two different ways to quantify uncertainty for task inference. In **Ent** the task t leading to the lowest entropy on $p(\mathbf{y} \mid \mathcal{D}^{(t)}; \tilde{\mathbf{x}})$ is selected. In **Agree**, which is meant to solely measure epistemic uncertainty, the task leading to the highest agreement in predictions across models drawn from $p(\mathbf{W} | \mathcal{D}^{(t)})$ is selected. Note that, ENT is applicable to deterministic solutions such as PR-DIRAC, but AGREE can only be estimated in a probabilistic setting. Although we generally consider task inference for individual samples, we also explore task inference for batches of 100 samples that are assumed to belong the same task, a variant we denote **BW**. Further details can be found in SM C.6, and in SM D.6 we consider using uncertainty for task-boundary detection when training without explicit access to task identity.

Revisiting task-specific posteriors. A crucial advantage of a Bayesian approach is the ability to update models as new evidence arrives. For instance, when continually learning a sequence of tasks, posteriors may undergo a post-hoc finetuning on stored coresets to mitigate catastrophic forgetting on the meta-model, especially for earlier tasks. Specifically, given a dataset split $\mathcal{D}^{(t)} \setminus \mathcal{C}^{(t)} \cup \mathcal{C}^{(t)}$, one can perform a final update $p(\mathbf{W}|\mathcal{D}^{(t)}) \propto p(\mathbf{W} \mid \mathcal{D}^{(t)} \setminus \mathcal{C}^{(t)}) p(\mathcal{C}^{(t)} \mid \mathbf{W}),$ using a stored coreset $C^{(t)}$ in conjunction with an already learned posterior approximation for $p(\mathbf{W} \mid \mathcal{D}^{(t)} \setminus \mathcal{C}^{(t)})$ that now acts as a prior. Interestingly, having access to coresets from all tasks can also be exploited to facilitate task inference via predictive uncertainty. Here we explore this idea by encouraging task-specific models to produce highly uncertain predictions for OOD samples (i.e., coresets from other tasks), an approach that we denote **CS** (SM C.7). Note that this does not violate CL constraints, as the coreset fine-tuning is performed after all tasks have been trained on. Intriguingly, training on OOD inputs makes these become in-distribution, and therefore model agreement (AGREE) as a way to infer task identity becomes inapplicable, which we empirically observe.

Reflection on prior-focused CL. Although so far we have only considered task-specific solutions, our framework can also be used in a PF-CL setting. In this case, the parameters θ are shared across tasks and no TC network is required, but the use of a WG hypernetwork to parametrize a shared implicit distribution $q_{\theta}(\mathbf{W})$ can still allow finding more powerful approximations (cf. Fig. 1). As opposed to

the PR-CL setting, the parameters θ are directly optimized. We refer to training a shared WG network via SSGE or AVB in a prior-focused way as **PF-SSGE** and **PF-AVB**.

Common PF-CL algorithms that consider *explicit* posterior approximations such as BbB and EWC can be viewed as instantiations of this framework. When these algorithms are used in a task-agnostic inference setting, they are often trained using a softmax that grows as new tasks are trained (e.g., van de Ven et al. (2020)). The use of a growing softmax causes the model-class parametrized by w to change over time, and therefore violates the Bayesian assumption that the approximate posterior is obtained from a model class containing the ground-truth model. If the number of tasks is known a priori, a simple solution is the use of a shared softmax spanning the outputs of all tasks. However, we observe this still performs poorly, since the softmax normalization pushes weights of output neurons of future tasks to become highly negative, hindering their ability to later adapt without catastrophic interference. To overcome these limitations, we propose to use these algorithms with a multi-head output instead. In this case, the learned parameters w consist of a set of shared weights ϕ and a set of task-specific output heads with weights $\{\xi^{(t)}\}_{t=1}^T$. The use of task-specific parameters requires knowledge about task identity, which in a task-agnostic inference setting can be inferred using predictive uncertainty. Note that this uncertainty is now task-specific as predictions for task t are made by marginalizing shared weights ϕ and task-specific weights $\xi^{(t)}$. For EWC, we refer to the growing softmax and multi-head scenarios as EWC-GH and EWC, respectively (cf. SM C.5.2). Notice that using BbB in a prior-focused setting corresponds to VCL (cf. SM C.5.1). As a final note, PF-CL methods in general do not require the notion of tasks, and can also be used within our PR-CL framework to continually learn individual tasks using non-i.i.d. data.

4. Experiments

In this section, we use the framework introduced in Sec. 3 to compare PR-CL and PF-CL empirically, using either *explicit* or *implicit* posterior approximations. We first consider two low-dimensional problems to build an intuition on the conceptual differences of the competing approaches, and then focus on a set of computer vision CL benchmarks.

To assess forgetting, we provide **during** scores, measured directly after training each task, and **final** scores, evaluated after training on all tasks. We consider two different testing scenarios: (1) either task-identity is explicitly given (**TG**) or (2) task-identity has to be inferred (**TI**), e.g. via predictive uncertainty. Importantly, task inference is performed for each sample in isolation and a sample is considered incorrectly classified if the wrong task is inferred. If not explicitly mentioned, FINAL performance scores are reported, and the

ENT criterion is used by default for task inference (TI-ENT). Supplementary results and controls are provided in SM D, and all experimental details can be found in SM E.²

4.1. 1D Regression

We start by studying the case of 1D polynomial regression, for which the predictive posterior can be easily visualized (cf. Fig. 3).

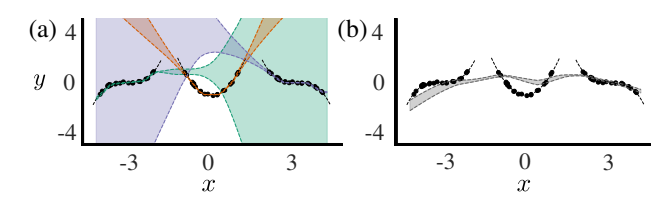


Figure 3. 1D polynomial regression task. (a) Three polynomials learned consecutively with PR-BBB. Different colors represent the task-specific posterior approximations within the final model. For an input point x the posterior with the lowest predictive uncertainty is chosen to make predictions. (b) Final approximation of the posterior $p(\boldsymbol{W} \mid \mathcal{D}^{(1:3)})$ using PF-SSGE. Prior-focused methods struggle with this simple regression problem, as good trade-off solutions are not present in the posterior of previous tasks. Shaded areas represent standard deviation of predictive distributions, and black dots correspond to training samples.

As is common for regression tasks, we consider a mean squared error (MSE) training objective, which corresponds to a Gaussian likelihood with fixed variance (cf. SM C.3.1). Therefore, all x-dependent uncertainty corresponds to model uncertainty, originating from the approximate posterior. We depict an example run of PR-BBB in Fig. 3a. As can be seen, each task-specific posterior fits the training data well and exhibits increasing uncertainty when leaving the indistribution domain, as desired for successful task inference. Quantitative results and illustrations for other methods as well as an analysis of the correlations and multi-modality that can be captured by implicit methods in weight space can be found in SM D.1. When studying low-dimensional problems, we generally found it easier to find viable hyperparameter configurations with implicit methods (such as PR-AVB or PR-SSGE) than with explicit ones.

Fig. 3b illustrates how the same set of tasks is learned by a prior-focused method. As we do not consider multi-head networks for the regression task, a single posterior has to be continually fitted to all polynomials and thus task-identity is not required. In our experiments all prior-focused methods struggle to find a good fit for those polynomials. Notably, we obtain such poor results even though we choose a set of tasks for which values at the boundaries can be easily connected.

²Source code for all experiments (including all baselines) is available at: https://github.com/chrhenning/posterior_replay_cl.

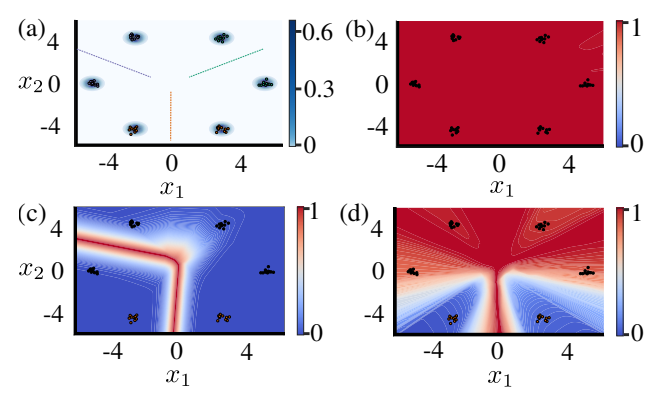


Figure 4. 2D mode classification. (a) Density map of the combined input distribution across tasks $p(\mathbf{x})$. Dots represent training points and colors indicate task-affiliation. Colored lines represent decision boundaries for each of the consecutively learned binary classification tasks. (b) - (d) Example uncertainty maps depicting the entropy of the predictive distribution across the input space covering all tasks. (b) Entropy of the prior predictive distribution, i.e., models are drawn from the prior. Entropy of predictive distribution induced by the approximate posterior of the orange-labeled task learned via PR-DIRAC (c) and PR-AVB (d).

Table 1. Accuracies of the 2D Mode Classification experiments (Mean \pm standard error of the mean (SEM) in %, n=10). Task identity is inferred via predictive using a minimum entropy (TI-ENT) or maximum model agreement (TI-AGREE) criterion.

	TI-ENT	TI-AGREE
PR-DIRAC PR-BBB PR-AVB PR-SSGE	44.90 ± 5.74 81.07 ± 6.78 98.57 ± 1.33 100.0 ± 0.00	$\begin{array}{c} \text{N/A} \\ 90.02 \pm 3.57 \\ 99.93 \pm 0.06 \\ 100.0 \pm 0.00 \end{array}$

4.2. 2D Mode Classification

To better understand the behavior of these methods in classification tasks, we consider a problem with 2D inputs, for which uncertainty can be visualized across in- and out-ofdistribution space. Classification tasks are of special interest because they apply a softmax to its outputs. This allows modeling arbitrary discrete distributions, and surprisingly often depicts meaningful OOD performance on highdimensional benchmarks without any treatment of model uncertainty (Snoek et al., 2019). Here, we specifically consider a Gaussian mixture with two modes per task, where each mode corresponds to a different label in a binary decision problem (cf. Fig. 4a). We report quantitative results in Table 1. Again, *implicit* methods maintain an advantage over explicit ones such as PR-BBB, presumably due to the increased flexibility in modelling the posterior parameter distribution. PR-DIRAC, which does not incorporate epistemic uncertainty, performs poorly on this benchmark. Note that TI-AGREE, which is indicative of the importance

Table 2. Accuracies of SplitMNIST experiments for (Mean \pm SEM in %, n=10), when task identity is provided (TG-ACC) and when it needs to be inferred (TI-ACC). Unless indicated otherwise, results are shown for an MLP with two hidden layers of 400 neurons, MLP-400,400.

	TG-Acc	TI-ACC
PR-DIRAC	99.65 ± 0.01	70.88 ± 0.61
PR-BBB	99.72 ± 0.02	71.73 ± 0.87
PR-RADIAL	99.64 ± 0.01	66.01 ± 0.92
PR-SSGE	99.77 ± 0.01	71.91 ± 0.79
EWC-GH	N/A	27.32 ± 0.60
EWC	96.40 ± 0.62	47.67 ± 1.52
VCL	96.45 ± 0.13	58.84 ± 0.64
PF-SSGE	99.02 ± 0.16	62.70 ± 1.32
PR-BBB-BW	99.72 ± 0.02	99.72 ± 0.02
PR-BBB-CS	98.50 ± 0.09	90.83 ± 0.24
PR-BBB (MLP-100,100)	99.75 ± 0.01	70.07 ± 0.56
PR-BBB (LENET)	99.20 ± 0.67	74.09 ± 1.38

of epistemic uncertainty for OOD detection, appears to be the most robust measure for task inference in this experiment. To better understand why differences arise between methods we provide uncertainty maps over the whole input space in Fig. 4. As expected, the prior predictive distribution exhibits high uncertainty everywhere (cf. Fig. 4b). Of particular interest is the difference between the uncertainty maps of PR-DIRAC (Fig. 4c) and PR-AVB (Fig. 4d). While PR-AVB approaches the desired behavior of depicting high-uncertainty when moving away from the training data of the corresponding task, PR-DIRAC displays arbitrary uncertainty away from the training data. We provide a more detailed analysis and complementary results in SM D.2.

4.3. SplitMNIST

To investigate how the different approaches scale to more complex datasets, we next consider SplitMNIST (Zenke et al., 2017), a popular variant of the MNIST dataset, adapted to CL by splitting the ten digit classes into five binary classification tasks. The results can be found in Table 2. While all methods achieve acceptable FINAL accuracies when task identity is provided, we observe large differences when the task needs to be inferred. Notably, all PR-CL approaches other than PR-RADIAL outperform the deterministic solution PR-DIRAC, highlighting the benefits of a Bayesian approach in a task-agnostic setting. Furthermore PR-CL methods, which use task-specific solutions, systematically outperform PF-CL. As expected, when a trade-off solution across tasks needs to be found, more flexible posterior approximations can facilitate finding suitable solutions, as illustrated by performance differences between PF-SSGE and prior-focused approaches with explicit distri-

Table 3. Accuracies of SplitCIFAR-10 experiments using a Resnet-32 (He et al., 2016) architecture (Mean \pm SEM in %, n=10).

	TG-Acc	TI-Acc
PR-DIRAC PR-BBB PR-SSGE	$\begin{array}{c} 93.77 \pm 0.31 \\ 95.43 \pm 0.11 \\ 92.83 \pm 0.16 \end{array}$	54.83 ± 0.79 61.90 ± 0.66 51.95 ± 0.53

butions such as EWC and VCL. Notably, the performance of PF-CL substantially improves when using uncertaintybased task inference, as reflected by the difference between EWC and EWC-GH. The high performance of PR-BBB-BW compared to PR-BBB illustrates that task inference becomes much easier when it is possible to use batches rather than single samples. In addition, using coresets to update task-specific posteriors at the end of training to encourage high uncertainty for OOD data is another way to considerably improve performance. Another factor influencing the methods' performance in a task-agnostic setting is the choice of main network architecture, as different architectures (in combination with the chosen weight prior) will induce different priors in function space (Wilson & Izmailov, 2020) and lead to a different OOD behavior of the Bayesian posterior. Indeed, we can observe for PR-BBB that increasingly complex architectures lead to higher TI-ACC. Further results can be found in SM D.3. These include DURING accuracies, accuracies using the AGREE criterion for task inference, detailed results for a LENET (LeCun et al., 1998) and MLP-100,100, as well as results on the PermutedMNIST CL benchmark (SM D.4).

4.4. SplitCIFAR-10

Finally, we test our framework on natural images using the CIFAR-10 dataset (Krizhevsky & Hinton, 2009). In particular, we consider SplitCIFAR-10, which consists of five tasks with two classes each. We report the results in Tables 3 and S9. We found considerable improvement through the incorporation of epistemic uncertainty via PR-BBB compared to PR-DIRAC. However, in contrast to low-dimensional problems, the *implicit* method *PR-SSGE* does not exhibit a competitive advantage compared to PR-DIRAC, as it appears to suffer from scalability issues, training instability and increased difficulty in finding suitable hyperparameter configurations.

5. Discussion

In this study we propose posterior-replay CL, a framework for continually learning task-specific posterior approximations within a single shared meta-model. We compare this approach to prior-focused CL, for which a single trade-off solution across all tasks is recursively obtained. Although both approaches overcome the need to train using i.i.d. sam-

ples by adopting a Bayesian perspective, we argue that seeking specialized solutions while transferring knowledge (e.g., through the shared meta-model) is a more versatile approach, since finding trade-off solutions might not always be feasible nor desirable. We empirically validate this view in a set of CL benchmarks using both simple posterior approximations, such as Gaussians, and complex implicit approximations parametrized by a neural network. Furthermore, although prior-focused methods are often portrayed as performing poorly in task-agnostic inference settings (e.g., van de Ven et al. (2020)), we show that their performance can be vastly improved by using a mixed strategy that includes both shared and task-specific parameters (e.g., by using a multi-head output).

Task-specificity in both posterior-replay and prior-focused methods comes, however, at the cost of having to know the task identity. If applicable, task identity can be inferred by an auxiliary system from contextual information (cf. von Oswald et al. (2020)). However, it is often assumed that input distributions across tasks are sufficiently distinct and that task-inference is possible by looking at the current input alone. Within our framework, input-based task-inference could be achieved by introducing inputs X and task embeddings E as additional random variables into the graphical model. This would naturally lead to an inference strategy as in Lee et al. (2020), where a task-conditioned generative model of X with tractable density is required. Learning generative models on high-dimensional data is a challenging problem. Furthermore, when tractable densities are accessible, they currently do not seem to reflect the underlying data-generative process (Nalisnick et al., 2019). To sidestep current limitations in modeling input distributions, we study instead the use of predictive uncertainty for task inference (cf. von Oswald et al. (2020)), and show that it is suitable for both Bayesian and deterministic solutions. Although the meaningfulness of uncertainty-based task-inference with plain deterministic models is questionable (Hein et al., 2019), methods such as the one proposed by Lakshminarayanan et al. (2020) that utilizes a deterministic distance preserving input-to-hidden mapping might be suitable for input-based task-inference. Nevertheless, deterministic solutions are always limited by the fact that parameters cannot be updated in a sound way when learning continually.

Taken together, our work shows that it is possible to continually learn a BNN per task without an increased parameter budget, and that finding a suitable trade-off solution across tasks can be facilitated through the use of more complex approximations and a set of task-specific parameters. Furthermore, our extensive evaluation of multiple posterior approximations across a wide range of problem settings gives valuable insights into their empirical performance and conceptual differences. Overall we believe this work, which highlights the diversity of Bayesian CL approaches, can inspire future research towards a constructive reflection on principled solutions to tackle CL.

Acknowledgements

This work was supported by the Swiss National Science Foundation (B.F.G. CRSII5-173721 and 315230_189251), ETH project funding (B.F.G. ETH-20 19-01) and funding from the Swiss Data Science Center (B.F.G, C17-18, J. v. O. P18-03). We are grateful for discussions with Harald Dermutz, Simone Carlo Surace and Jean-Pascal Pfister. We also would like to thank Sebastian Farquhar for discussions on Radial posteriors and for proofreading our implementation of this method.

References

- Arjovsky, M. and Bottou, L. Towards principled methods for training generative adversarial networks. In 5th International Conference on Learning Representations, ICLR 2017, Toulon, France, April 24-26, 2017, Conference Track Proceedings, 2017. URL https://openreview.net/forum?id=Hk4_qw5xe.
- Bachem, O., Lucic, M., and Krause, A. Coresets for non-parametric estimation the case of dp-means. In Bach, F. and Blei, D. (eds.), *Proceedings of the 32nd International Conference on Machine Learning*, volume 37 of *Proceedings of Machine Learning Research*, pp. 209–217, Lille, France, 07–09 Jul 2015. PMLR.
- Blei, D. M., Kucukelbir, A., and McAuliffe, J. D. Variational inference: A review for statisticians. *Journal of the American Statistical Association*, 112(518):859–877, 2017. doi: 10.1080/01621459.2017.1285773.
- Blundell, C., Cornebise, J., Kavukcuoglu, K., and Wierstra, D. Weight uncertainty in neural networks. In Bach, F. and Blei, D. (eds.), *Proceedings of the 32nd International Conference on Machine Learning*, volume 37 of *Proceedings of Machine Learning Research*, pp. 1613–1622, Lille, France, 07–09 Jul 2015. PMLR.
- Chang, O., Flokas, L., and Lipson, H. Principled weight initialization for hypernetworks. In *International Conference on Learning Representations*, 2020.
- Ehret, B., Henning, C., Cervera, M. R., Meulemans, A., von Oswald, J., and Grewe, B. F. Continual learning in recurrent neural networks. In *International Conference on Learning Representations*, 2021.
- Farquhar, S. and Gal, Y. Towards Robust Evaluations of Continual Learning. *Lifelong Learning: A Reinforcement Learning Approach Workshop at ICML*, 2018a.

- Farquhar, S. and Gal, Y. A unifying bayesian view of continual learning. *Bayesian Deep Learning Workshop at NeurIPS*, 2018b.
- Farquhar, S., Osborne, M. A., and Gal, Y. Radial bayesian neural networks: Beyond discrete support in large-scale bayesian deep learning. In Chiappa, S. and Calandra, R. (eds.), *Proceedings of the Twenty Third International Conference on Artificial Intelligence and Statistics*, volume 108 of *Proceedings of Machine Learning Research*, pp. 1352–1362. PMLR, 26–28 Aug 2020.
- Goodfellow, I., Pouget-Abadie, J., Mirza, M., Xu, B., Warde-Farley, D., Ozair, S., Courville, A., and Bengio, Y. Generative adversarial nets. In Ghahramani, Z., Welling, M., Cortes, C., Lawrence, N. D., and Weinberger, K. Q. (eds.), Advances in Neural Information Processing Systems 27, pp. 2672–2680. Curran Associates, Inc., 2014.
- Gretton, A., Borgwardt, K. M., Rasch, M. J., Schölkopf, B., and Smola, A. A kernel two-sample test. *Journal of Machine Learning Research*, 13(25):723–773, 2012.
- Ha, D., Dai, A., and Le, Q. Hypernetworks. In 5th International Conference on Learning Representations, ICLR 2017, 2017.
- He, K., Zhang, X., Ren, S., and Sun, J. Deep residual learning for image recognition. In *Proceedings of the IEEE conference on computer vision and pattern recognition*, pp. 770–778, 2016.
- He, X., Sygnowski, J., Galashov, A., Rusu, A. A., Teh, Y. W., and Pascanu, R. Task agnostic continual learning via meta learning. *arXiv preprint arXiv:1906.05201*, 2019.
- Hein, M., Andriushchenko, M., and Bitterwolf, J. Why relu networks yield high-confidence predictions far away from the training data and how to mitigate the problem. In *Proceedings of the IEEE/CVF Conference on Computer Vision and Pattern Recognition*, pp. 41–50, 2019.
- Henning, C., von Oswald, J., Sacramento, J., Surace, S. C., Pfister, J.-P., and Grewe, B. F. Approximating the predictive distribution via adversarially-trained hypernetworks. In *NeurIPS Bayesian Deep Learning Workshop*, 2018.
- Hinton, G., Vinyals, O., and Dean, J. Distilling the knowledge in a neural network. *arXiv preprint arXiv:1503.02531*, 2015.
- Hochreiter, S. and Schmidhuber, J. Flat minima. *Neural Computation*, 9(1):1–42, January 1997.
- Hu, T., Chen, Z., Sun, H., Bai, J., Ye, M., and Cheng, G. Stein neural sampler. *arXiv preprint arXiv:1810.03545*, 2018.

- Huszár, F. Variational inference using implicit distributions. *arXiv preprint arXiv:1702.08235*, 2017.
- Huszár, F. Note on the quadratic penalties in elastic weight consolidation. *Proceedings of the National Academy of Sciences*, 115(11):E2496–E2497, March 2018.
- Joseph, K. and Balasubramanian, V. N. Meta-consolidation for continual learning. In Advances in Neural Information Processing Systems, 2020.
- Kendall, A. and Gal, Y. What uncertainties do we need in bayesian deep learning for computer vision? In Guyon,
 I., Luxburg, U. V., Bengio, S., Wallach, H., Fergus, R.,
 Vishwanathan, S., and Garnett, R. (eds.), *Advances in Neural Information Processing Systems*, volume 30, pp. 5574–5584. Curran Associates, Inc., 2017.
- Kingma, D. P. and Welling, M. Auto-encoding variational bayes. In Bengio, Y. and LeCun, Y. (eds.), 2nd International Conference on Learning Representations, ICLR 2014, Banff, AB, Canada, April 14-16, 2014, Conference Track Proceedings, 2014.
- Kingma, D. P., Salimans, T., and Welling, M. Variational dropout and the local reparameterization trick. In Cortes, C., Lawrence, N., Lee, D., Sugiyama, M., and Garnett, R. (eds.), *Advances in Neural Information Processing Systems*, volume 28, pp. 2575–2583. Curran Associates, Inc., 2015.
- Kirkpatrick, J., Pascanu, R., Rabinowitz, N., Veness, J., Desjardins, G., Rusu, A. A., Milan, K., Quan, J., Ramalho, T., Grabska-Barwinska, A., Hassabis, D., Clopath, C., Kumaran, D., and Hadsell, R. Overcoming catastrophic forgetting in neural networks. *Proceedings of the National Academy of Sciences*, 114(13):3521–3526, March 2017.
- Krizhevsky, A. and Hinton, G. Learning multiple layers of features from tiny images. *Master's thesis, Department of Computer Science, University of Toronto*, 2009.
- Krueger, D., Huang, C.-W., Islam, R., Turner, R., Lacoste, A., and Courville, A. Bayesian Hypernetworks. *arXiv:1710.04759 [cs, stat]*, October 2017. arXiv: 1710.04759.
- Lakshminarayanan, B., Pritzel, A., and Blundell, C. Simple and scalable predictive uncertainty estimation using deep ensembles. In Guyon, I., Luxburg, U. V., Bengio, S., Wallach, H., Fergus, R., Vishwanathan, S., and Garnett, R. (eds.), *Advances in Neural Information Processing Systems*, volume 30, pp. 6402–6413. Curran Associates, Inc., 2017.

- Lakshminarayanan, B., Tran, D., Liu, J., Padhy, S., Bedrax-Weiss, T., and Lin, Z. Simple and principled uncertainty estimation with deterministic deep learning via distance awareness. In *Advances in Neural Information Processing Systems* 33, 2020.
- LeCun, Y., Bottou, L., Bengio, Y., and Haffner, P. Gradient-based learning applied to document recognition. *Proceedings of the IEEE*, 86(11):2278–2324, 1998.
- Lee, K., Lee, H., Lee, K., and Shin, J. Training confidence-calibrated classifiers for detecting out-of-distribution samples. In *International Conference on Learning Representations*, 2018. URL https://openreview.net/forum?id=ryiAv2xAZ.
- Lee, S., Ha, J., Zhang, D., and Kim, G. A neural dirichlet process mixture model for task-free continual learning. In *International Conference on Learning Representations*, 2020.
- Li, H., Barnaghi, P., Enshaeifar, S., and Ganz, F. Continual learning using bayesian neural networks. *IEEE Transactions on Neural Networks and Learning Systems*, 2020.
- Li, Y. and Turner, R. E. Gradient estimators for implicit models. In *International Conference on Learning Repre*sentations, 2018.
- Liu, Q., Lee, J., and Jordan, M. A kernelized stein discrepancy for goodness-of-fit tests. In Balcan, M. F. and Weinberger, K. Q. (eds.), *Proceedings of The 33rd International Conference on Machine Learning*, volume 48 of *Proceedings of Machine Learning Research*, pp. 276–284, New York, New York, USA, 20–22 Jun 2016. PMLR.
- Louizos, C. and Welling, M. Multiplicative Normalizing Flows for Variational Bayesian Neural Networks. In Proceedings of the 34th International Conference on Machine Learning - Volume 70, ICML'17, pp. 2218–2227. JMLR.org, 2017.
- MacKay, D. J. A practical bayesian framework for backpropagation networks. *Neural computation*, 4(3):448–472, 1992.
- MacKay, D. J. *Information theory, inference and learning algorithms*. Cambridge university press, 2003.
- Martens, J. New insights and perspectives on the natural gradient method. *Journal of Machine Learning Research*, 21(146):1–76, 2020.
- Mescheder, L., Nowozin, S., and Geiger, A. Adversarial variational bayes: Unifying variational autoencoders and generative adversarial networks. In *Proceedings of the 34th International Conference on Machine Learning*, volume 70 of *Proceedings of Machine Learning Research*,

- pp. 2391–2400, International Convention Centre, Sydney, Australia, 06–11 Aug 2017. PMLR.
- Nalisnick, E., Matsukawa, A., Teh, Y. W., Gorur, D., and Lakshminarayanan, B. Do deep generative models know what they don't know? In *International Conference on Learning Representations*, 2019.
- Nguyen, C. V., Li, Y., Bui, T. D., and Turner, R. E. Variational continual learning. In 6th International Conference on Learning Representations, ICLR 2018, Vancouver, BC, Canada, April 30 May 3, 2018, Conference Track Proceedings, 2018.
- Nielsen, F. Cramér-rao lower bound and information geometry. In *Connected at Infinity II*, pp. 18–37. Springer, 2013.
- Nowozin, S., Cseke, B., and Tomioka, R. f-gan: Training generative neural samplers using variational divergence minimization. In Lee, D., Sugiyama, M., Luxburg, U., Guyon, I., and Garnett, R. (eds.), Advances in Neural Information Processing Systems, volume 29, pp. 271–279. Curran Associates, Inc., 2016.
- Oswald, J. V., Kobayashi, S., Sacramento, J., Meulemans, A., Henning, C., and Grewe, B. F. Neural networks with late-phase weights. In *International Conference on Learning Representations*, 2021.
- Papamakarios, G., Nalisnick, E., Rezende, D. J., Mohamed, S., and Lakshminarayanan, B. Normalizing flows for probabilistic modeling and inference. arXiv preprint arXiv:1912.02762, 2019.
- Parisi, G. I., Kemker, R., Part, J. L., Kanan, C., and Wermter, S. Continual lifelong learning with neural networks: A review. *Neural Networks*, 113:54–71, May 2019. ISSN 0893-6080. doi: 10.1016/j.neunet.2019.01.012.
- Pascanu, R. and Bengio, Y. Revisiting natural gradient for deep networks. *arXiv preprint arXiv:1301.3584*, 2013.
- Pawlowski, N., Brock, A., Lee, M. C., Rajchl, M., and Glocker, B. Implicit weight uncertainty in neural networks. *arXiv preprint arXiv:1711.01297*, 2017.
- Rebuffi, S.-A., Kolesnikov, A., Sperl, G., and Lampert, C. H. icarl: Incremental classifier and representation learning. In *Proceedings of the IEEE conference on Computer Vision and Pattern Recognition*, pp. 2001–2010, 2017.
- Ritter, H., Botev, A., and Barber, D. A scalable laplace approximation for neural networks. In *International Conference on Learning Representations*, 2018.
- Schmidhuber, J. Learning to Control Fast-Weight Memories: An Alternative to Dynamic Recurrent Networks. *Neural*

- Comput., 4(1):131–139, Jan 1992. ISSN 0899-7667. doi: 10.1162/neco.1992.4.1.131.
- Schwarz, J., Czarnecki, W., Luketina, J., Grabska-Barwinska, A., Teh, Y. W., Pascanu, R., and Hadsell, R. Progress & compress: A scalable framework for continual learning. In Dy, J. and Krause, A. (eds.), *Proceedings of the 35th International Conference on Machine Learning*, volume 80 of *Proceedings of Machine Learning Research*, pp. 4528–4537, Stockholmsmässan, Stockholm Sweden, 10–15 Jul 2018. PMLR.
- Shi, J., Sun, S., and Zhu, J. A spectral approach to gradient estimation for implicit distributions. In Dy, J. and Krause, A. (eds.), *Proceedings of the 35th International Conference on Machine Learning*, volume 80 of *Proceedings of Machine Learning Research*, pp. 4644–4653, Stockholmsmässan, Stockholm Sweden, 10–15 Jul 2018. PMLR.
- Shin, H., Lee, J. K., Kim, J., and Kim, J. Continual Learning with Deep Generative Replay. In Guyon, I., Luxburg, U. V., Bengio, S., Wallach, H., Fergus, R., Vishwanathan, S., and Garnett, R. (eds.), *Advances in Neural Information Processing Systems 30*, pp. 2990–2999. Curran Associates, Inc., 2017.
- Snoek, J., Ovadia, Y., Fertig, E., Lakshminarayanan, B., Nowozin, S., Sculley, D., Dillon, J., Ren, J., and Nado, Z. Can you trust your model's uncertainty? evaluating predictive uncertainty under dataset shift. In *Advances* in *Neural Information Processing Systems*, pp. 13969– 13980, 2019.
- Swaroop, S., Nguyen, C. V., Bui, T. D., and Turner, R. E. Improving and understanding variational continual learning. *Continual Learning Workshop at NeurIPS*, 2018.
- Tuor, T., Wang, S., and Leung, K. Continual learning without knowing task identities: Do simple models work?, 2021.
- van de Ven, G. M. and Tolias, A. S. Generative replay with feedback connections as a general strategy for continual learning. *arXiv preprint arXiv:1809.10635*, 2018.
- van de Ven, G. M. and Tolias, A. S. Three scenarios for continual learning. *arXiv*, Apr 2019.
- van de Ven, G. M., Siegelmann, H. T., and Tolias, A. S. Brain-inspired replay for continual learning with artificial neural networks. *Nature communications*, 11(1):1–14, 2020.
- von Oswald, J., Henning, C., Sacramento, J., and Grewe, B. F. Continual learning with hypernetworks. In *International Conference on Learning Representations*, 2020.

- Wenzel, F., Roth, K., Veeling, B., Swiatkowski, J., Tran, L., Mandt, S., Snoek, J., Salimans, T., Jenatton, R., and Nowozin, S. How good is the Bayes posterior in deep neural networks really? In III, H. D. and Singh, A. (eds.), *Proceedings of the 37th International Conference on Machine Learning*, volume 119 of *Proceedings of Machine Learning Research*, pp. 10248–10259. PMLR, 13–18 Jul 2020.
- Wilson, A. G. and Izmailov, P. Bayesian deep learning and a probabilistic perspective of generalization. In *Advances in Neural Information Processing Systems*, 2020.
- Wortsman, M., Ramanujan, V., Liu, R., Kembhavi, A., Rastegari, M., Yosinski, J., and Farhadi, A. Supermasks in superposition. In *Advances in Neural Information Processing Systems*, 2020.
- Zenke, F., Poole, B., and Ganguli, S. Continual Learning Through Synaptic Intelligence. In *Proceedings of the 34th International Conference on Machine Learning - Volume* 70, ICML'17, pp. 3987–3995. JMLR.org, 2017.
- Zeno, C., Golan, I., Hoffer, E., and Soudry, D. Task agnostic continual learning using online variational bayes. *arXiv* preprint arXiv:1803.10123, 2018.
- Zhang, C., Bengio, S., Hardt, M., Recht, B., and Vinyals, O. Understanding deep learning requires rethinking generalization. In *International Conference on Learning Representations*, 2017.

Supplementary Material: Posterior Meta-Replay for Continual Learning

Christian Henning*, Maria R. Cervera*, Francesco D'Angelo, Johannes von Oswald, Regina Traber, Benjamin Ehret, Seijin Kobayashi, João Sacramento, Benjamin F. Grewe

Table S1. List of acronyms.

ML	Machine learning
CL	Continual learning
BNN	Bayesian neural network
VI	Variational inference
ELBO	Evidence lower-bound
KL	Kullback-Leibler divergence
FKL	Forward Kullback-Leibler divergence
RKL	Reverse Kullback-Leibler divergence
W2	2-Wasserstein distance
MC	Monte Carlo
PF-CL	Prior-focused CL
PR-CL	Posterior-replay CL
M	Main network
WG	Weight generator
TC	Task-conditioning network
BW	Task inference using batches
CS	Final fine-tuning using coresets
SP	Separate posteriors per task
TG	Task identity is given
TI	Task identity is inferred
Ent	Task inference via minimum entropy
CONF	Task inference via maximum confidence
AGREE	Task inference via maximum model agreement
OOD	Out of distribution
SH	Shared (non-growing) output head
GH	Growing output head
SEM	Standard error of the mean
MSE	Mean-squared error
SD	Standard deviation
MLP	Multilayer perceptron
AVB	Adversarial variational Bayes
ВвВ	Bayes-by-Backprop
EWC	Elastic weight consolidation
SSGE	Spectral Stein gradient estimator
VCL	Variational continual learning

A. Acronyms

For clarity, we provide a list of acronyms used throughout the paper in Table S1.

B. Summary of Notation

We summarize here the mathematical notation used throughout the paper and reintroduce the role of important variables. Whenever applicable, we denote random variables by capital letters, random variates by lowercase letters and sample spaces using calligraphic font, e.g., the prior density of $w \in \mathcal{W}$ is p(W = w). In general, sets use calligraphic font. Vectors are assumed to be column vectors and highlighted as bold symbols. Indexing is performed using subscripts, e.g., x_i is the i-th component of $\mathbf{x} \in \mathcal{X}$. Superscripts are used to

disambiguate external factors such as task identity. Matrices also use capital letters, and it is clearly stated whenever a variable has to be interpreted as matrix, e.g., the *Fisher Information matrix* F.

In this study, we distinguish between three different networks with clearly defined roles (plus a discriminator network when using AVB). The main network (M), $\hat{y} =$ $f_{\rm M}({\bf x},{\bf w})$, processes inputs x to generate predictions $\hat{{\bf y}}$ using trainable parameters w. This notation is chosen for mathematical convenience, but it should be noted that in most cases $f_{\rm M}(\cdot)$ represents a likelihood function. For instance, in the case of a C-way classification with labels $y \in \mathcal{Y} = \{1, \dots, C\}$, the output of the main network is an element of the probability simplex $\Delta(\mathcal{Y})$, and in regression $f_{\rm M}(\cdot)$ represents the mean of a normal distribution $\mathcal{N}(f_{\mathbf{M}}(\cdot), \sigma_{\mathbf{II}}^2)$ with variance $\sigma_{\mathbf{II}}^2$. The task-conditioned hypernetwork (TC), $\boldsymbol{\theta}^{(t)} = f_{\text{TC}}(\mathbf{e}^{(t)}, \boldsymbol{\psi})$, has parameters $\boldsymbol{\psi}$ and processes task embeddings $e^{(t)}$ to generate the parameters $\theta^{(t)}$ of the weight generator (WG). In the deterministic case (e.g., PR-DIRAC), the weight generator simply reduces to $\mathbf{w}^{(t)} \equiv \boldsymbol{\theta}^{(t)} = f_{\text{WG}}(\cdot, \boldsymbol{\theta}^{(t)})$. In all other cases, it transforms noise samples $z \sim p(\mathbf{Z})$ into main network parameter configurations.

A dataset is a set of input-output tuples $\mathcal{D} = \{(\mathbf{x}^{(n)}, \mathbf{y}^{(n)})\}_{n=1}^{N}$. If not noted otherwise, a dataset is considered an i.i.d. sample from some unknown data-generating process $\mathcal{D} \stackrel{i.i.d.}{\sim} p(\mathbf{X})p(\mathbf{Y} \mid \mathbf{X})$.

We consider a Bayesian treatment of main network parameters \mathbf{w} to incorporate model uncertainty (MacKay, 1992). The prior is denoted by $p(\mathbf{W})$, the likelihood by $p(\mathcal{D} \mid \mathbf{W}) \equiv \prod_{n=1}^N p(\mathbf{y}^{(n)} \mid \mathbf{W}; \mathbf{x}^{(n)})$, the posterior parameter distribution by $p(\mathbf{W} \mid \mathcal{D})$ and the posterior predictive distribution for an unseen input $\tilde{\mathbf{x}}$ by $p(\mathbf{Y} \mid \mathcal{D}; \tilde{\mathbf{x}})$. We consider families of distributions parametrized by $\boldsymbol{\theta}$ to approximate the posterior parameter distribution $q_{\boldsymbol{\theta}}(\mathbf{W}) \approx p(\mathbf{W} \mid \mathcal{D})$, e.g., for the deterministic case we have $q_{\boldsymbol{\theta}}(\mathbf{W}) = \delta(\boldsymbol{\theta} - \mathbf{W})$, where $\delta(\cdot)$ denotes the Dirac delta function.

C. Algorithms

In this section we provide details about the different algorithms used throughout the paper. We start by quickly reviewing variational inference, and explaining how it can be applied to task-conditioned hypernetworks in the context of CL in order to obtain task-specific approximate posterior distributions. Then, we present several variational algorithms that we employed to obtain the approximate posteriors, ei-

ther based on a predefined function (explicit posterior) or based on a parametrization by an auxiliary network (implicit posterior). We also explain how prior-focused CL can be achieved within our framework, and present the algorithms that can be used to learn *explicit* posteriors. Additionally, we explain how prior-focused CL can be rendered more flexible by allowing the parameter posteriors to be approximated by *implicit* distributions, and by incorporating a set of task-specific parameters alongside the shared ones. Because task-specific solutions require having access to the identity of the task, we explain how task identity can be inferred via predictive uncertainty for both prior-focused and posteriorreplay approaches. Finally, we explain how coresets can be used in our framework to perform a fine-tuning stage after training which mitigates forgetting and facilitates task inference.

C.1. Variational inference

Whenever confronted with unseen inputs $\tilde{\mathbf{x}}$, we aspire to obtain predictions via the posterior predictive distribution: $p(\mathbf{y} \mid \mathcal{D}; \tilde{\mathbf{x}}) = \int_{\mathbf{W}} p(\mathbf{y} \mid \mathbf{W}; \tilde{\mathbf{x}}) p(\mathbf{W} | \mathcal{D}) d\mathbf{W}$. Unfortunately, the posterior parameter distribution $p(\mathbf{W}|\mathcal{D})$ is in general intractable. Furthermore, since sampling cannot be efficiently performed and would require high storage demands, we approximate this distribution in order to evaluate the posterior predictive distribution. For this purpose, we apply variational inference (VI), a standard approximate probabilistic inference technique (see e.g., Blei et al. (2017)) where we look for approximations $q_{\theta}(\mathbf{W})$ within a certain family of distributions \mathcal{Q} , referred to as the variational family, with members parametrized by $\theta \in \Theta$. In VI, this problem is solved by optimizing for nearest approximations within Q according to some divergence, most often the Kullback-Leibler (KL) divergence: $KL(q_{\theta}(\mathbf{W}) \mid\mid p(\mathbf{W} \mid \mathcal{D}))$. The choice of the reverse KL allows rewriting the above expression such that it does not contain the intractable posterior. The resulting expression (known as the evidence lower bound; *ELBO*) is therefore a suitable optimization objective that needs to be maximized:

$$\mathbb{E}_{q_{\boldsymbol{\theta}}(\mathbf{W})} \left[\log p(\mathcal{D} \mid \mathbf{W}) \right] - \text{KL}(q_{\boldsymbol{\theta}}(\mathbf{W}) \mid\mid p(\mathbf{W})) \quad (2)$$

where the first term corresponds to minimizing the negativelog likelihood of the data \mathcal{D} (cf. SM C.3.1), and the second term can be seen as a regularization that aims to match the approximation $q_{\theta}(\mathbf{W})$ to the prior $p(\mathbf{W})$, and is referred to as *prior-matching term*. Finding an optimal approximation within the variational family amounts to optimizing the parameters θ . Since in our framework these are task-specific and their optimization depends only on the corresponding dataset $\mathcal{D}^{(t)}$ we write from here on $q_{\theta(t)}(\mathbf{W})$.

C.2. Task-conditioned hypernetworks

Task-conditioned hypernetworks, which generate taskspecific weights for a main network, have recently been proposed as an effective method to continually learn several tasks (von Oswald et al., 2020). The outputs of the hypernetwork are made task-specific by providing low-dimensional task embeddings $e^{(t)}$ as input, which are learned continually alongside the hypernetwork's parameters ψ . Catastrophic forgetting can be prevented using a simple L2 regularizer (cf. Eq. 1 in the main text) which makes sure that the outputs of the hypernetwork for previously learned tasks do not change. Notably, shifting CL to the meta-level simplifies the problem considerably, because only a single input-output mapping per task needs to be fixed. It should be noted that von Oswald et al. (2020) also investigated the regularizer in Eq. 1 with long task sequences (e.g., 250 tasks), where a fixed-size, random subset of previous tasks was chosen at every training iteration for regularization. In this way, the regularization cost is constant and does not depend on the number of tasks.

Here we consider hypernetworks that parameterize target models in a compressed form using a simple but effective technique called *chunking*: the hypernetwork is iteratively invoked using an additional input c at each step, which addresses a distinct subset of parameters (e.g., a distinct layer of the target neural network). To be precise, chunk embeddings $\mathbf{c}^{(l)}$, l = 1..L, are unconditional parameters (i.e., not task-specific). Thus, the hypernetwork parameters ψ can be split into a set of chunk embeddings $\{\mathbf{c}^{(l)}\}_{l=1}^{L}$ and a set of weights $\tilde{\psi}$, which are the actual weights of the network that produces individual chunks. This introduces soft weight sharing, as the entire set of target model parameters w depends on ψ . Note, that modern graphics hardware allows the parallel generation of all chunks (batch-processing). For more details, please refer to von Oswald et al. (2020) and Ehret et al. (2021). For all experiments other than the lowdimensional toy problems, we apply the chunking strategy to the TC and WG networks. Low-dimensional problems utilize MLP hypernetworks, where w is directly the output of the network. Both task and chunk embeddings are initialized according to a normal distribution with zero mean, whose variance is considered a hyperparameter.

In their original formulation, hypernetworks for CL provide a single main network weight configuration per task (**PR-Dirac**). Here, we extend this deterministic approach to a probabilistic setting and aim to model task-specific *distributions* over main network weights instead. Therefore, the outputs of the hypernetwork can no longer be interpreted as the weights **w** of the main network, but rather as parameters $\theta^{(t)}$ defining the approximate distribution $q_{\theta^{(t)}}(\mathbf{W})$, from which weights **w** for the main network can be sampled. In practice, $q_{\theta^{(t)}}(\mathbf{W})$ is given by a function $f_{\mathbf{WG}}(\mathbf{z}, \theta^{(t)})$,

which also depends on a base distribution $p(\mathbf{Z})$ from which inputs \mathbf{z} for the hypernetwork are sampled.

Crucially, in this probabilistic setting, catastrophic forgetting is avoided via a regularizer that prevents the distributions $q_{\boldsymbol{\theta}^{(t)}}(\mathbf{W})$ of previously learned tasks to change, hence our naming posterior meta-replay. Whenever the utilized variational family for approximate posteriors has an analytic expression for a divergence measure, this can be achieved by turning the original hypernetwork regularizer into a divergence measure between the distributions (cf. Eq. 10) before and after any given task is being learned. However divergence measures cannot always be analytically evaluated, for example if the distributions are *implicit*, in which case other solutions are necessary. One option is to use a sample-based distance estimate between the distributions (Gretton et al., 2012; Liu et al., 2016), which would act upon the output of the WG network (i.e., the weight samples). However, due to the dimensionality of w, meaningful distance estimates in distribution space might be prohibitively expensive since the regularizer has to be evaluated in every training iteration. For this reason, whenever no analytic divergence measure is available, we resort to the use of a mean-squared error (MSE) regularizer at the output of the TC network (Eq. 1), as done in the deterministic case considered by von Oswald et al. (2020). Therefore, rather than ensuring that a distribution does not change, we ensure that the parameters of a distribution do not change. Note however, that this treatment forces an interpretation onto the TC network as encoding a Gaussian likelihood with isotropic variance.

While in our experiments forgetting is not a prevailing issue and we therefore were not urged to improve upon this simple regularization, we would still like to comment on potential improvements that can be considered by future work. One option would be to assign importance values to individual outputs of the TC network and thus transform the isotropic regularization of Eq. 1 into a weighted sum per previous task. Such importance values could incorporate the curvature of the loss landscape. As the task-specific loss is data-dependent, the importance values would need to be computed at the end of the training of each task, where data is still accessible. In our case, the task-specific loss is the ELBO (Eq. 2), which embodies the KL to the posterior $p(\mathcal{D} \mid \mathbf{W})$. Thus, if importance values reflect the Hessian of the ELBO with respect to the outputs of the TC network, the CL regularization would target our posterior approximation criterion (i.e., the ELBO) directly, ensuring that parameter changes are only tolerated if the ELBO remains stable. In SM. F.2 we further elaborate on how importance values could be constructed such that this simple type of regularization can be interpreted as preserving distances in distribution space. Nonetheless, an imminent drawback of this procedure is the need to store the importance values of

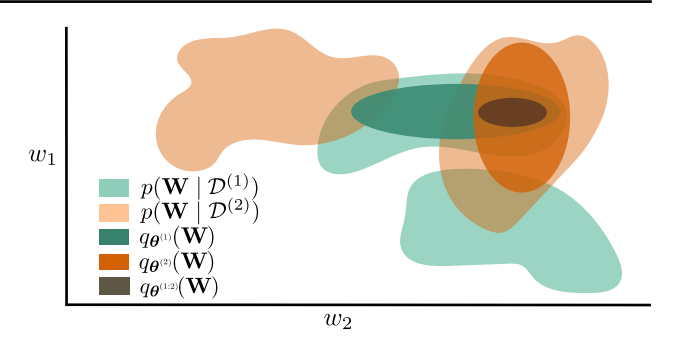


Figure S1. Differences between prior-focused and posterior-replay CL approaches when using Gaussian posterior approximations with diagonal covariance. In this case, the proposed posterior-replay framework can capture one mode of each task-specific posterior via $q_{\theta^{(1)}}(\mathbf{W})$ and $q_{\theta^{(2)}}(\mathbf{W})$. In contrast, a prior-focused method with this type of approximation (e.g., EWC (Kirkpatrick et al., 2017) or VCL (Nguyen et al., 2018)) has to assume that the currently found mode $q_{\theta^{(1:2)}}(\mathbf{W})$ also contains admissible solutions for upcoming tasks.

each previous task.³ However, the memory implications of this shortcoming can be alleviated by using compression schemes for importance values or by distilling them into an auxiliary network (Hinton et al., 2015).

C.3. Posterior-Replay with explicit parametric distributions

We now present the algorithms that can be used to obtain what we refer to as *explicit* approximate posterior distributions, i.e., simple posterior approximations $q_{\theta^{(t)}}(\mathbf{W})$ that can be sampled from according to a predefined function (cf. Eq. 3 and Eq. 11).

C.3.1. BAYES-BY-BACKPROP

Blundell et al. (2015) present Bayes-by-Backprop (BbB), a VI algorithm that uses a mean-field Gaussian approximation, i.e., $q_{\theta}(\mathbf{W}) = \prod_{i} \mathcal{N}(W_{i}; \mu_{i}, \sigma_{i}^{2})$, where θ consists of vectors μ and σ^{2} containing a mean and variance for each weight. To be able to optimize these two vectors, the authors make use of the *reparametrization trick* (Kingma & Welling, 2014), which allows gradient computation with respect to μ and σ through the stochastic sampling process of $q_{\theta}(\mathbf{W})$. Specifically, samples \mathbf{w} are obtained via:

$$\mathbf{w} = \boldsymbol{\mu} + \boldsymbol{\sigma} \odot \boldsymbol{\epsilon} \tag{3}$$

where $\epsilon \sim \mathcal{N}(0, \mathbf{I})$.

Recall, that optimizing the ELBO (cf. Eq. 2) requires estimating the negative log-likelihood (NLL) $-\mathbb{E}_{q_{\boldsymbol{\theta}}(\mathbf{W})}[\log p(\mathcal{D} \mid \mathbf{W})], \text{ which in practice is achieved}$

³Note, that also the original EWC formulation required the storage of one Fisher matrix per task (Kirkpatrick et al., 2017).

via a Monte-Carlo estimate of K samples $\mathbf{w}^{(k)} \sim q_{\boldsymbol{\theta}}(\mathbf{W})$

$$NLL \approx -\frac{1}{K} \sum_{k=1}^{K} \log p(\mathcal{D} \mid \mathbf{W} = \mathbf{w}^{(k)})$$
 (4)

As a full summation $\log p(\mathcal{D} \mid \mathbf{W}) = \sum_{n=1}^N \log p(\mathbf{y}^{(n)} \mid \mathbf{W}; \mathbf{x}^{(n)})$ over the whole dataset at every training iteration is prohibitively expensive, this term is approximated via mini-batches \mathcal{B} of size $N_{\rm mb}$, which requires a corrective scaling

$$NLL \approx -\frac{1}{K} \sum_{k=1}^{K} \frac{N}{N_{\text{mb}}} \sum_{(\mathbf{x}, \mathbf{y}) \in \mathcal{B}} \log p(\mathbf{y} \mid \mathbf{w}^{(k)}; \mathbf{x})$$
 (5)

How to compute the term $\log p(\mathbf{y} \mid \mathbf{w}; \mathbf{x})$ depends on the problem at hand. In regression tasks, it is common to model the likelihood as a Gaussian distribution. For simplicity, we only consider 1D regression and a model likelihood with fixed variance σ_{11}^2 such that:

$$\log p(y \mid \mathbf{w}; x) = \operatorname{const} - \frac{1}{2\sigma_{\text{II}}^2} (f_{\mathbf{M}}(x, \mathbf{w}) - y)^2$$
 (6)

Dropping all constant terms that do not affect the optimization, the NLL can be written as a properly scaled $(\frac{N}{2\sigma_z^2})$ mean-squared error (MSE) loss inside a Monte-Carlo esti-

$$NLL \approx \frac{N}{2KN_{\text{mb}}\sigma_{\text{ll}}^2} \sum_{k=1}^{K} \sum_{(x,y) \in \mathcal{B}} \left(f_{\text{M}}(x, \mathbf{w}^{(k)}) - y \right)^2 \quad (7)$$

In C-way classification problems, the likelihood of class c is computed as:

$$p(Y = c \mid \mathbf{w}; \mathbf{x}) = \operatorname{sm}(f_{\mathbf{M}}(\mathbf{x}, \mathbf{w}))_{c}$$
(8)

where $sm(\cdot)$ refers to the softmax, assuming the main network produces unnormalized logits for mathematical convenience. Under this notation, the NLL for classification problems can be estimated as follows:

$$\begin{aligned} \text{NLL} &\approx -\frac{N}{KN_{\text{mb}}} \sum_{k=1}^{K} \sum_{(\mathbf{x}, y) \in \mathcal{B}} \log \left(\text{sm} \left(f_{\text{M}}(\mathbf{x}, \mathbf{w}^{(k)}) \right)_{y} \right) \\ &= \frac{N}{KN_{\text{mb}}} \sum_{k=1}^{K} \sum_{(\mathbf{x}, y) \in \mathcal{B}} \left(\\ &\underbrace{-\sum_{c=1}^{C} [c = y] \log \left(\text{sm} \left(f_{\text{M}}(\mathbf{x}, \mathbf{w}^{(k)}) \right)_{c} \right) \right)}_{\text{cross-entropy loss with 1-hot targets}} \end{aligned} \tag{9}$$

where [.] denotes the Iverson bracket.

The second term in the ELBO, i.e., the *prior-matching term*, can be analytically evaluated if a Gaussian prior is used.

We adapt the BbB algorithm to our PR-CL framework by having a task-conditioned (TC) network that generates taskspecific $\mu^{(t)}$ and $\sigma^{(t)}$ (Fig. S1). Since outputs of the TC network are real-valued, variances $\sigma^{(t)}$ are obtained through a softplus transformation of the network's outputs. The current task's loss $\mathcal{L}_{task}(\psi, \mathbf{e}^{(t)}, \mathcal{D}^{(t)})$ corresponds to the negative ELBO and can be estimated as described above, where we use the analytic expression for the prior-matching term.

Since approximate posteriors correspond to Gaussian distributions, the CL regularizer can take the form of an explicit divergence measure in distribution space computed solely based on the TC network's output. We experiment with the forward (FKL) and reverse KL (RKL), and the 2-Wasserstein distance (W2). Specifically, the loss when learning task t therefore becomes:

$$\mathcal{L}^{(t)}(\boldsymbol{\psi}, \mathcal{E}, \mathcal{D}^{(t)}) = \mathcal{L}_{\text{task}}(\boldsymbol{\psi}, \mathbf{e}^{(t)}, \mathcal{D}^{(t)}) + \beta \sum_{t' < t} \mathbf{D} \left(q_{\boldsymbol{\theta}^{(t', *)}}(\mathbf{W}) || q_{\boldsymbol{\theta}^{(t')}}(\mathbf{W}) \right)$$
(10)

where $\mathrm{D}(\cdot||\cdot)$ corresponds to one of the above mentioned divergence measures and $\boldsymbol{\theta}^{(t',*)} \equiv f_{\mathrm{TC}}(\mathbf{e}^{(t',*)}, \boldsymbol{\psi}^*)$ are the parameters of the posterior approximation obtained from a checkpoint of the TC hypernetwork before learning task t (cf. Eq. 1). In practice, we do not observe a notable difference between any of these divergence measures and the L2 regularization applied in Eq. 1.

As a variance reduction trick to improve training stability, we also experiment with the local reparametrization trick (Kingma et al., 2015) whenever the main network has an MLP architecture. Whether or not this trick is used is determined by a hyperparameter and therefore selected by the hyperparameter search of each experiment conducted with BbB or VCL (cf. SM C.5.1).

C.3.2. RADIAL POSTERIORS

Intuitively, one would expect that the probability mass of a Gaussian lies around the mean. This is however not the case in high dimensions, where the probability mass is clustered in a thin hyper-annulus far away from the mean. This happens because a sample point from an isotropic, highdimensional Gaussian distribution can be interpreted as many sample points from the corresponding 1D Gaussian distribution, therewith representing with high probability an element of the typical set. Farquhar et al. (2020) argues that training BNNs with a mean-field Gaussian approximation (as in BbB), can lead to gradient estimates with high variance and impaired training stability due to the effects

that arise due to typicality in isotropic, high-dimensional Gaussian distributions. Based on this insight, Farquhar et al. (2020) propose the following corrective normalization to Eq. 3, and argue it helps recover the intuitive behavior of Gaussian distributions in low dimensions:

$$\mathbf{w} = \boldsymbol{\mu} + \boldsymbol{\sigma} \odot \frac{\boldsymbol{\epsilon}}{\|\boldsymbol{\epsilon}\|} \cdot r \tag{11}$$

where $r \sim \mathcal{N}(0, 1)$ and $\epsilon \sim \mathcal{N}(0, \mathbf{I})$. Here, we apply the corrective normalization layer-wise, but treating weights and biases separately, such that the dimensions of \mathbf{I} correspond to the number of weights or biases in a given layer.

When computing the *prior-matching term* between a *radial* approximation and a Gaussian prior $p(\mathbf{W})$, we use the following expression for the negative entropy of a *radial* distribution (cf. Eq. 5 in Farquhar et al. (2020)):

$$\int q_{\theta}(\mathbf{W}) \log q_{\theta}(\mathbf{W}) d\mathbf{W} = -\sum_{i} \log \sigma_{i} + \text{const} \quad (12)$$

The cross-entropy term is approximated via an MC estimate with samples from the *radial* posterior. Note, that the log-density of the Gaussian prior can be computed analytically.

Again, in our framework the task-specific means μ and "variances" σ^2 are generated by a TC hypernetwork, whose outputs need to be regularized to prevent forgetting (cf. SM C.3.1). Because an analytic expression for a divergence between *radial* distributions is unknown, we resort to the L2 hypernetwork regularizer (Eq. 1) when working with *radial* distributions.

C.4. Posterior-Replay with implicit distributions

We also explore the use of *implicit* $q_{\theta^{(t)}}(\mathbf{W})$ distributions as approximate posteriors. In our framework, these are parametrized by an auxiliary WG network, that has parameters $\theta^{(t)}$ and receives samples from an arbitrary base distribution $p(\mathbf{Z})$ as inputs. In our experiments, we always consider a Gaussian base distribution with zero mean, and experiment with different variances.

The use of implicit posterior approximations introduces a challenge when optimizing the *prior-matching* term of the *ELBO*, since we do not have access to the analytic expression of the density, nor to its entropy. This problem can be avoided when the change-of-variables formula is applicable, i.e., when using an invertible architecture for the weight-generator network f_{WG} with tractable base distribution $p(\mathbf{Z})$ (cf. normalizing flows (Papamakarios et al., 2019)). In this case, the ELBO objective can be approximated via an MC estimate and optimized via automatic differentiation. Alternative approaches sidestep the need to have invertible networks, and aim to find other estimates that allow optimizing the *ELBO* objective. Multiple studies

have already investigated the use of weight generators for BNNs (Krueger et al., 2017; Henning et al., 2018), ranging from sample-based estimates of the prior-matching term (Pawlowski et al., 2017) to the use of normalizing flows with shared influence on a set of weights for improved scalability (Louizos & Welling, 2017). Within the deep learning community, generative adversarial networks (GANs, Goodfellow et al. (2014)) represent the most successful use case of implicit distributions. This approach is purely samplebased and requires an auxiliary network that engages in a minimax optimization. A wide range of loss functions can be used to approximately optimize different kinds of divergences or distances, including the KL required for the prior-matching term, (Nowozin et al., 2016) as done in AVB (cf. SM C.4.1). However, as training corresponds to playing a non-convex game and an inner-loop optimization is required, optimization difficulties arise when applying GAN-like approaches to high-dimensional problems. We experienced these difficulties and therefore also explore alternative ways to train implicit distributions, e.g., methods based on Stein's identity (cf. SM C.4.2). In practice, approaches that do not require invertible networks are used with architectures that have a support of measure zero in weight space \mathcal{W} , which causes the KL to be ill-defined. We comment on this issue in SM C.4.3.

C.4.1. ADVERSARIAL VARIATIONAL BAYES

Adversarial variational Bayes (AVB, Mescheder et al. (2017)) was introduced as a method to estimate the log density ratio of the *prior-matching term* by using the GAN framework. More specifically, the *prior-matching term* (Eq. 2) can be rewritten as $\mathbb{E}_{q_{\theta}(\mathbf{W})} \big[\log q_{\theta}(\mathbf{W}) - \log p(\mathbf{W}) \big]$, and AVB introduces an auxiliary *discriminator* network (**D**) that, within each training iteration, learns to approximate $\log q_{\theta}(\mathbf{W}) - \log p(\mathbf{W})$. Mescheder et al. (2017) show that this is achieved for a discriminator that maximizes the following expression:

$$\mathbb{E}_{q_{\boldsymbol{\theta}}(\mathbf{W})}[\log \sigma(f_{D}(\mathbf{W}))] + \mathbb{E}_{p(\mathbf{W})}\left[\log(1 - \sigma(f_{D}(\mathbf{W})))\right]$$
(13)

where $\sigma(\cdot)$ denotes the logistic sigmoid function and f_D the function performed by the discriminator. Having the optimal discriminator $f_D^*(\mathbf{w})$, the *prior-matching term* can be approximated via a Monte-Carlo sample:

$$\mathbb{E}_{q_{\boldsymbol{\theta}}(\mathbf{W})} \left[\log \frac{q_{\boldsymbol{\theta}}(\mathbf{W})}{p(\mathbf{W})} \right] = \mathbb{E}_{q_{\boldsymbol{\theta}}(\mathbf{W})} \left[f_{\mathbf{D}}^*(\mathbf{W}) \right]$$

$$\approx \frac{1}{K} \sum_{k=1}^{K} f_{\mathbf{D}}^*(\mathbf{w}^{(k)}) \qquad (14)$$

This means that at every training iteration of θ (or in our case ψ) the parameters of the discriminator should be trained to optimality. In practice, however, one only fine-tunes the discriminator weights for a few iterations in the inner loop.

Note, that training requires access to $\nabla_{\theta} \mathbb{E}_{q_{\theta}(\mathbf{W})} [f_{\mathrm{D}}^{*}(\mathbf{W})]$, and that the optimal parameter configuration of the discriminator might also depend on θ as it is an outcome of the optimization procedure described in Eq. 13. Fortunately, as shown in Mescheder et al. (2017), the term $\mathbb{E}_{q_{\theta}(\mathbf{W})}[\nabla_{\theta}f_{\mathrm{D}}^{*}(\mathbf{W})]$ vanishes and no backpropagation through the discriminator is required.

We also employ a trick suggested in Mescheder et al. (2017), termed *adaptive contrast*, which can be used whenever analytic access to the prior density is guaranteed (which is not the case when using AVB in a prior-focused setting, PF-AVB, except for the first task). The incentive for the trick is the fact that a density ratio, especially in high-dimensions, has high variance. Therefore, an auxiliary Gaussian distribution $r_{\alpha}(\mathbf{W})$ is introduced, whose mean and variance parameters are set to the empirical mean and variance of $q_{\theta}(\mathbf{W})$, assuming that the ratio when involving such $r_{\alpha}(\mathbf{W})$ is "easier" to estimate. The ELBO is then rewritten in the following way to include $r_{\alpha}(\mathbf{W})$:

$$\mathbb{E}_{q_{\theta}(\mathbf{W})} \left[\log p(\mathcal{D} \mid \mathbf{W}) \right] - \text{KL}(q_{\theta}(\mathbf{W}) \mid\mid p(\mathbf{W}))$$

$$= \mathbb{E}_{q_{\theta}(\mathbf{W})} \left[\log p(\mathcal{D} \mid \mathbf{W}) - \log q_{\theta}(\mathbf{W}) + \log r_{\alpha}(\mathbf{W}) - \log r_{\alpha}(\mathbf{W}) + \log p(\mathbf{W}) \right]$$

$$= \mathbb{E}_{q_{\theta}(\mathbf{W})} \left[\log p(\mathcal{D} \mid \mathbf{W}) - \log r_{\alpha}(\mathbf{W}) + \log p(\mathbf{W}) - \tilde{f}_{D}^{*}(\mathbf{W}) \right]$$

$$(15)$$

where now $\tilde{f}_{\rm D}^*(\mathbf{w})$ is trained to approximate the log-density ratio $\log q_{\theta}(\mathbf{W}) - \log r_{\alpha}(\mathbf{W})$.

Because of this minimax optimization, AVB suffers in our experiments from scalability issues,⁴ and we therefore only experimented with it for low-dimensional problems, where it turns out to be in general the best method, both in terms of performance of individual runs and in ease of finding suitable hyperparameters.

An interesting question regarding AVB is the choice of the discriminator's architecture, which processes complete weight samples w to determine whether they originate from the prior or from the approximate posterior distribution. For low-dimensional problems, we use MLP architectures since the dimensionality of w is only in the order of 100 weights. For high-dimensional problems, where using a plain MLP is infeasible, we experimented with a chunking approach. Specifically, we used one MLP to reduce the dimensionality of individual weight chunks, which are then concatenated and fed as input to a second MLP that generates the actual output of the discriminator. However, we did not succeed with this approach, and we leave the scaling of AVB to large main networks as an open problem for future work.

C.4.2. SPECTRAL STEIN GRADIENT ESTIMATOR

Stein's identity and the related Stein discrepancy have also been investigated to develop training methods for *implicit* distributions (Hu et al., 2018). Li & Turner (2018) and Shi et al. (2018) observed that the training of *implicit* distributions (e.g., via VI) often only requires access to $\nabla_{\mathbf{w}} \log q_{\theta}(\mathbf{w})$, a quantity that appears in Stein's identity. Notably, both approaches do no require an auxiliary network nor an inner-loop optimization.

Li & Turner (2018) uses an MC estimate of Stein's identity in combination with ridge regression to obtain $\nabla_{\mathbf{w}} \log q_{\boldsymbol{\theta}}(\mathbf{w})$ estimates. Unfortunately, the method can only be used to estimate this quantity for sample points retrieved from $q_{\boldsymbol{\theta}}(\mathbf{w})$. When requiring an estimate for sample points obtained from a different distribution, as it is the case for the cross-entropy term appearing in PF-SSGE, this method is not applicable.

Therefore, we consider an alternative, the spectral Stein gradient estimator (SSGE, Shi et al. (2018)), whose inner workings are briefly sketched below for completeness.

Recall that our ultimate goal is to find the parameters θ that maximize the *ELBO*, and we therefore need to evaluate the following expression:

$$\nabla_{\boldsymbol{\theta}} E L B O = \nabla_{\boldsymbol{\theta}} \mathbb{E}_{q_{\boldsymbol{\theta}}(\mathbf{W})} \Big[\log p(\mathcal{D} \mid \mathbf{W}) \Big]$$
$$- \nabla_{\boldsymbol{\theta}} \mathbb{E}_{q_{\boldsymbol{\theta}}(\mathbf{W})} \Big[q_{\boldsymbol{\theta}}(\mathbf{W}) \Big] + \nabla_{\boldsymbol{\theta}} \mathbb{E}_{q_{\boldsymbol{\theta}}(\mathbf{W})} \Big[p(\mathbf{W}) \Big]$$
(16)

Thus, the gradient acts on three distinct terms, the first term simply corresponds to the negative log-likelihood (NLL) when learning on the data \mathcal{D} , and we refer to the other two terms as the *entropy* and the *cross-entropy*. In this specific case, the NLL and cross-entropy term can be approximated using an MC estimate, and their gradient computation through individual samples becomes feasible by using the reparametrization trick. However, as explained previously, the entropy term is difficult to compute since we do not have access to the density of $q_{\theta}(\mathbf{W})$. This term can be rewritten as follows:

$$\nabla_{\boldsymbol{\theta}} \mathbb{E}_{q_{\boldsymbol{\theta}}(\mathbf{W})} \Big[q_{\boldsymbol{\theta}}(\mathbf{W}) \Big] = \nabla_{\boldsymbol{\theta}} \int_{\mathbf{w}} q_{\boldsymbol{\theta}}(\mathbf{w}) \log q_{\boldsymbol{\theta}}(\mathbf{w}) d\mathbf{w}$$

$$= \nabla_{\boldsymbol{\theta}} \int_{\mathbf{z}} p(\mathbf{z}) \log q \big(f_{\text{WG}}(\mathbf{z}, \boldsymbol{\theta}), \boldsymbol{\theta} \big) d\mathbf{z}$$

$$= \int_{\mathbf{z}} p(\mathbf{z}) \nabla_{\boldsymbol{\theta}} \log q \big(f_{\text{WG}}(\mathbf{z}, \boldsymbol{\theta}), \boldsymbol{\theta} \big) d\mathbf{z}$$

$$= \mathbb{E}_{p(\mathbf{z})} \Big[\nabla_{\boldsymbol{\theta}} \log q \big(f_{\text{WG}}(\mathbf{Z}, \boldsymbol{\theta}), \boldsymbol{\theta} \big) \Big]$$

$$= \mathbb{E}_{p(\mathbf{z})} \Big[\nabla_{\boldsymbol{\theta}} \log q \big(f_{\text{WG}}(\mathbf{Z}, \boldsymbol{\theta}), \hat{\boldsymbol{\theta}} \big) \Big|_{\hat{\boldsymbol{\theta}} = \boldsymbol{\theta}} \Big]$$

$$= \mathbb{E}_{p(\mathbf{z})} \Big[\nabla_{\mathbf{w}} \log q \big(\mathbf{W}, \boldsymbol{\theta} \big) \Big|_{W = f_{\text{WG}}(\mathbf{Z}, \boldsymbol{\theta})} \nabla_{\boldsymbol{\theta}} f_{\text{WG}}(\mathbf{Z}, \boldsymbol{\theta}) \Big]$$
(17)

⁴Note, also Pawlowski et al. (2017) reports difficulties when applying AVB to BNNs.

where to get the second line we have used the following reparametrization $\mathbf{w} = f_{\mathrm{WG}}(\mathbf{z}, \boldsymbol{\theta})$ and $\mathbf{z} \sim p(\mathbf{Z})$, and rewritten $q_{\boldsymbol{\theta}}(\mathbf{W})$ as $q(\mathbf{W}, \boldsymbol{\theta})$ for clarity. Furthermore, to obtain the fifth line we computed the total derivative, and directly used the fact that $\mathbb{E}_{p(\mathbf{Z})} \big[\nabla_{\boldsymbol{\theta}} \log q(\mathbf{W}, \boldsymbol{\theta}) \big|_{\mathbf{w} = f_{\mathrm{WG}}(\mathbf{z}, \boldsymbol{\theta})} \big]$ cancels out. Here is the derivation for completeness:

$$\mathbb{E}_{p(\mathbf{Z})} \left[\nabla_{\boldsymbol{\theta}} \log q(\mathbf{W}, \boldsymbol{\theta}) \big|_{\mathbf{W} = f_{\text{WG}}(\mathbf{Z}, \boldsymbol{\theta})} \right]$$

$$= \mathbb{E}_{q_{\boldsymbol{\theta}}(\mathbf{W})} \left[\nabla_{\boldsymbol{\theta}} \log q(\mathbf{W}, \boldsymbol{\theta}) \right]$$

$$= \int_{\mathbf{w}} q_{\boldsymbol{\theta}}(\mathbf{w}) \nabla_{\boldsymbol{\theta}} \log q(\mathbf{w}, \boldsymbol{\theta}) d\mathbf{w}$$

$$= \int_{\mathbf{w}} q_{\boldsymbol{\theta}}(\mathbf{w}) \frac{1}{q_{\boldsymbol{\theta}}(\mathbf{w})} \nabla_{\boldsymbol{\theta}} q(\mathbf{w}, \boldsymbol{\theta}) d\mathbf{w}$$

$$= \nabla_{\boldsymbol{\theta}} \int_{\mathbf{w}} q(\mathbf{w}, \boldsymbol{\theta}) d\mathbf{w} = \nabla_{\boldsymbol{\theta}} 1 = 0 \qquad (18)$$

Coming back to Eq. 17, we see that two gradients need to be computed within the expectation. The second term $\nabla_{\boldsymbol{\theta}} f_{\text{WG}}(\mathbf{z}, \boldsymbol{\theta})$ is simply the gradient of the output of the weight-generator hypernetwork with respect to its own parameters, and can therefore be easily obtained using automatic differentiation. The expression $\nabla_{\mathbf{w}} \log q_{\boldsymbol{\theta}}(\mathbf{w})$ is not accessible for implicit distributions, and needs to be estimated.

SSGE provides a way to estimate $\nabla_{\mathbf{w}} \log q_{\boldsymbol{\theta}}(\mathbf{w})$ by considering a spectral decomposition:

$$\nabla_{w_i} \log q_{\boldsymbol{\theta}}(\mathbf{w}) = \sum_{j=1}^{\infty} \gamma_{ij} \varphi_j(\mathbf{w})$$
 (19)

where φ are the eigenfunctions of a covariance kernel $k(\mathbf{w}^i, \mathbf{w}^j)$ with respect to $q_{\theta}(\mathbf{w})$ and γ_{ij} are the coefficients of the spectral series. Both need to be estimated. The Nyström method is used to approximate the eigenfunctions. For this, SSGE considers the following eigenvalue problem $K\mathbf{u} \approx \lambda \mathbf{u}$, where $K \in \mathbb{R}^{S \times S}$ is the Gram matrix: $K_{ij} = k(\mathbf{w}^i, \mathbf{w}^j)$, S is the number of samples used for the gradient estimation. We only consider the radial basis function (RBF) kernel in this work. The J eigenvectors $\mathbf{u}^1 \dots \mathbf{u}^J$ with the J largest eigenvalues $\lambda_1 \geq \dots \geq \lambda_J$ are computed and later will be selected to approximate the spectral series. We discuss below how to set J. The j-th eigenfunction can now be estimated based on the Nyström method with:

$$\varphi_j(\mathbf{w}) = \frac{\sqrt{S}}{\lambda_j} \sum_{s=1}^S u_s^j k(\mathbf{w}, \mathbf{w}^s)$$
 (20)

where u_s^j denotes the s-th element of the j-th eigenvector. Finally, Stein's identity allows finding the following expression for the coefficients γ :

$$\gamma_{ij} = -\frac{1}{\sqrt{S}\lambda_j} \sum_{n=1}^{S} \sum_{s=1}^{S} \nabla_{w_i^n} k(\mathbf{w}^n, \mathbf{w}^s) u_s^j$$
 (21)

The estimated eigenfunctions and the corresponding coefficients can then be inserted back into a finite form of Eq. 19 to estimate $\nabla_{\mathbf{w}} \log q_{\theta}(\mathbf{w})$, and multiplied by the gradient of $f_{\mathbf{WG}}$ with respect to θ that we obtain via automatic differentation. Finally, taking the expectation over the base distribution $p(\mathbf{Z})$ allows obtaining an estimate for the gradient of the entropy term in the ELBO (Eq. 17). Note, if θ is the output of a TC network, then the gradient estimate $\nabla_{\theta} \mathbb{E}_{q_{\theta}(\mathbf{W})} \Big[q_{\theta}(\mathbf{W}) \Big]$ has to be further backpropagated to the parameters of the TC network, where it is accumulated with the gradient of the remaining loss terms, all of which have been automatically computed via automatic differentiation.

The use of SSGE introduces three extra hyperparameters that need to be tuned: the width of the RBF kernel, the number of samples S used for the eigenvalue decomposition, and the number J of eigenfunctions. For the kernel width, we explored setting it to some arbitrary small value or to the median of pairwise distances between all samples, as described in the original paper (Shi et al., 2018). In our results, this choice did not considerably impact performance. For the number of eigenfunctions, we experimented with directly setting J to some fixed value or, as suggested in the original paper, with setting it based on a certain ratio τ of cumulative eigenvalues (i.e., select the minimum number of eigenfunctions J such that $\sum_{j=1}^{J} \frac{\lambda_j}{\lambda_j} > \tau$).

C.4.3. SUPPORT OF IMPLICIT APPROXIMATE POSTERIOR DISTRIBUTIONS

Special attention needs to be payed to the support of the approximate posterior distribution when it is parametrized by an auxiliary network. Indeed, when using a WG architecture for which the output size is larger than the input size, or that contains some bottleneck layer, the support of $q_{\theta}(\mathbf{W})$ will be limited to a set of measure zero (cf. Lemma 1 in Arjovsky & Bottou (2017)). This causes the *prior-matching term* of the ELBO to be ill-defined as the KL definition requires $q_{\theta}(\mathbf{W})$ to be absolutely continuous with respect to $p(\mathbf{W})$. To overcome this limitation, we injected small noise perturbations to the outputs of the WG, e.g.,

$$\mathbf{w} \sim q_{\boldsymbol{\theta}}(\mathbf{W}) \Leftrightarrow \mathbf{w} = f_{\mathrm{WG}}(\mathbf{z}, \boldsymbol{\theta}) + \mathbf{u}$$
 (22)

with $\mathbf{z} \sim p(\mathbf{Z})$ and $\mathbf{u} \sim p(\mathbf{U})$, where $p(\mathbf{U})$ is an additional noise distribution. Note, when using the reparametrization trick to rewrite expected values with respect to $q_{\boldsymbol{\theta}}(\mathbf{W})$, one now has to integrate over the joint of \mathbf{Z} and \mathbf{U} .

Due to practical considerations, we use the following simplification in our implementation:

$$\mathbf{w} \sim q_{\theta}(\mathbf{W}) \Leftrightarrow \mathbf{w} = f_{\text{WG}}(\mathbf{z}_{:n_z}, \boldsymbol{\theta}) + \sigma_{\text{noise}}\mathbf{z}$$
 (23)

where $\mathbf{z}_{:n_z}$ refers to the first n_z elements of the vector \mathbf{z} ,

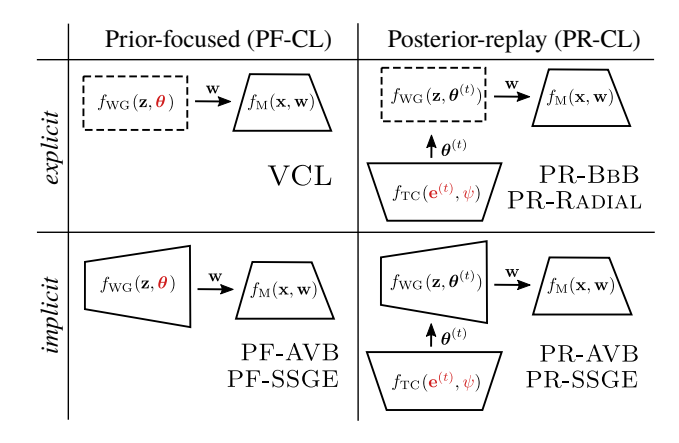


Figure S2. Summary of the different algorithms used to train BNNs, and how they fit into the described framework. We distinguish between approaches that learn a single shared posterior across tasks (PF-CL) and approaches that learn task-specific posteriors (PR-CL). We consider both *explicit* and *implicit* posterior approximations. Red color indicates the parameters that are learned in each scenario.

and both σ_{noise} and n_z are hyperparameters.

C.5. Prior-Focused Continual Learning

Prior-focused CL (Farquhar & Gal, 2018b) is an alternative Bayesian approach to CL that is commonly used in the literature. As opposed to PR-CL, a single set of shared parameters is recursively updated, and finding suitable solutions therefore relies on the existence of trade-off solutions across tasks. We first describe VCL and EWC, two existing algorithms that use a Gaussian approximation for the shared posterior, and then discuss how our framework can be used to render PF-CL more flexible through the use of implicit distributions. Note that PF-CL approaches can be implemented within our framework by directly learning a single set of parameters θ that define the shared posterior distribution, which is recursively instantiated as prior. Since θ is not task-specific, no TC network is required. An overview of how PF-CL and PR-CL approaches fit in our proposed framework is given in Fig. S2.

C.5.1. VARIATIONAL CONTINUAL LEARNING

Variational continual learning (VCL, Nguyen et al. (2018); Swaroop et al. (2018)) was introduced as a way to continually learn a single mean-field Gaussian posterior approximation across tasks by doing a recursive Bayesian update via VI. More specifically, VCL aims to learn a single approximate posterior $q_{\theta^{(1:T)}}(\mathbf{W})$ by recursively considering the posterior of the previous task as the prior for the new task:

$$q_{\boldsymbol{\theta}^{(1:T)}}(\mathbf{W}) \propto p(\mathcal{D}^{(T)} \mid \mathbf{W}) q_{\boldsymbol{\theta}^{(1:T-1)}}(\mathbf{W})$$
 (24)

where $q_{\theta^{(1:T-1)}}(\mathbf{W})$ is an approximation to the previous posterior $p(\mathbf{W} \mid \mathcal{D}^{(1:T-1)})$. Importantly, the CL requirements are not violated since only data from the current task $\mathcal{D}^{(T)}$ is required for the update. To learn the approximate posteriors, VCL uses BbB, and learns a mean-field Gaussian approximation parametrized by a mean and variance per weight, which are optimized by using the *reparametrization trick* (Eq. 3). An interesting contribution of this method is the mathematically sound posterior update based on coresets (i.e., a small set of samples stored from each task, Rebuffi et al. (2017); Bachem et al. (2015)) within their Bayesian framework. Importantly, the role of coresets in their approach is to help mitigate catastrophic forgetting. In contrast, in this work we mainly use coresets to facilitate task inference in a task-agnostic setting (see SM C.7 for details).

In our framework, VCL is realized via a main network and a simple WG function with parameters θ as depicted in Fig. 2 for BbB. Conceptual differences between using BbB in a prior-focused setting (VCL), and using BbB using a posterior-replay approach (PR-BBB) are illustrated in Figure S1. We study this method in a multihead setting, where each head is task-specific and leads to a task-specific approximate posterior that induces epistemic uncertainty. Therefore, the predictive uncertainty of each head has a task-specific influence that we exploit for task inference.

C.5.2. ELASTIC WEIGHT CONSOLIDATION

Kirkpatrick et al. (2017) propose elastic weight consolidation (EWC), a CL algorithm that limits the plasticity of weights that are considered important for solving previous tasks, and therefore mitigates forgetting. In contrast to VCL, the algorithm is based on a Laplace approximation of the posterior (MacKay, 1992). For completeness, we detail here the derivation of this algorithm, specifically of its more mathematically sound variant *Online EWC* (Huszár, 2018; Schwarz et al., 2018), which we simply refer to as *EWC* for brevity. Afterwards, we explain how this algorithm is commonly used in the literature in a task-agnostic setting, and propose an alternative solution based on a combination of shared and task-specific parameters that leads to improved performance.

Online EWC. The core idea of EWC (and of priorfocused methods in general) simply consists in performing a recursive Bayesian update of a single posterior distribution as new tasks arrive:

$$p(\mathbf{W} \mid \mathcal{D}^{(1:T)}) = \frac{p(\mathcal{D}^{(T)} \mid \mathbf{W})p(\mathbf{W} \mid \mathcal{D}^{(1:T-1)})}{p(\mathcal{D}^{(T)} \mid \mathcal{D}^{(1:T-1)})} \quad (25)$$

where we have used the fact that $\mathcal{D}^{(1:T-1)}$ and $\mathcal{D}^{(T)}$ are conditionally independent given **W**. For simplicity, we start

by considering T=2:

following expression:

$$p(\mathbf{W} \mid \mathcal{D}^{(1:2)}) = \frac{p(\mathcal{D}^{(2)} \mid \mathbf{W})p(\mathbf{W} \mid \mathcal{D}^{(1)})}{p(\mathcal{D}^{(2)} \mid \mathcal{D}^{(1)})}$$
(26)

This is almost identical to the original formulation (cf. Eq 2. in Kirkpatrick et al. (2017)), except that the denominator contains $p(\mathcal{D}^{(2)} \mid \mathcal{D}^{(1)})$ and not simply $p(\mathcal{D}^{(2)})$, since the datasets are only conditionally independent, as noted by Huszár (2018). Optimizing the parameters **W** corresponds to finding their most probable value given the data:

$$\arg \min_{\mathbf{W}} \left\{ -\log p(\mathbf{W} \mid \mathcal{D}^{(1:2)}) \right\} \Leftrightarrow \tag{27}$$

$$\arg \min_{\mathbf{W}} \left\{ -\log p(\mathcal{D}^{(2)} \mid \mathbf{W}) - \log p(\mathbf{W} \mid \mathcal{D}^{(1)}) \right\}$$

where we have dropped constant terms. Notice that $-\log p(\mathcal{D}^{(2)}\mid\mathbf{W})$ is simply the negative log-likelihood and can easily be computed. The second term, $\log p(\mathbf{W}\mid\mathcal{D}^{(1)})$ is generally intractable, and for this reason we consider a second order Taylor approximation around the minimum that was found after learning the first task $\mathbf{w}_{\text{MAP}}^{(1)}$, corresponding to the maximum a posteriori (MAP) estimate. First

order terms vanish around the minimum and we obtain the

$$\log p(\mathbf{W} \mid \mathcal{D}^{(1)}) \approx const +$$

$$\frac{1}{2} (\mathbf{W} - \mathbf{w}_{MAP}^{(1)})^T \mathcal{H}_{\log p(\mathbf{w} \mid \mathcal{D}^{(1)})} \Big|_{\mathbf{w} = \mathbf{w}_{MAP}^{(1)}} (\mathbf{W} - \mathbf{w}_{MAP}^{(1)})$$

where $\mathcal{H}_{\log p(\mathbf{W}|\mathcal{D}^{(1)})}$ denotes the Hessian of $\log p(\mathbf{W} \mid \mathcal{D}^{(1)})$, which can be rewritten as:

$$\mathcal{H}_{\log p(\mathbf{W}|\mathcal{D}^{(1)})} = \mathcal{H}_{\log p(\mathcal{D}^{(1)}|\mathbf{W})} + \mathcal{H}_{\log p(\mathbf{W})}$$

$$= \nabla_{\mathbf{w}} \nabla_{\mathbf{w}}^{T} \left[\sum_{n=1}^{N} \log p(\mathbf{y}^{(1,n)} \mid \mathbf{W}, \mathbf{x}^{(1,n)}) - \frac{1}{2\sigma_{prior}^{2}} \|\mathbf{W}\|_{2}^{2} \right]$$

$$= \sum_{n=1}^{N} \mathcal{H}_{\log p(\mathbf{y}^{(1,n)}|\mathbf{W}, \mathbf{x}^{(1,n)})} - \frac{1}{\sigma_{prior}^{2}} I \qquad (29)$$

where $\mathbf{x}^{(1,n)}$ denotes the n-th sample of the first task and where we have used the fact that all N samples are independent given \mathbf{w} . Furthermore, we have assumed a Gaussian prior such that $p(\mathbf{W}) = \mathcal{N}(0, I\sigma_{prior}^2)$, where I is the identity matrix. Recall the relationship between the Hessian and the Fisher information matrix F (e.g., cf. Eq. 3/4 in Martens (2020)):

$$F = -\mathbb{E}_{p(\mathbf{y}|\mathbf{W},\mathbf{x})} \Big[\mathcal{H}_{\log(\mathbf{y}|\mathbf{W},\mathbf{x})} \Big]$$
(30)

Note that so far we have considered x fixed, but the model should perform well with respect to the input distribution

 $p(\mathbf{x})$:

$$\mathbb{E}_{p(\mathbf{x})} \left[-F \right] = \mathbb{E}_{p(\mathbf{x})p(\mathbf{y}|\mathbf{W},\mathbf{x})} \left[\mathcal{H}_{\log p(\mathbf{y}|\mathbf{W},\mathbf{x})} \right]$$

$$\approx \frac{1}{N} \sum_{n=1}^{N} \mathcal{H}_{\log p(\tilde{\mathbf{y}}^{(n)}|\mathbf{W},\mathbf{x}^{(n)})}$$
(31)

where the approximation in the last line comes from a Monte-Carlo estimate using N samples drawn from the joint $p(\mathbf{y} \mid \mathbf{W}, \mathbf{x})p(\mathbf{x})$. Assuming \mathbf{w} has been trained to optimality, i.e., $p(\mathbf{y} \mid \mathbf{W}, \mathbf{x}) \approx p(\mathbf{y} \mid \mathbf{x})$ for $\mathbf{x} \sim p(\mathbf{x})$, the samples used in Eq. 29 and Eq. 31 are essentially from the same joint distribution and we can write:

$$\frac{1}{N} \sum_{n=1}^{N} \mathcal{H}_{\log p(\mathbf{y}^{(n)}|\mathbf{W},\mathbf{x}^{(n)})} \approx \frac{1}{N} \sum_{n=1}^{N} \mathcal{H}_{\log p(\tilde{\mathbf{y}}^{(n)}|\mathbf{W},\mathbf{x}^{(n)})}$$
(32)

to obtain the following expression:

$$\mathcal{H}_{\log p(\mathbf{W}|\mathcal{D}^{(1)})} \approx -NF_{emp} - \frac{1}{\sigma_{prior}^2}I$$
 (33)

where we have introduced the empirical Fisher, which is obtained using the sample points from the actual dataset \mathcal{D} , but given the optimality assumption above here it simply corresponds to $F_{emp} = \mathbb{E}_{p(\mathbf{x})}[F]$. Plugging this result into Eq. 28, while using a diagonal approximation of the empirical Fisher matrix, and extending it to an arbitrary number of tasks by iteratively computing the posterior, we obtain the following expression (cf. Eq. 11 in Huszár (2018)):

$$\log p(\mathbf{W} \mid \mathcal{D}^{(1:T)}) \approx const + \log p(\mathcal{D}^{(T)} \mid \mathbf{W}) - (34)$$

$$\frac{1}{2} \sum_{i} \left(\sum_{t < T} N^{(t)} F_{emp_{i}^{(t)}} + \frac{1}{\sigma_{prior}^{2}} \right) (w_{i} - w_{\text{MAP}, i}^{(T-1)})^{2}$$

where $N^{(t)}$ denotes the size of $\mathcal{D}^{(t)}$. Thus, per weight w_i there is a scalar importance value $\sum_{t < T} N^{(t)} F_{emp_i^{(t)}} + \frac{1}{\sigma_{prior}^2}$ which can be computed online such that there is no need to maintain the empirical Fisher matrices of individual tasks. This is in contrast to the original EWC formulation Kirkpatrick et al. (2017), where each Fisher matrix had to be maintained in memory.

Crucially, in order to relate the sum over Hessians in Eq. 29 to the Fisher information matrix, we have to assume that $p(\mathbf{y} \mid \mathbf{W}, \mathbf{x})$ and $p(\mathbf{y} \mid \mathbf{x})$ are identical for $\mathbf{x} \sim p(\mathbf{x})$. In this case, the empirical Fisher and the (expected) Fisher are also identical and it mathematically does not matter which of the two is used for the algorithm.

⁵Note, that for mathematical convenience we include the expectation over $p(\mathbf{x})$ in the definition of the empirical Fisher.

Multihead EWC. When EWC is used in a task-agnostic inference setting, it is often trained with an output softmax that grows as new tasks are trained (e.g., van de Ven et al. (2020)), which we refer to as EWC-GH. In this setting, where EWC performs poorly, the Bayesian assumption that the model class contains the ground-truth model is violated, since the model-class changes whenever the softmax changes in size. A simple way to overcome this issue when the number of tasks is known in advance, is to use a shared softmax that spans the outputs of all tasks from the beginning of training, which we refer to as EWC-SH. However, as we will show, this approach still performs poorly. We hypothesize this is due to the fact that the role played by output connections for their corresponding task is in conflict with that played for all other tasks (i.e., because the shared softmax pushes the weights of future heads to be highly negative). As a solution, we propose the use of a multihead when applying EWC to a task-agnostic inference setting (simply referred to as EWC). This results in a hybrid PF-CL approach, where the learned parameters w consist of a set of shared weights ϕ and a set of task-specific output heads with weights $\{\xi^{(t)}\}_{t=1}^T$. Now, Eq. 26 becomes:

$$p(\phi, \boldsymbol{\xi}^{(1:2)} \mid \mathcal{D}^{(1:2)})$$

$$= \frac{p(\mathcal{D}^{(2)} \mid \phi, \boldsymbol{\xi}^{(2)}) p(\phi, \boldsymbol{\xi}^{(1)} \mid \mathcal{D}^{(1)}) p(\boldsymbol{\xi}^{(2)})}{p(\mathcal{D}^{(2)} \mid \mathcal{D}^{(1)})}$$
(35)

Repeating the procedure in the original derivation, i.e. considering a Taylor approximation around optimal parameters and recursively computing the posterior, we obtain the following expression:

$$\log p(\phi, \boldsymbol{\xi}^{(1:T)} \mid \mathcal{D}^{(1:T)}) \approx const$$

$$+ \log p(\mathcal{D}^{(T)} \mid \phi, \boldsymbol{\xi}^{(T)}) + \log p(\boldsymbol{\xi}^{(T)})$$

$$- \frac{1}{2} \sum_{i} \left(\sum_{t \in T} N^{(t)} F_{emp_{i}^{(t)}} + \frac{1}{\sigma_{prior}^{2}} \right) (w_{i} - w_{\text{MAP}, i}^{(T-1)})^{2}$$

where we have assumed that all parameters $\mathbf{w} = [\phi, \boldsymbol{\xi}^{(1)}, \dots, \boldsymbol{\xi}^{(T)}]$ share the same prior. Importantly, for any t, $F_{emp^{(t)}}$ is a square diagonal matrix of dimension $\dim(\mathbf{w})$, where all entries related to weights $\boldsymbol{\xi}^{(s)}$ for $s \neq t$ are zero.

Recall, that the EWC importance values are reminiscent of the entries of a precision matrix of a multivariate Gaussian with diagonal covariance matrix. Together with the final MAP estimate $\mathbf{w}_{\text{MAP}}^{(T)}$ of $p(\mathbf{W} \mid \mathcal{D}^{(1:T)})$ we can explicitly construct the following approximate posterior in (Online) multihead EWC:

$$\log p(\boldsymbol{\phi}, \boldsymbol{\xi}^{(1:T)} \mid \mathcal{D}^{(1:T)}) =$$

$$\mathcal{N}\left(\mathbf{w}_{\text{MAP}}^{(T)}, \left[\frac{1}{\sigma_{prior}^{2}} I + \sum_{t=1}^{T} N^{(t)} F_{emp^{(t)}}\right]^{-1}\right)$$
(37)

This posterior induces predictive uncertainty at each output head, which can be used for task inference in task-agnostic inference settings.

C.5.3. PRIOR-FOCUSED CL WITH IMPLICIT DISTRIBUTIONS

Both VCL and EWC use a Gaussian approximation for the shared posterior. This means that, not only a tradeoff solution across tasks needs to be found, but also that the expressivity of this posterior with respect to unknown future tasks is limited. To overcome this limitation, we explore PF-CL with a more flexible variational family, a family of *implicit* distributions parametrized by a neural network. Although this approach does not overcome the need to find trade-off solutions across tasks, it can make better use of the existing overlaps by capturing, for example, multi-modality. Within our framework, PF-CL with an implicit posterior distribution can be realised by directly learning the parameters θ of a WG hypernetwork. This can be achieved using algorithms for learning with implicit distributions, such as AVB or SSGE, and we therefore refer to these methods as PF-AVB and PF-SSGE.

If not noted otherwise, we also consider a hybrid approach with task-specific weights introduced by a multihead main network, such that task-inference through task-specific predictive uncertainty is possible.

C.6. Task inference

When confronted with an unseen input $\tilde{\mathbf{x}}$, algorithms that maintain task-specific solutions, such as our PR-CL framework, first have to explicitly assign the input to a certain task. In this work, we exclusively consider inferring task identity via predictive uncertainty, and explore three different ways of quantifying uncertainty as outlined below.

The quantities ENT and CONF are only considered in classification tasks and are computed directly from the posterior predictive distribution $p(\mathbf{y} \mid \mathcal{D}^{(t)}; \tilde{\mathbf{x}}) = \int_{\mathbf{W}} p(\mathbf{y} \mid \mathbf{W}; \tilde{\mathbf{x}}) p(\mathbf{W} \mid \mathcal{D}^{(t)}) \, d\mathbf{W}$. Due to intractability of this integral, we resort to a Monte-Carlo (MC) estimate using K = 100 models drawn from the approximate posterior parameter distribution $q_{\boldsymbol{\theta}^{(t)}}(\mathbf{W})$ of each task:

$$p(\mathbf{y} \mid \mathcal{D}^{(t)}; \tilde{\mathbf{x}}) \approx \frac{1}{K} \sum_{k=1}^{K} p(\mathbf{y} \mid \mathbf{w}^{(t,k)}; \tilde{\mathbf{x}})$$
 (38)

with $\mathbf{w}^{(t,k)} \sim q_{\boldsymbol{\theta}^{(t)}}(\mathbf{W})$. Note that for deterministic approaches such as PR-DIRAC, only K=1 is applicable. In the ENT criterion, the task leading to the lowest entropy is selected:

$$t_{\text{ENT}} = \underset{t \in 1..T}{\arg \min} \mathcal{H} \left\{ p(\mathbf{y} \mid \mathcal{D}^{(t)}; \tilde{\mathbf{x}}) \right\}$$
(39)

where $\mathcal{H}\{\}$ denotes the entropy functional. In the CONF criterion, the task leading to the highest confidence is selected:

$$t_{\text{CONF}} = \underset{t \in 1...T}{\text{arg max}} \max_{\mathbf{y} \in \mathcal{Y}} p(\mathbf{y} \mid \mathcal{D}^{(t)}; \tilde{\mathbf{x}})$$
(40)

where \mathcal{Y} denotes the set of class labels, which indeed could be task-specific.

These two criteria intuitively correspond to choosing the model with the most peaky predictive distribution, i.e. the highest certainty in the predicted class. However, uncertainty in the predictive distribution can also arise indistribution due to noisy data, i.e., aleatoric uncertainty. In order to quantify epistemic uncertainty only, we additionally study model agreement as uncertainty measure. Note that, in regions where sufficient data has been observed, models drawn from the posterior parameter distribution should converge towards the data-generating distribution $p(\mathbf{Y} \mid \mathbf{X})$ and should therefore agree among each other. Conversely, regions where those models disagree have not observed enough data and can be considered OOD. This intuition should be captured in AGREE, where the task leading to the strongest agreement between models is selected. For C-way classification, we compute this quantity as the average standard deviation of predicted likelihood values for K models $\mathbf{w}^{(t,k)} \sim q_{\boldsymbol{\theta}^{(t)}}(\mathbf{W})$:

$$t_{\text{AGREE}} = \underset{t \in 1..T}{\text{arg min}} \frac{1}{C} \sum_{c=1}^{C} \text{SD} \left\{ p(Y = c \mid \mathbf{w}^{(t,k)}; \tilde{\mathbf{x}}) \quad \forall k \right\}$$

$$\tag{41}$$

where $SD(\cdot)$ refers to the standard deviation of the given set of values.

Note, that choosing to use predictive uncertainty for taskinference is a heuristic choice and, to the best of our knowledge, there is no guarantee that predictive uncertainty can lead to principled OOD detection in general. However, except when exploring hybrid approaches, practitioners have to trade-off pros and cons when selecting a CL method that can be deployed in a task-agnostic setting. As discussed in the main text, if task-identity can be inferred from inputs alone, in theory it seems reasonable to perform task inference directly on approximations of the unknown input distributions $p^{(t)}(\mathbf{x})$, e.g., via tractable density access Lee et al. (2020). While in practice this approach still seems to be out of reach for high-dimensional problems (Nalisnick et al., 2019), generative models for data replay have been successfully applied to CL (Shin et al., 2017; van de Ven & Tolias, 2018; von Oswald et al., 2020). In this case, when a new task is trained, generated data from past tasks is replayed to train in a pseudo-i.i.d. setting. Because of the pseudo-parallel training on all tasks, task inference does not have to be handled explicitly anymore. Note, however, that a conceptual disadvantage exists when using replay approaches, i.e., the problem of training with non-i.i.d. data is

actually not addressed and rather side-stepped completely for the target network by shifting CL to the generative model. Finally, we want to stress again that the task-identity can also be externally provided to the TC, e.g., by an auxiliary system that processes context data (different than the main network's input) (He et al., 2019; von Oswald et al., 2020).

C.7. Posterior-Replay CL with Coreset Fine-Tuning

As opposed to the deterministic setting, already acquired knowledge can be updated in a principled way when using a Bayesian perspective. When continually learning a sequence of tasks, this allows approximate posteriors to be revisited as new data comes in. This can be used in our PR-CL framework to mitigate forgetting by storing task-specific coresets and using them to refresh all task-specific posteriors in a small fine-tuning stage at the end of training.

Specifically, we consider a dataset split per task $\mathcal{D}^{(t)} \setminus \mathcal{C}^{(t)} \cup \mathcal{C}^{(t)}$, where $\mathcal{D}^{(t)} \setminus \mathcal{C}^{(t)}$ is used for the initial CL training phase, and $\mathcal{C}^{(t)}$ is maintained in memory for the fine-tuning stage. More explicitly, when continually learning our metamodel we approximate the following posteriors:

$$q_{\tilde{\boldsymbol{\theta}}^{(t)}}(\mathbf{W}) \approx p(\mathbf{W} \mid \mathcal{D}^{(t)} \setminus \mathcal{C}^{(t)})$$
 (42)

after which $\mathcal{D}^{(t)} \setminus \mathcal{C}^{(t)}$ can be discarded, and only a small-sized coreset $\mathcal{C}^{(t)}$ needs to be maintained in memory until all tasks are learned.

The fine-tuning stage at the end of training is then performed in a multitask fashion on the stored coresets, which are all simultaneously available. To see how this final update can be performed we write our posterior distribution as follows:

$$p(\mathbf{W} \mid \mathcal{D}^{(t)}) = \frac{p(\mathbf{W})p(\mathcal{D}^{(t)} \mid \mathbf{W})}{p(\mathcal{D}^{(t)})}$$

$$= \frac{p(\mathbf{W})p(\mathcal{D}^{(t)} \setminus \mathcal{C}^{(t)} \mid \mathbf{W})p(\mathcal{C}^{(t)} \mid \mathbf{W})}{p(\mathcal{D}^{(t)} \setminus \mathcal{C}^{(t)}, \mathcal{C}^{(t)})}$$

$$\propto \frac{p(\mathbf{W})p(\mathcal{D}^{(t)} \setminus \mathcal{C}^{(t)} \mid \mathbf{W})p(\mathcal{C}^{(t)} \mid \mathbf{W})}{p(\mathcal{D}^{(t)} \setminus \mathcal{C}^{(t)})}$$

$$= p(\mathbf{W} \mid \mathcal{D}^{(t)} \setminus \mathcal{C}^{(t)})p(\mathcal{C}^{(t)} \mid \mathbf{W})$$
(43)

where we have used the fact that $\mathcal{D}^{(t)}\setminus\mathcal{C}^{(t)}$ and $\mathcal{C}^{(t)}$ are conditionally independent given \mathbf{W} . Eq. 43 shows that the desired posteriors $p(\mathbf{W}\mid\mathcal{D}^{(t)})$ can be obtained via a Bayesian update of the continually learned posteriors $p(\mathbf{W}\mid\mathcal{D}^{(t)}\setminus\mathcal{C}^{(t)})$ by using the task-specific coreset $\mathcal{C}^{(t)}$. Recall that in VI, we approximate this posterior with a distribution $q_{\boldsymbol{\theta}^{(t)}}(\mathbf{W})$ by minimizing $\mathrm{KL}(q_{\boldsymbol{\theta}^{(t)}}(\mathbf{W})\mid\mid p(\mathbf{W}\mid\mathcal{D}^{(t)}))$. Based on our dataset split, the expression to be minimized can be rewritten as $\mathrm{KL}(q_{\boldsymbol{\theta}^{(t)}}(\mathbf{W})\mid\mid \zeta p(\mathbf{W}\mid\mathcal{D}^{(t)}\setminus\mathcal{C}^{(t)})p(\mathcal{C}^{(t)}\mid\mathbf{W}))$, where ζ is a normalization constant that accounts for the fact that we dropped $\mathcal{C}^{(t)}$ from the denominator. Replacing $p(\mathbf{W}\mid\mathcal{D}^{(t)}\setminus\mathcal{C}^{(t)})$ by the approximations $q_{\tilde{\boldsymbol{\theta}}^{(t)}}(\mathbf{W})$ learned continually, we obtain the

following VI objective:

$$\underset{\boldsymbol{\theta}^{(t)}}{\operatorname{arg \, min}} \operatorname{KL}\left(q_{\boldsymbol{\theta}^{(t)}}(\mathbf{W}) \mid\mid \zeta q_{\tilde{\boldsymbol{\theta}}^{(t)}}(\mathbf{W}) p(\mathcal{C}^{(t)} \mid \mathbf{W})\right) \quad (44)$$

$$= \underset{\boldsymbol{\theta}^{(t)}}{\operatorname{arg \, min}} \left[\operatorname{KL}\left(q_{\boldsymbol{\theta}^{(t)}}(\mathbf{W}) \mid\mid q_{\tilde{\boldsymbol{\theta}}^{(t)}}(\mathbf{W})\right) - \mathbb{E}_{q_{\boldsymbol{\theta}^{(t)}}}\left[\log p(\mathcal{C}^{(t)} \mid \mathbf{W})\right] \right]$$

Note that the second term corresponds to integrating the evidence from the coreset into the new posterior, and therefore simply corresponds to minimizing the negative log-likelihood on the coreset $\mathcal{C}^{(t)}$, while the first term ensures that the posterior does not change much, preventing forgetting. Notably, the KL term is now between two distributions from the same variational family, reminiscent of prior-focused learning as discussed in SM C.5. Therefore, it can be analytically evaluated for PR-BBB while other methods require estimation, e.g., using AVB or SSGE.

Crucially, having coresets available at the end of training can also be used to facilitate task inference based on predictive uncertainty (refer to SM C.6 for details). To do this, we perform the final update on a set of modified coresets, which encourage the prediction of a task-specific model on OOD data (i.e., on a coreset from another task) to be highly uncertain. More specifically, we use the modified coresets:

$$\tilde{\mathcal{C}}^{(t)} = \mathcal{C}^{(t)} \cup \bigcup_{s \in \{1, \dots, T\} \setminus \{t\}} \hat{\mathcal{C}}^{(s)}$$

$$\tag{45}$$

where $\hat{\mathcal{C}}^{(s)}$ is constructed from the same inputs contained in $\mathcal{C}^{(s)}$ but the labels are replaced by high uncertainty labels. We enforce high uncertainty in OOD inputs by either setting high-entropy softmax labels (i.e., uniform distribution; eg., cf. Lee et al. (2018)), or by using different random labels per mini-batch.

Intriguingly, when training with data from other tasks, this data becomes in-distribution and cannot be considered OOD anymore. Therefore, we expect our task-inference criterion AGREE, which is designed to capture only epistemic uncertainty, to become less reliable. In other terms, what was previously OOD data, that could have been detected via epistemic uncertainty, now became in-distribution data with high aleatoric uncertainty due to the way we design training targets. This intuition is reflected in our empirical observations (cf. SM D).

D. Supplementary Experiments and Results

In this section, we extend the results presented in the main text, and provide a more detailed discussion. Furthermore, we report additional baselines and supplementary experiments such as PermutedMNIST (cf. SM D.4).

In addition to the methods and baselines that have already been introduced, we consider the following variations. To investigate the role played by the shared meta-model, we consider independently trained models per task (*separate posteriors:* **SP**); a baseline that by design is not affected by catastrophic interference, and therefore leads to identical TG-DURING and TG-FINAL scores. In this setting, task-specific solutions cannot benefit from knowledge transfer, but they are also less limited because the capacity of the meta-model is not shared with previous tasks.

We distinguish two cases for this baseline. In the first case, there is no TC network and θ is trained directly (denoted SP-<METHOD>, e.g., **SP-BbB**). However, one has to keep in mind that the underlying architecture in combination with the chosen weight prior defines a prior in function space that will affect predictive uncertainty (cf. Sec. 3 and Wilson & Izmailov (2020)), and it is therefore unclear how comparable task-inference scores based on predictive uncertainty are in this case, e.g., between SP-BBB and PR-BBB. For this reason, we include a second SP baseline where the TC network remains but has no dedicated functional purpose (denoted SP-TC-<METHOD>, e.g., SP-TC-BbB). Note that for this baseline, one TC network with a single task embedding is learned per task.

As a potential upper-bound we also consider **Fine-Tuning**, which simply refers to the continuous deterministic training of a main network without undertaking any measures against catastrophic forgetting. Thus, the achieved TG-DURING score can benefit from transfer while not being restricted to finding any trade-off that accommodates past tasks. In this case, the hyperparameter configuration is selected based on the best TG-DURING score. We only searched hyperparameters for this baseline in the PermutedMNIST and SplitCIFAR experiments, because the TG-DURING scores of other experiments are often maxed out.

All results involving Bayesian methods use a standard Gaussian prior $p(\mathbf{W}) = \mathcal{N}(\mathbf{0}, I)$. For high-dimensional problems and for methods trained with variational inference, we explore tempering the posterior to increase training stability (cf. SM E.3). Specifically, we downscale the prior-matching term, which effectively increases the emphasis on matching the data well (cf. SM E in Wenzel et al. (2020)). Note, no such posterior tempering is used when studying the lowdimensional problems in SM D.1 and SM D.2. Importantly, whenever applicable and unless noted otherwise, all hyperparameter configurations have been selected based on the TI-ENT criterion. Hence, reported task-given (TG) scores do not necessarily reflect the ability of a method to combat forgetting. However, in most cases, forgetting does not seem to be a major challenge in the experiments we consider, and the reported TG-DURING and TG-FINAL scores are often very close. Please refer to SM E for details on the experimental setup and hyperparameter searches.

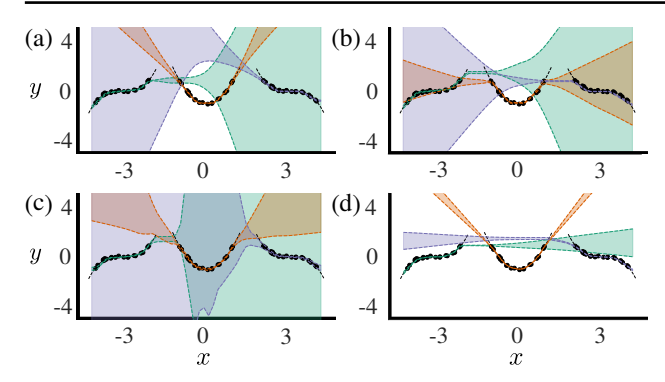


Figure S3. 1D polynomial regression task, where three polynomials need to be learned consecutively. Different colors represent the task-specific posterior approximations within the final model when training with different PR-CL algorithms: (a) PR-BBB, (b)PR-RADIAL, (c) PR-AVB, (d) PR-SSGE. The illustrations sketch the idea behind task inference via predictive uncertainty, i.e., for an input point x the posterior with the lowest predictive uncertainty can be chosen to make predictions. Note, if the input does not lie in the in-distribution space of any task, predictive uncertainty will be high for all posteriors.

D.1. 1D Polynomial Regression

In this section we expand on the discussion from Sec. 4.1 on continually learning a set of low-dimensional regression tasks. Details about the dataset can be found in SM E.1. Quantitative results for a ReLU MLP-10,10 main network can be found in Table S2.

PR-CL methods are all able to fit the polynomials well and do not seem to be affected by catastrophic interference. Notably, due to the choice of Gaussian likelihood with fixed variance (cf. Eq. 7), the likelihood function is not able to represent x-dependent (aleatoric) uncertainty. Therefore, all x-dependent uncertainty corresponds to model uncertainty, which is not captured by PR-DIRAC. Interestingly, the reported PR-AVB run is always able to pick the right task embedding in a random-seed robust way, such that final TG and TI scores are identical. All reported PF-CL methods use a single head main network and therefore do not require task inference. Instead, they have to learn a single posterior continually that captures well all data across tasks. Here, we observe that these methods greatly suffer from the stability-plasticity dilemma (Parisi et al., 2019): having enough plasticity to accommodate new tasks causes catastrophic interference with existing knowledge, while excessive protection of the existing shared posterior does not give the flexibility required to fit new data.

Supplementary qualitative plots showing the final approximate posteriors found by the PR-CL methods are depicted in Fig. S3. While these plots convey the intuition behind uncertainty-based task inference, it should be noted that the ground-truth posterior shape is unknown, and that hyperpa-

rameters have a strong influence on these plots.

Finally, to highlight a potential advantage of *implicit* methods, we qualitatively investigate the found posterior approximations by PR-AVB in Fig. S4. We provide joint density plots (using kernel density estimation) for random pairs of weights as well as Pearson correlation matrices for a random subset of weights. Note that these plots are not cherry-picked and are representative of the found posterior approximations. Weights in the posteriors of all tasks seem to be highly correlated, which is also to be expected for the unknown ground-truth posterior, since individual weight changes will affect the behavior of the neural network function and should therefore be coordinated to maintain stable in-distribution predictions. This is in contrast to mean-field approximations such as PR-BBB and PR-RADIAL, which by design are not able to capture weight correlations. In addition, the joint distribution plots for PR-AVB often exhibit multi-modality. Presumably, this could be beneficial for OOD detection and thus task inference, since different modes in the posterior landscape may represent very different functions that exert vastly different behavior on OOD data. However, such argument is purely speculative and should be considered with care given that single high-dimensional posterior modes might be flat in many directions and thus also be able to capture a diverse set of functions (Hochreiter & Schmidhuber, 1997; Oswald et al., 2021).

D.2. 2D Mode Classification

Next, we reconsider the 2D mode classification introduced in Sec. 4.2. All results are obtained with a ReLU MLP-10,10 main network. Details about this synthetic dataset can be found in SM E.2, and quantitative results are reported in Table S3.

As reflected in the TG-FINAL scores, forgetting is not a concern in this benchmark. Instead, the relevance of this experiment is rooted in the ability to gain insights on how task inference based on predictive uncertainty works in classification tasks. Recall, that the softmax likelihood function can represent arbitrary x-dependent discrete distributions, which (in contrast to Sec. 4.1) allows the model to exhibit x-dependent aleatoric uncertainty. Deterministic approaches such as PR-DIRAC only have access to aleatoric uncertainty, and therefore rely solely on it for task inference. However this has certain limitations since aleatoric uncertainty is only calibrated in-distribution. For instance, the typical cross-entropy loss criterion used for classification tasks can be linked to the minimization of the quantity: $\mathbb{E}_{p(\mathbf{X})}[\mathrm{KL}(p(\mathbf{Y} \mid \mathbf{X})||p(\mathbf{Y} \mid \mathbf{W}; \mathbf{X}))]$, where $p(\mathbf{X})p(\mathbf{Y} \mid \mathbf{X})$ denotes the unknown underlying datagenerating process and $p(Y \mid W; X)$ is the model likelihood. Thus, the behaviour of aleatoric uncertainty as re-

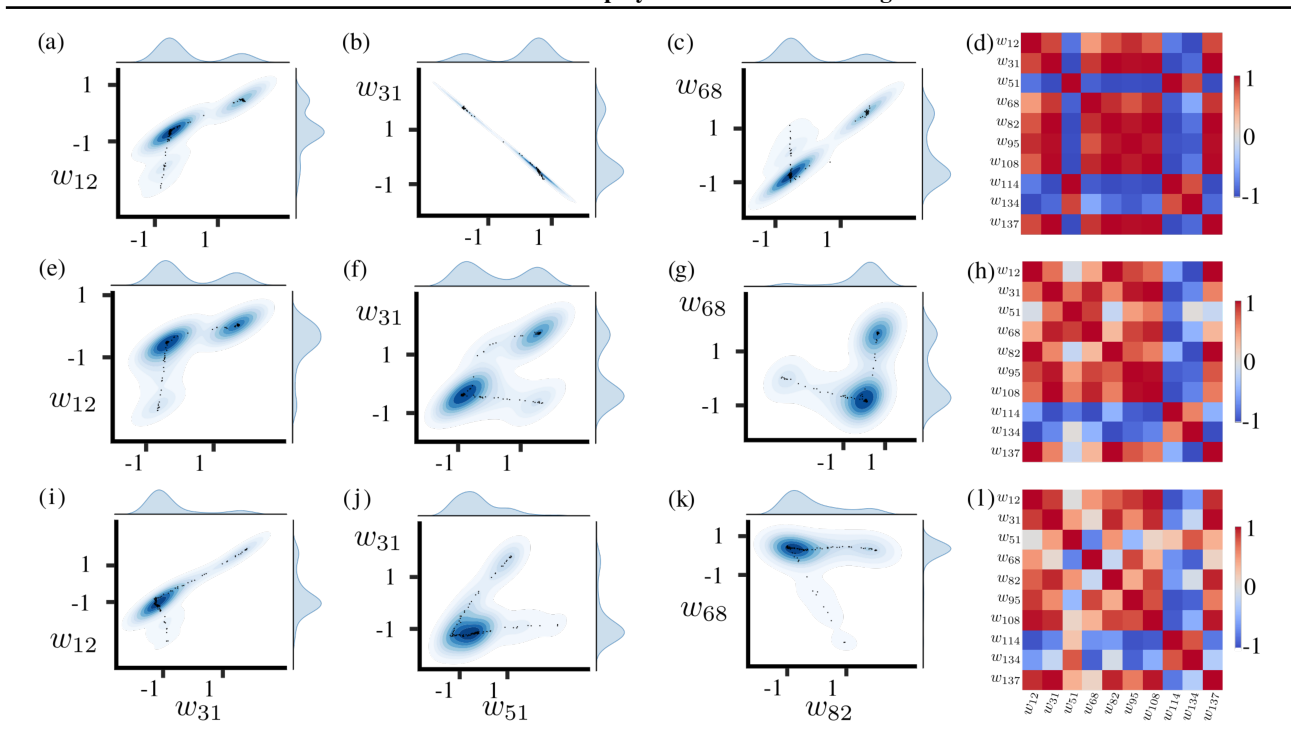


Figure S4. Example illustrations of weight distributions captured by the final approximate posteriors when learning the 1D polynomial regression task with PR-AVB. (a)-(c) Joint density plots of task 1 for three random pairs of weights. (d) Weight correlations in task 1 for a subset of randomly chosen weights. The same is depicted for the approximate posterior of task 2 (e)-(h) and task 3 (i)-(l). Note, that unlike unimodal mean-field approximations (cf. PR-BBB and PR-RADIAL), implicit methods can capture correlations between weights and multi-modality.

flected in $p(\mathbf{Y} \mid \mathbf{W}; \mathbf{X})$ for OOD data (e.g., outside the support of $p(\mathbf{X})$) is not calibrated and can indeed be harmful for OOD detection (e.g., Hein et al. (2019)). This intuition is validated by our PR-DIRAC results, which exhibit rather arbitrary behavior on OOD data (Fig. S6). This might also explain why there is a notable difference in the results reported for PR-DIRAC and SP-DIRAC in Table S3, while probabilistic PR-CL methods behave similarly.

We provide uncertainty maps for all studied probabilistic PR-CL methods in Fig. S5. A desirable behavior for good OOD detection would entail having low uncertainty only where the training data of the corresponding task resides, while having high uncertainty elsewhere. As opposed to the deterministic case, Bayesian approaches reflect this intuition (cf. Fig. S6), despite not being perfect OOD detectors. Note that, since the uncertainty map of the true Bayesian posterior is unknown, it remains unclear whether this imperfection originates from the approximate nature of the used posteriors, or whether it is innate to the real posterior. Importantly, the displayed uncertainty maps represent aggregated results over many models drawn from the approximate posteriors. Therefore, an interesting question arises, i.e., whether the depicted uncertainty maps result from models having high aleatoric uncertainty on OOD data, or from individual models behaving very differently on OOD data. To answer this

question, we plot the softmax entropy maps for individual models drawn from the posterior of PR-AVB in Fig. S7. Uncertainty maps from individual models look very different, suggesting that epistemic uncertainty is crucial for OOD detection in this experiment. This is supported by the fact that the ENT uncertainty map looks very similar to that obtained with AGREE, even though ENT is supposed to capture both aleatoric and epistemic uncertainty. However, one needs to keep in mind that these are qualitative results which strongly depend the selected hyperparameter configuration, as can be seen for the chosen PR-SSGE results.

In this experiment, PF-CL methods perform worse in uncertainty-based task inference than PR-CL methods. A reason could be the impaired ability of PF-CL methods to capture task-specific epistemic uncertainty. This may be due to the fact that data from all tasks is used to train a shared body, and thus the posterior models drawn from it should lead to similar hidden activations (i.e., low epistemic uncertainty) for data from all tasks. Thus, epistemic uncertainty, which we saw above is crucial for task inference, will mainly be introduced by the task-specific outputs heads which process those hidden activations. In contrast, the posterior of all weights in PR-CL methods has only ever seen data from one task and can therefore exhibit high epistemic uncertainty when computing hidden activations for

Table S2. Mean-squared-error (MSE) values for the 1D polynomial regression experiments. TI-MSE refers to the MSE when making predictions using the task embedding leading to lowest uncertainty for the given input. The column ACC-INFERENCE reports the accuracy for how often the correct task-embedding was chosen for (in-distribution) test inputs. Note, that single-head PF-CL methods do not require task-inference, and thus the distinction between TG and TI does not apply (Mean \pm SEM, ACC-INFERENCE in %, n=10).

	TG-MSE-DURING	TG-MSE-FINAL	TI-MSE	ACC-INFERENCE
PR-DIRAC PR-BBB PR-RADIAL PR-AVB PR-SSGE	$\begin{array}{c} 0.01007 \pm 0.00170 \\ 0.01036 \pm 0.00112 \\ 0.01238 \pm 0.00184 \\ 0.00504 \pm 0.00061 \\ 0.00236 \pm 0.00016 \end{array}$	$\begin{array}{c} 0.01037 \pm 0.00162 \\ 0.01037 \pm 0.00121 \\ 0.01108 \pm 0.00090 \\ 0.00712 \pm 0.00181 \\ 0.00251 \pm 0.00020 \end{array}$	$\begin{array}{c} \text{N/A} \\ 0.01175 \pm 0.00103 \\ 0.03996 \pm 0.02377 \\ 0.00712 \pm 0.00181 \\ 0.00476 \pm 0.00208 \end{array}$	$\begin{array}{c} \text{N/A} \\ 98.07 \pm 0.53 \\ 96.19 \pm 1.77 \\ 100.00 \pm 0.00 \\ 99.80 \pm 0.13 \end{array}$
EWC VCL PF-AVB PF-SSGE	$\begin{array}{c} 0.08004 \pm 0.02444 \\ 0.09787 \pm 0.00982 \\ 0.24125 \pm 0.00315 \\ 0.01546 \pm 0.00082 \end{array}$	2.55570 ± 1.07003 0.23889 ± 0.06711 0.46187 ± 0.07851 2.09433 ± 0.78611	N/A N/A N/A N/A	N/A N/A N/A N/A

Table S3. Accuracies for the 2D mode classification experiments (Mean \pm SEM in %, n=10).

	TG-during	TG-FINAL	TI-ENT	TI-CONF	TI-AGREE
PR-DIRAC PR-BBB PR-RADIAL PR-AVB PR-SSGE	$\begin{array}{c} 100.0 \pm 0.00 \\ 100.0 \pm 0.00 \\ 95.08 \pm 2.38 \\ 100.0 \pm 0.00 \\ 100.0 \pm 0.00 \end{array}$	$\begin{array}{c} 99.78 \pm 0.21 \\ 100.0 \pm 0.00 \\ 95.08 \pm 2.38 \\ 100.0 \pm 0.00 \\ 100.0 \pm 0.00 \end{array}$	$44.90 \pm 5.74 81.07 \pm 6.78 54.50 \pm 5.01 98.57 \pm 1.33 100.0 \pm 0.00$	$45.43 \pm 5.84 \\ 81.07 \pm 6.78 \\ 54.50 \pm 5.01 \\ 98.57 \pm 1.33 \\ 100.0 \pm 0.00$	$\begin{array}{c} \text{N/A} \\ 90.02 \pm 3.57 \\ 76.33 \pm 4.18 \\ 99.93 \pm 0.06 \\ 100.0 \pm 0.00 \end{array}$
SP-DIRAC SP-BBB SP-AVB	N/A N/A N/A	$100.0 \pm 0.00 \\ 100.0 \pm 0.00 \\ 100.0 \pm 0.00$	70.92 ± 4.96 85.13 ± 2.58 95.00 ± 2.09	74.17 ± 3.78 85.13 ± 2.58 95.00 ± 2.09	N/A 87.92 ± 2.29 98.62 ± 1.23
VCL PF-AVB PF-SSGE	$100.0 \pm 0.00 \\ 100.0 \pm 0.00 \\ 100.0 \pm 0.00$	$100.0 \pm 0.00 98.17 \pm 1.57 95.92 \pm 1.71$	45.17 ± 3.80 64.53 ± 4.99 50.00 ± 3.33	45.17 ± 3.80 64.53 ± 4.99 49.40 ± 3.06	47.13 ± 4.26 65.40 ± 5.05 50.02 ± 3.33

data from different tasks.

We also experiment with multi-head EWC (EWC), for which we obtain chance level predictions. To understand this effect, let's recall that EWC relies on the post-hoc construction of the posterior, for which the computation of the empirical Fisher information matrix is required in order to approximate the loss curvature. In our results, we observe that some of the computed Fisher values are zero. Looking at Eq. 37 one can see that whenever Fisher values are very low for a certain weight, the variance of the posterior for that weight will be dominated by the variance of the prior, which was set to one in our experiments. We hypothesize that such high variance for certain weights in the constructed posterior is the reason for the low performance displayed by EWC in such a small network. Note, that the empirical Fisher values are computed as a sum of squared log-likelihood gradients computed across the whole training set. These gradients are zero for some weights, which might be due to overfitting; a conceivable problem given the low dataset size. We observed the same issue when testing multi-head EWC for the 1D regression experiment. Intriguingly, this observation

also implies that the empirical Fisher approximation failed to appropriately approximate the Hessian and thus capture loss curvature.

D.3. SplitMNIST

Here we provide additional results obtained for the SplitM-NIST experiment. In particular, we compare the different methods for three different main network architectures: Table S4 contains results obtained with a ReLU MLP with two hidden layers of 100 neurons (MLP-100,100), Table S5 for an MLP-400,400 and Table S6 for a Lenet (LeCun et al., 1998) with a kernel size of 5, 20 resp. 50 feature maps in the two convolutional layers and 500 units in the penultimate fully-connected layer.

Some general trends can be observed independent of the main network architecture used. Catastrophic forgetting is not a major issue in this experiment, as illustrated by similar TG-DURING and TG-FINAL scores across methods. Only prior-focused approaches seem slightly affected by forgetting and sometimes exhibit a slight drop in TG-

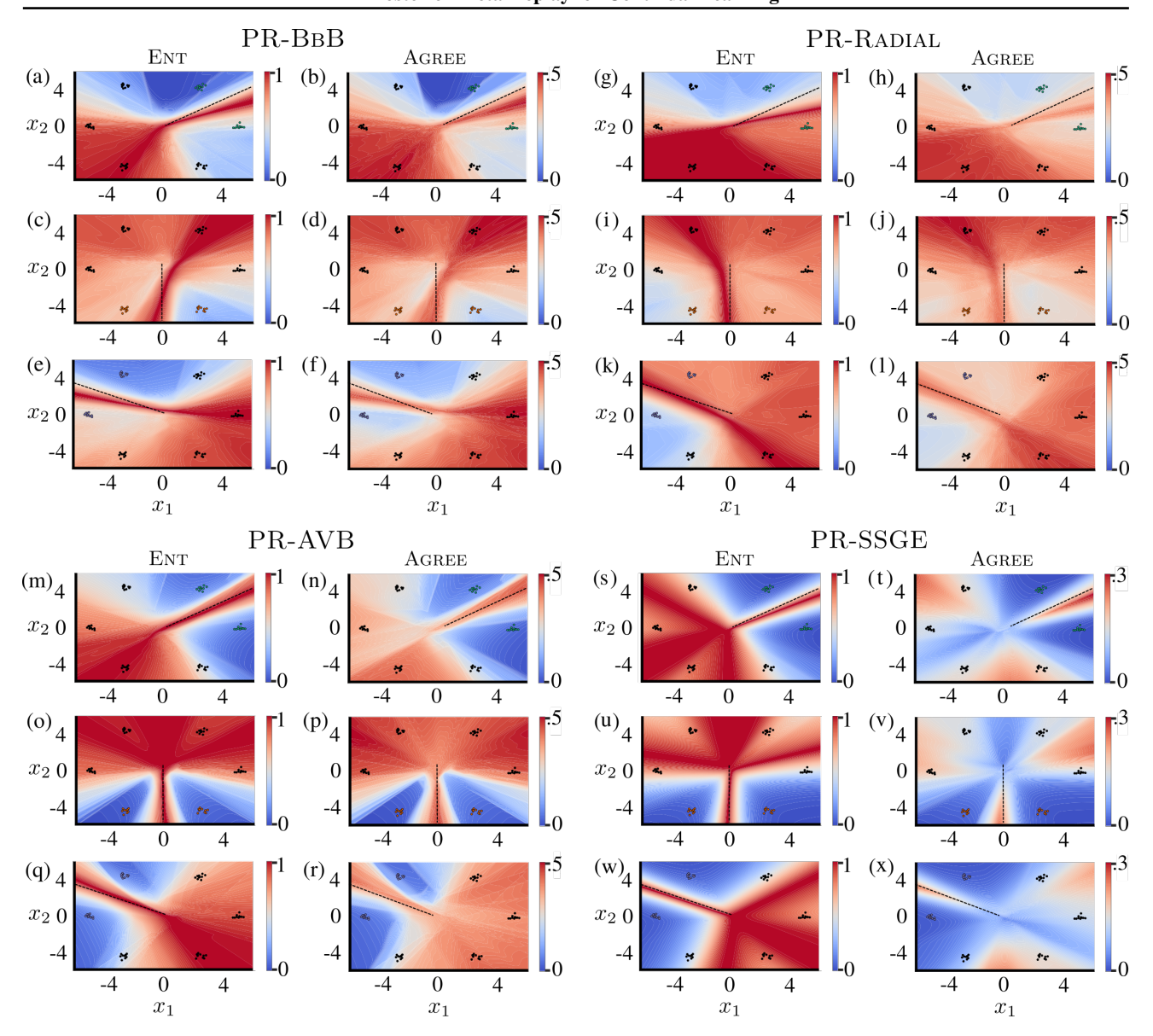


Figure S5. 2D mode classification uncertainty maps for probabilistic PR-CL approaches. (a) Entropy of the predictive distribution (ENT) of task 1 across the input space covering in-distribution domains of all tasks, when training with PR-BBB. Dots represent training points and colors indicate task-affiliation. The dashed line represents the decision boundary for task 1. (b) Same as (a) but uncertainty here reflects model agreement (AGREE). The same uncertainty maps are produced using the final approximate posteriors for task 2 (c)-(d) and 3 (e)-(f). To show qualitative results for several probabilistic PR-CL approaches, the uncertainty maps (a)-(f) are repeated for PR-RADIAL (g)-(l), PR-AVB (m)-(r) and PR-SSGE (s)-(x).

FINAL accuracies, which however stay above 96% for all methods and architectures. Much wider variations can be observed in the task-agnostic setting where task identity needs to be inferred. Despite the fact that we could improve upon previously reported results for the PR-DIRAC baseline in MLP-400,400 (termed HNET+ENT in von Oswald et al. (2020)), this deterministic solution generally performs worse at inferring task identity than probabilistic approaches, notably PR-BBB. Interestingly, PR-BBB con-

sistently outperforms PR-RADIAL in this experiment by a large extent, which is in disagreement with the performance gains reported by Farquhar et al. (2020) on other datasets. A potential cause for the differences in performance can be that, as opposed to Farquhar et al. (2020), we tempered the posteriors (Wenzel et al., 2020). This was done because successful training for both PR-RADIAL and PR-BBB could only be accomplished when notably reducing the prior influence in the loss computation. When using *implicit* posterior

Table S4. Accuracies of SplitMNIST experiments when using an MLP-100,100 (Mean \pm SEM in $\%$, $n=10$). Column TI represents
TI-ENT accuracies if applicable. Otherwise this column is used to report results of methods that learn a shared softmax across all tasks.

	TG-during	TG-FINAL	TI	TI-CONF	TI-AGREE
PR-DIRAC PR-BBB PR-RADIAL PR-SSGE EWC-GH EWC-SH EWC VCL	99.72 ± 0.01 99.75 ± 0.01 99.55 ± 0.06 99.66 ± 0.02 N/A N/A 99.01 ± 0.03 97.83 ± 0.03	99.72 ± 0.01 99.75 ± 0.01 99.43 ± 0.10 99.65 ± 0.02 N/A N/A 97.79 ± 0.30 96.05 ± 0.21	63.41 ± 1.54 70.07 ± 0.56 63.00 ± 1.56 66.15 ± 0.92 28.15 ± 0.51 29.67 ± 0.86 46.61 ± 1.26 51.45 ± 1.11	48.41 ± 1.02 65.34 ± 0.66 64.03 ± 1.19 47.89 ± 0.67 N/A N/A 46.63 ± 1.27 51.45 ± 1.11	N/A 70.11 ± 0.54 63.06 ± 1.55 66.20 ± 0.92 N/A N/A 19.97 ± 0.01 51.50 ± 1.22
PF-SSGE PR-BBB-BW PR-BBB-CS	99.74 ± 0.01 99.75 ± 0.01 99.41 ± 0.04	96.48 ± 0.54 99.75 ± 0.01 98.70 ± 0.05	51.26 ± 1.72 99.75 ± 0.01 90.42 ± 0.19	49.64 ± 1.72 99.75 ± 0.01 90.42 ± 0.19	51.59 ± 1.64 99.75 ± 0.01 59.09 ± 0.64

distributions via PR-SSGE, performance gains can be observed over PR-BBB for MLP-400,400 and LENET main networks. Using SSGE to learn a single *implicit* posterior distribution (PF-SSGE) leads however to a significant drop in performance across architectures, which highlights the potential of a system that learns task-specific posteriors. Yet, compared to prior-focused approaches that do not use *implicit* distributions, PF-SSGE generally performs better, illustrating that more flexible posterior approximations can lead to improved performance when trade-off solutions need to be found.

When applied with a growing (EWC-GH) or shared softmax (EWC-SH), EWC leads to very poor results in all architectures, even though we manage to considerably improve upon the existing EWC-GH* baseline. The use of a multihead significantly improves performance, but even in this case the performance of EWC remains well below other PF-CL methods such as VCL. A potential cause is the post-hoc construction of the posterior in EWC, as noted in SM D.2.

Note that, if task-inference performance is above chancelevel for individual inputs, it can be improved as a simple statistical effect by looking at multiple samples belonging to the same task. Indeed, in all three architectures, we observe that performance in a task-agnostic setting can be dramatically improved when task inference is performed on a set of 100 samples rather than individual ones. Task-inference becomes perfect in all three architectures, leading to identical final TG and TI accuracies. Even though we only report results for BbB (PR-BbB-BW), all methods equally benefit from such aggregated task inference. An additional way to considerably improve task-inference performance is the use of coresets in a fine-tuning stage at the end of training (CS). This approach leads to results that are comparable to prior work based on generative replay (e.g., DGR*, HNET+TIR**).

Although this approach leads to lower performance than the use of batches for inferring the task, the use of coresets does not rely on the assumption that a set of samples belongs to the same task, and when such an assumption is plausible both tricks can be simultaneously used to further boost performance.

The relative behavior of the three criteria for quantifying uncertainty is also stable across architectures. ENT and AGREE generally lead to very similar results, while CONF often performs worse, except for EWC and VCL, where all three approaches behave similarly. Interestingly, when using coresets to facilitate task inference, OOD data becomes indistribution, and hinders the ability of the AGREE criterion to infer task identity, as shown by our TI-AGREE results for PR-BBB-CS.

Training separate posteriors per task (SP) controls for the influence of the shared system on performance and uncertainty-based task-inference. Our results for MLP-400,400 indicate that the CL performance of PR-DIRAC and PR-SSGE is very close to what is achieved when a different model can be allocated per task. To our surprise, however, BbB exhibits lower performance when used to learn independent posteriors (SP-BBB), than when used in a CL setting (PR-BBB). Since PR-SSGE does not exhibit the same trend, the cause is likely not rooted in Bayesian inference for this model class, but rather in the particular approximation used. Interestingly, the SP performance achieved in the deterministic case and with BbB (SP-DIRAC, SP-BBB) improves marginally when the parameters of the approximate posteriors are not learned directly, but generated by a hypernetwork (SP-TC-DIRAC, SP-TC-BBB). The results are somewhat different for a LENET, where learning separate posteriors leads to a much larger performance improvement in SP-DIRAC and SP-BBB compared to the PR-CL setting. In this case, however, the use of a hypernetwork to generate main network weights does not

Table S5. Accuracies of SplitMNIST experiments when using an MLP-400,400 (Mean \pm SEM in %, n=10). Column TI represents TI-ENT accuracies if applicable. Otherwise this column is used to report results of methods that learn a shared softmax across all tasks. Results denoted with a * are taken from van de Ven & Tolias (2019) and those denoted with a ** are taken from von Oswald et al. (2020). SI stands for *synaptic intelligence* (Zenke et al., 2017), and DGR for *deep generative replay* Shin et al. (2017). HNET+TIR and HNET+R are CL methods based on hypernetwork-protected replay proposed in von Oswald et al. (2020).

	TG-during	TG-FINAL	TI	TI-CONF	TI-AGREE
PR-DIRAC PR-BBB PR-RADIAL PR-SSGE EWC-GH EWC-SH EWC VCL PF-SSGE	$\begin{array}{c} 99.65 \pm 0.02 \\ 99.73 \pm 0.01 \\ 99.64 \pm 0.01 \\ 99.78 \pm 0.01 \\ \text{N/A} \\ \text{N/A} \\ 99.70 \pm 0.01 \\ 96.66 \pm 0.19 \\ 99.79 \pm 0.01 \end{array}$	$\begin{array}{c} 99.65 \pm 0.01 \\ 99.72 \pm 0.02 \\ 99.64 \pm 0.01 \\ 99.77 \pm 0.01 \\ \text{N/A} \\ \text{N/A} \\ 96.40 \pm 0.62 \\ 96.45 \pm 0.13 \\ 99.02 \pm 0.16 \\ \end{array}$	70.88 ± 0.61 71.73 ± 0.87 66.01 ± 0.92 71.91 ± 0.79 27.32 ± 0.60 30.21 ± 0.52 47.67 ± 1.52 58.84 ± 0.64 62.70 ± 1.32	56.56 ± 0.64 67.42 ± 0.68 61.56 ± 0.38 55.15 ± 0.67 N/A N/A 47.67 ± 1.52 58.84 ± 0.64 61.62 ± 1.31	N/A 71.73 ± 0.85 66.22 ± 0.93 71.43 ± 0.77 N/A N/A 47.52 ± 1.48 56.54 ± 0.94 62.76 ± 1.31
PR-BBB-BW PR-BBB-CS	$99.73 \pm 0.01 99.34 \pm 0.05$	$99.72 \pm 0.02 98.50 \pm 0.09$	$99.72 \pm 0.02 90.83 \pm 0.24$	$99.72 \pm 0.02 90.83 \pm 0.24$	$99.72 \pm 0.02 59.74 \pm 0.59$
SP-DIRAC SP-BBB SP-SSGE	N/A N/A N/A	99.77 ± 0.01 99.81 ± 0.00 99.76 ± 0.04	70.39 ± 0.27 68.40 ± 0.23 71.53 ± 1.34	63.69 ± 0.10 63.37 ± 0.85 68.50 ± 0.99	N/A 68.37 ± 0.24 71.36 ± 1.31
SP-TC-DIRAC SP-TC-BBB	N/A N/A	$\begin{array}{c} 99.79 \pm 0.02 \\ 99.77 \pm 0.01 \end{array}$	$71.84 \pm 0.49 \\ 72.74 \pm 0.45$	$50.69 \pm 1.23 \\ 72.87 \pm 0.57$	N/A 72.79 ± 0.45
EWC-GH* SI-GH* DGR* PR-DIRAC** HNET+TIR** HNET+R**	N/A N/A N/A N/A N/A N/A	N/A N/A N/A N/A N/A N/A	19.96 ± 0.07 19.99 ± 0.06 91.79 ± 0.32 69.48 ± 0.80 89.59 ± 0.59 95.30 ± 0.13	N/A N/A N/A N/A N/A N/A	N/A N/A N/A N/A N/A N/A

lead to increased SP performance, highlighting the complicated influence of the architectural setup on uncertainty, and therefore task inference.

When comparing the behavior of individual methods for different architectures, we generally observe improved uncertainty-based task inference with increasing main network complexity (i.e., the results obtained for MLP-100,100 are generally worse than for MLP-400,400, which in turn are worse than for LENET). This is especially noticeable for PR-DIRAC, PR-SSGE, VCL and PF-SSGE, whereas the performance of EWC in all three considered settings is similar. We speculate that improved performance in increasingly complex architectures is due to differences in the resulting inductive biases (cf. Wilson & Izmailov (2020)). For example, compared to an MLP, a convolutional architecture such as Lenet is supposed to have a much better inductive bias towards data with local structure (e.g., SplitM-NIST), and might therefore be better suited for detecting whether an image belongs to a certain task or not.

D.4. PermutedMNIST

In this section, we consider the PermutedMNIST benchmark, another adaptation of MNIST to CL, where different

tasks are obtained by applying, for each task, a different pixel permutation to the input digits. The results of learning ten different tasks with an MLP with two hidden layers of 100 neurons (MLP-100,100) are presented in Table S7, and with an MLP with two hidden layers of 1000 neurons (MLP-1000,1000) in Table S8. Note that, for compatibility with previous literature (van de Ven & Tolias, 2019; von Oswald et al., 2020), the experiments with the MLP-1000,1000 are done by padding the original MNIST images with zeros before applying the permutation, which results in inputs of size 32×32 instead of the original 28×28 dimensions.

In the MLP-100,100 experiments (Table S7), catastrophic forgetting is successfully prevented by all PR-CL methods, as indicated by the similar performance in TG-DURING and TG-FINAL accuracies. Note, that if no explicit CL strategy is applied as in FINE-TUNING, severe catastrophic interference can be observed for this small network architecture. In a setting where task identity is given (TG), all methods perform similarly, except for PR-SSGE which exhibits slightly lower performance. However, whenever task identity needs to be inferred, all three probabilistic methods outperform PR-DIRAC, highlighting the advantages of using a Bayesian approach for inferring task identity via predictive uncertainty. In agreement with our SplitM-

Table S6. Accuracies of SplitMNIST experiments when using a Lenet (Mean \pm SEM in %, n=10). Column TI represents TI-ENT accuracies if applicable. Otherwise this column is used to report results of methods that learn a shared softmax across all tasks.

	TG-during	TG-FINAL	TI	TI-CONF	TI-AGREE
PR-DIRAC	99.92 ± 0.01	99.87 ± 0.04	72.33 ± 2.75	57.22 ± 3.25	N/A
PR-BBB	98.96 ± 0.90	99.20 ± 0.67	74.09 ± 1.38	67.39 ± 1.39	74.13 ± 1.33
PR-RADIAL	99.85 ± 0.03	99.78 ± 0.05	68.99 ± 2.06	64.63 ± 2.79	69.41 ± 2.12
PR-SSGE	99.89 ± 0.01	99.89 ± 0.01	77.56 ± 1.01	57.29 ± 1.89	77.55 ± 1.02
EWC-GH	N/A	N/A	27.62 ± 0.55	N/A	N/A
EWC-SH	N/A	N/A	26.01 ± 1.02	N/A	N/A
EWC	98.09 ± 0.75	97.17 ± 0.54	49.78 ± 2.20	49.77 ± 2.20	49.85 ± 2.11
VCL	98.03 ± 0.07	97.43 ± 0.12	63.05 ± 0.63	63.05 ± 0.63	62.24 ± 0.73
PF-SSGE	99.94 ± 0.00	99.37 ± 0.10	74.18 ± 1.00	38.15 ± 0.90	74.12 ± 1.01
PR-BBB-BW	98.96 ± 0.90	99.20 ± 0.67	99.20 ± 0.67	99.20 ± 0.67	99.20 ± 0.67
PR-BBB-CS	99.76 ± 0.02	99.62 ± 0.02	95.73 ± 0.05	95.73 ± 0.05	60.69 ± 1.13
SP-DIRAC	N/A	99.92 ± 0.00	85.50 ± 0.28	70.98 ± 0.34	N/A
SP-BBB	N/A	99.93 ± 0.00	85.52 ± 0.45	71.22 ± 1.41	85.47 ± 0.45
SP-TC-DIRAC	N/A	99.91 ± 0.00	82.85 ± 0.60	55.38 ± 0.25	N/A
SP-TC-BBB	N/A	99.92 ± 0.00	84.16 ± 0.42	84.06 ± 0.41	84.04 ± 0.38

Table S7. Accuracies of PermutedMNIST-10 experiments when using an MLP-100,100 (Mean \pm SEM in %, n=10).

	TG-during	TG-FINAL	TI-ENT	TI-CONF	TI-AGREE
PR-DIRAC PR-BBB PR-RADIAL PR-SSGE	95.70 ± 0.03 95.44 ± 0.04 94.31 ± 0.03 93.58 ± 0.10	95.05 ± 0.04 94.35 ± 0.06 94.30 ± 0.03 92.88 ± 0.10	75.84 ± 0.51 89.90 ± 0.33 81.78 ± 0.36 78.94 ± 0.73	75.14 ± 0.50 88.38 ± 0.33 79.87 ± 0.33 77.43 ± 0.73	$\begin{array}{c} \text{N/A} \\ 70.52 \pm 0.86 \\ 76.73 \pm 0.45 \\ 68.93 \pm 0.88 \end{array}$
FINE-TUNING	97.44 ± 0.01	47.89 ± 0.46	N/A	N/A	N/A

NIST results, PR-BBB performs considerably better than PR-RADIAL. PR-SSGE, despite using more flexible *implicit* distributions, performs poorly compared to PR-BBB. Note that, here, individual tasks are more difficult than in SplitMNIST, and a method as complex as SSGE might be disproportionately affected by an increase in task difficulty. As opposed to our SplitMNIST results, when comparing different methods to quantify uncertainty for task inference one can observe that ENT systematically yields the best results, closely followed by CONF. However, when applicable, accuracies based on the AGREE criterion lead to lower performance. A potential reason could be that all employed approximate inference methods lead to poor approximations that do not capture the space of admissible solutions well.

Similar trends can be observed for the MLP-1000,1000 (Table S8). Catastrophic forgetting only seems to be an issue for the prior-focused methods EWC and VCL. Interestingly, the FINE-TUNING baseline shows that, despite not adopting any strategy for CL, catastrophic interference is also not very severe due to the capacity of this large network. We could not find viable hyperparameter configurations for an *implicit* prior-focused method, i.e., PF-SSGE, and therefore do not report results for this method. The deterministic

solution PR-DIRAC performs surprisingly well, specially in a task-agnostic setting (TI in the Table), for which we significantly improve upon the previous baseline (PR-DIRAC**), and that is only outperformed by PR-BBB and methods based on replay. Interestingly, despite having similar performance when task identity is given (especially EWC), PF-CL approaches perform considerably worse than PR-CL approaches whenever task identity needs to be inferred. The performance we obtain for EWC in a task-agnostic setting is, however, vastly superior to that reported by prior work (EWC-GH* and SI-GH*), highlighting the benefits of using a multihead architecture in PF-CL. Again, when task identity needs to be inferred, ENT results in the best performance, but as opposed to the MLP-100,100 case, AGREE often leads to comparable results. While results reported by prior work when using generative replay methods (DGR, HNET+TIR and HNET+R) perform best, the gap with PR-BBB, which does not use generative models, is small.

When comparing the results obtained with both architectures, as expected, performance is slightly higher for the larger MLP when task identity is given. This gap in performance is much more noticeable when task identity needs to be inferred. However, this could also be explained by the

Table S8. Accuracies of PermutedMNIST-10 experiments when using an MLP-1000,1000 (Mean \pm SEM in %, n=10). Column TI represents TI-ENT accuracies if applicable. Otherwise this column is used to report results of methods that learn a shared softmax across all tasks. Results denoted with * are taken from van de Ven & Tolias (2019) and those denoted with ** are taken from von Oswald et al. (2020). SI stands for *synaptic intelligence* (Zenke et al., 2017), and DGR for *deep generative replay* Shin et al. (2017). HNET+TIR and HNET+R are CL methods based on hypernetwork-protected replay proposed in von Oswald et al. (2020).

	TG-during	TG-FINAL	TI	TI-CONF	TI-AGREE
PR-DIRAC	96.78 ± 0.03	96.73 ± 0.03	94.15 ± 0.18	93.41 ± 0.16	N/A
PR-BBB	96.33 ± 0.02	96.21 ± 0.03	96.14 ± 0.03	95.86 ± 0.05	85.92 ± 0.32
PR-RADIAL	97.19 ± 0.02	97.19 ± 0.02	92.92 ± 0.20	92.68 ± 0.19	92.26 ± 0.19
PR-SSGE	97.57 ± 0.02	97.39 ± 0.02	93.58 ± 0.13	93.39 ± 0.12	93.02 ± 0.10
EWC	96.87 ± 0.02	94.73 ± 0.11	81.12 ± 0.62	79.32 ± 0.59	79.46 ± 0.57
VCL	95.15 ± 0.02	89.72 ± 0.24	85.40 ± 0.49	81.66 ± 0.56	79.80 ± 0.86
FINE-TUNING	98.13 ± 0.01	90.08 ± 0.45	N/A	N/A	N/A
EWC-GH*	N/A	N/A	33.88 ± 0.49	N/A	N/A
SI-GH*	N/A	N/A	29.31 ± 0.62	N/A	N/A
DGR*	N/A	N/A	96.38 ± 0.03	N/A	N/A
PR-DIRAC**	N/A	N/A	91.75 ± 0.21	N/A	N/A
HNET+TIR**	N/A	N/A	97.59 ± 0.01	N/A	N/A
HNET+R**	N/A	N/A	97.76 ± 0.76	N/A	N/A

fact that for the larger MLP, the dimensionality of the input images is considerably larger due to padding, which might render task inference easier.

D.5. SplitCIFAR-10

Our results from the SplitCIFAR-10 experiment (cf. Sec. 4.4) are reported in Table S9. All experiments are conducted with a Resnet-32 as main network (He et al., 2016) using batch normalization in all convolutional layers. The batch normalization weights are part of the trainable weights captured by the WG system. The batchnorm statistics are checkpointed and stored at the end of training for each task. Specifically, in the final model, each task embedding has an associated set of batchnorm statistics that will be loaded into the main network when the task embedding is selected.

In this experiment, PR-BBB performs best, followed by PR-DIRAC. As for PermutedMNIST, PR-SSGE struggles, potentially due to the increased task difficulty. All three task-inference criteria perform similar, with ENT usually leading to the best results. The FINE-TUNING baseline reveals that PR-CL methods slightly suffer from a stability-plasticity dilemma, and the use of a shared meta-model seems to affect TG-DURING accuracies.

Multi-head VCL performs poorly in this benchmark. The correct task identity is chosen below chance level, which indicates that inducing task-specific uncertainty by the output head only is not sufficient for this challenging benchmark. We also experimented with multi-head EWC but observed instabilities similar to those reported in SM D.2. In particular, some weights had very low Fisher values, which led to high variance in the predictions made by the post-hoc

constructed posterior, even in-distribution.⁶ The growing softmax baselines, EWC-GH and VCL-GH, perform at chancel level as only instances from the last task are correctly classified.

As consistently observed in all our experiments, PR-RADIAL underperforms PR-BBB. While this is in disagreement with the superior performance obtained with Radial posteriors in (Farquhar et al., 2020), their results were obtained for a medical dataset, and are therefore not comparable to the experiments that we consider. We leave it open for future work to investigate under which scenarios PR-RADIAL might be a useful replacement for PR-BBB.

D.6. Task boundary detection during training

So far, we assumed that task identity is known during training. To overcome this constraint, methods for task boundary detection can be used, and the use of uncertainty for this purpose was already proposed by Farquhar & Gal (2018a).

Here we analyze, for PermutedMNIST, the feasibility of task boundary detection based on the uncertainty computed on a training batch, and compare it to using the loss as a boundary indicator. We consider the entropy of the predictive distribution as uncertainty measure (ENT). In both cases, the transitions to new tasks can be detected based on peaks in the evolution of the signals. The criterion for

⁶Note, a heuristic modification would be to train the multihead network with EWC, but to omit the post-hoc posterior construction (cf. Eq. 37). In this case, there is still task-specific aleatoric uncertainty (similar to PR-DIRAC), but no epistemic uncertainty and therewith no instability issues arising from the posterior construction using the EWC importance values.

	TG-during	TG-FINAL	TI-ENT	TI-CONF	TI-AGREE
PR-DIRAC PR-BBB PR-RADIAL PR-SSGE	$\begin{array}{c} 94.59 \pm 0.10 \\ 95.59 \pm 0.08 \\ 94.82 \pm 0.12 \\ 94.25 \pm 0.07 \end{array}$	$\begin{array}{c} 93.77 \pm 0.31 \\ 95.43 \pm 0.11 \\ 94.67 \pm 0.15 \\ 92.83 \pm 0.16 \end{array}$	54.83 ± 0.79 61.90 ± 0.66 52.89 ± 1.19 51.95 ± 0.53	54.83 ± 0.79 61.90 ± 0.64 52.89 ± 1.19 51.93 ± 0.52	$\begin{array}{c} \text{N/A} \\ 61.36 \pm 0.71 \\ 50.92 \pm 1.50 \\ 51.81 \pm 0.48 \end{array}$
SP-DIRAC SP-BBB	N/A N/A	95.42 ± 0.13 96.06 ± 0.06	58.67 ± 0.94 61.35 ± 0.91	58.62 ± 0.93 61.36 ± 0.91	N/A 59.24 ± 1.05
EWC-GH VCL-GH VCL	N/A N/A 95.78 ± 0.09	N/A N/A 61.09 ± 0.54	20.40 ± 0.95 19.84 ± 0.53 15.97 ± 1.91	N/A N/A 15.86 ± 1.90	N/A N/A 15.86 ± 1.88
FINE-TUNING	96.59 ± 0.03	60.25 ± 0.77	N/A	N/A	N/A

Table S9. Accuracies of SplitCIFAR-10 experiments (Mean \pm SEM in %, n=10).

boundary detection can be implemented as a simple threshold crossing. As both loss and uncertainty will stay high in the initial phase of training on a new task, the detection algorithm is paused for a grace period after a detected transition. Furthermore, to improve detection stability, loss and uncertainty can be considered over a window of several training iterations.

To compare how useful loss and uncertainty values are for detecting task boundaries, we analyze the sensitivity of the two approaches to the choice of the detection threshold when using a grace period of 1000 iterations and a detection window of 10 iterations (Fig. S8). The threshold value that detects task boundaries without errors is bounded from above by the minimum of the values at actual task boundaries (such that all boundaries are detected), and from below by the maximum value outside of task boundary periods (such that false positives are avoided). While perfect boundary detection is possible with both signals, we found that the range of viable thresholds is much larger for the uncertainty signal (65.80% of the signal range) than for the loss signal (14.11% of the signal range).

These results suggest that task boundary detection based on an uncertainty measure might be a more robust way to detect task boundaries during training compared to a loss criterion. Interestingly, using uncertainty for task boundary detection does not require access to labelled data, as opposed to a criterion based on the loss. However, an uncertainty criterion relies on the assumption that input distributions of subsequent tasks are sufficiently distinct, which might not always be case. Crucially, both of these simple threshold criteria assume some sort of continuity for the training of individual tasks.

E. Experimental Details

In this section, we provide detailed descriptions of the two low-dimensional problems considered in this paper, and explain how hyperparameter configurations were chosen for all methods and experiments. The exact hyperparameter choice of all reported experiments can be found in the code repository accompanying the paper, which also contains the instructions to reproduce all results.

E.1. 1D Polynomial Regression Dataset

The 1D polynomial regression dataset consists of three tasks, each defined by a different ground-truth function $g^{(t)}(x)$ that operates on a specific input domain $p^{(t)}(X)$:

$$g^{(1)}(x) = (x+3)^3$$
 $p^{(1)}(X) = \mathcal{U}(-4, -2)$ (46)
 $g^{(2)}(x) = 2x^2 - 1$ $p^{(2)}(X) = \mathcal{U}(-1, 1)$
 $g^{(3)}(x) = (x-3)^3$ $p^{(3)}(X) = \mathcal{U}(2, 4)$

where $\mathcal{U}(a,b)$ denotes a continuous uniform distribution between the bounds a and b. Note that input domains are non-overlapping, and therefore task identity can be inferred by looking at the inputs alone.

20 noisy training samples are collected from each of these polynomials according to $\{(x,y) \mid y=g^{(t)}(x)+\epsilon$ with $\epsilon \sim \mathcal{N}(0,\sigma^2), x \sim p^{(t)}(X)\}$. We set $\sigma=0.05$ in this experiment. We also scale the NLL properly using $\sigma_{\rm II}=0.05$ (cf. Eq. 7) to circumvent model misspecification when testing Bayesian approaches.

E.2. 2D Mode Classification Dataset

The 2D Mode Classification experiment is comprised of three binary classification tasks. The 2D inputs x are sampled from a Gaussian mixture model with six modes and uniform mixing coefficients:

$$p(\mathbf{X}) = \sum_{t=1}^{6} \frac{1}{6} \mathcal{N}(\mathbf{X}; \boldsymbol{\mu}^{(t)}, \boldsymbol{\Sigma}^{(t)})$$
 (47)

We set $\Sigma^{(t)} = (0.2)^2 I$ for $t \in \{1, ..., 6\}$ and equidistantly locate the modes in a circle of radius five around the origin.

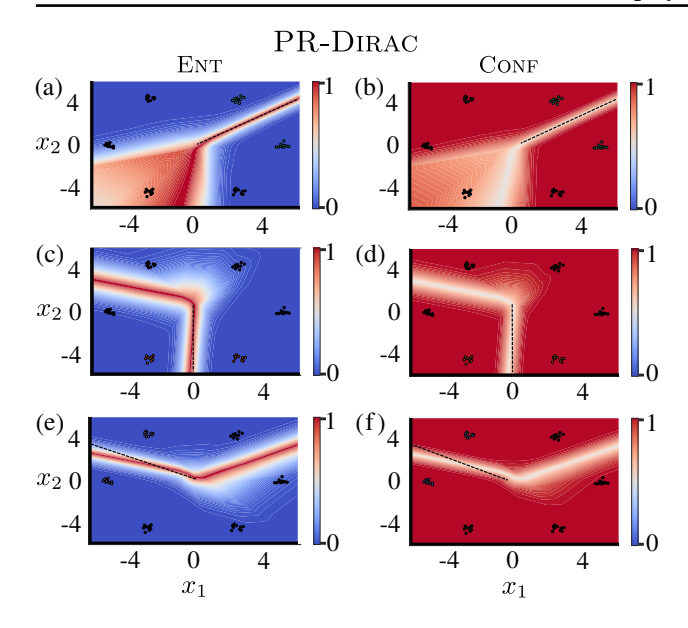


Figure S6. 2D mode classification uncertainty maps for PR-DIRAC. (a) Entropy of the predictive distribution (ENT) of task 1 across the input space covering in-distribution domains of all tasks. Dots represent training points and colors indicate task-affiliation. The dashed line represents the decision boundary for task 1. Same as (a) but uncertainty here reflects the confidence of the predictive distribution (CONF). The same uncertainty maps are produced using the final approximate posteriors for task 2 (c)-(d) and 3 (e)-(f).

Specifically, the angular position of each mode was determined by $\alpha^{(t)} = \frac{t-0.5}{6} 2\pi$, and the corresponding Cartesian coordinates by: $\mu^{(t)} = [5\sin(\alpha^{(t)}), 5\cos(\alpha^{(t)})]^T$. The dataset contains 10 training samples per mode, i.e., 20 training samples per task.

E.3. Hyperparameter selection

To gather the results, we performed extensive hyperparameter searches for all the methods across all experiments. Unless noted otherwise, we selected the hyperparameter configurations according to the best performance in a taskagnostic setting using the ENT criterion. In Table S10 we describe the basic grid of hyperparameter values used for all methods. Note that we only report the initial search grid from which a random subset of 100 calls was generated. The results of this initial search were thoroughly evaluated and the grid was fine-tuned individually for each method and experiment if parameter choices appeared inappropriate. Notably, the network architectures differ considerably across methods and across experiments, and the lists below are not exhaustive. We use chunked hypernetworks (cf. Sec. C.2) with architectures where the total number of parameters of the TC system is smaller than dim(w), except for low-dimensional problems where we only experiment with

non-compressive MLP hypernetworks. In addition, we experiment with principled hypernetwork initializations (e.g., cf. Chang et al. (2020)), that we adapted for chunked hypernetworks. However, we do not find a noticeable influence of the initialization on the training outcome when using the Adam optimizer. The hyperparameter searches were performed on the ETH Leonhard scientific compute cluster. For exact configurations of the reported results, please refer to our list of command line calls provided in the README files of the accompanying code base.

F. Further Discussion and Remarks

F.1. Runtime and storage complexity

A BNN has an intrinsic runtime disadvantage during inference compared to a deterministic network due to the incorporation of model uncertainty. As in practical scenarios the posterior predictive distribution cannot be analytically evaluated, it has to be approximated via an MC estimate (cf. Eq. 38). Thus, if the MC estimate incorporates K samples from the approximate parameter posterior, then inference of every input is approximately K times as expensive as for a deterministic model.

Task inference via predictive uncertainty comes into play as an additional factor during inference, since the predictive distribution has to be estimated for every task in order to chose the prediction corresponding to lowest uncertainty. Hence, inference time is additionally increased by a factor T. Note, this is not the case for the considered multi-head PF-CL methods, where in every forward pass the output of all T heads is computed anyways. Certainly, proper parallelization on modern graphics hardware can ensure that these extra demands are not noticeably reflected in the actual runtime.

During training via variational inference, BNNs require an MC estimate of the NLL term (cf. Eq. 2), which also corresponds to a linear increase for the loss computation compared to the deterministic case. However, it should be noted that this hyperparameter $K_{\rm NLL}$ (the MC sample size) is often chosen to be rather small, e.g., $K_{\rm NLL}=1$.

Apart from these general remarks, we also would like to comment on method-specific resource demands.

BbB and Radial posteriors. Both methods are very similar in their implementation as well as their resource complexity. A notable difference is, that an analytic expressions for the *prior-matching term* is known for BbB when using certain priors, while the training of radial posteriors requires an MC estimate of the involved cross-entropy term (cf. SM C.3.2). Compared to the deterministic case, the number of trainable parameters is doubled (a mean and variance per weight) in both cases.

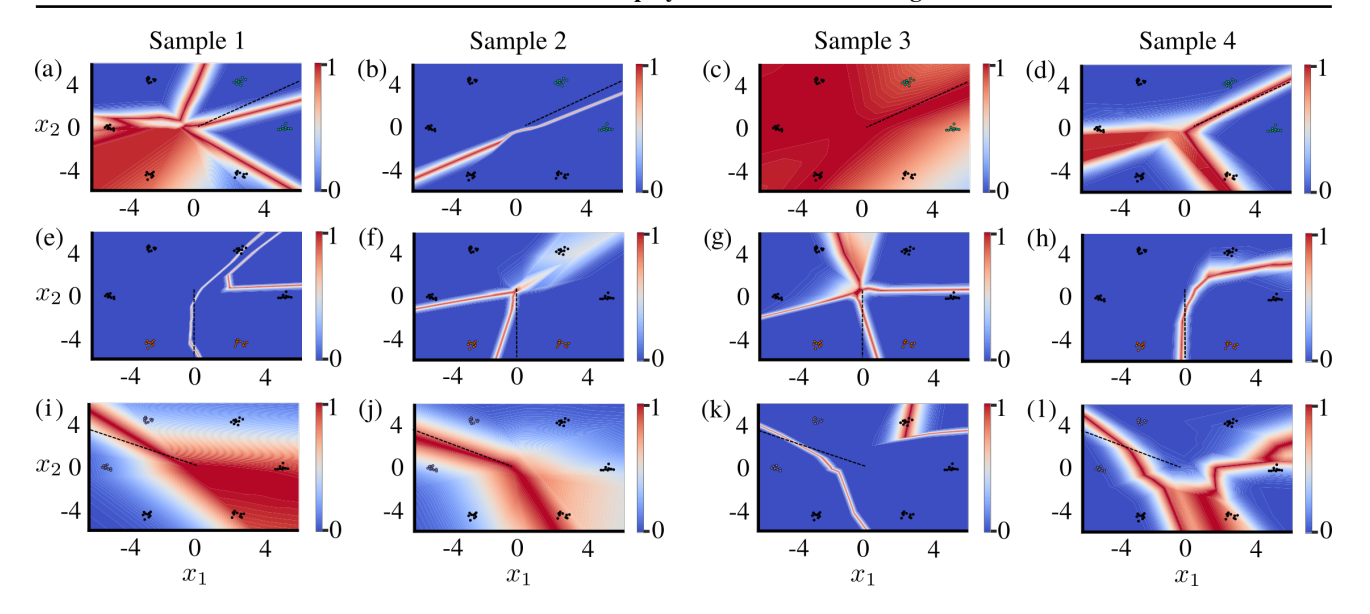


Figure S7. 2D mode classification uncertainty maps of single sample points drawn from the final approximate posteriors trained with PR-AVB. (a) Entropy of the softmax output for a sample point $\mathbf{w} \sim q_{\boldsymbol{\theta}^{(1)}}(\mathbf{W})$ of task 1 across the input space covering in-distribution domains of all tasks. (b)-(d) same as (a) for different sample points $\mathbf{w} \sim q_{\boldsymbol{\theta}^{(1)}}(\mathbf{W})$. Posterior draws for task 2 using $q_{\boldsymbol{\theta}^{(2)}}(\mathbf{W})$ are shown in (e)-(h) and for task 3 using $q_{\boldsymbol{\theta}^{(3)}}(\mathbf{W})$ are shown in (i)-(l), respectively. Intriguingly, individual models tend to be overconfident (similar to Fig. S6), and different models exhibit very different uncertainty behavior. Thus, the overall uncertainty reflected in the predictive distribution (cf. Fig. S5) is likely induced through model uncertainty.

Implicit methods. Implicit methods, such as AVB and SSGE, require an additional neural network that in combination with the base distribution forms the approximate posterior. The architecture of this WG network is a hyperparameter. Note, that the choice of architecture has a considerable influence on runtime and storage complexity. Every sample drawn from such an approximate posterior requires a forward pass through the WG network.

AVB requires yet another network during training, the discriminator. Also here, the architecture of the discriminator is a hyperparameter. In every training iteration, the discriminator is optimized inside an inner-loop for a predefined number of steps. For loss computation, the *prior-matching term* has to be evaluated via an MC sample, where forward passes through the discriminator are required.

SSGE requires an eigendecomposition at every training iteration which has cubic runtime complexity in the number of samples S used for the construction of the kernel matrix (cf. SM 19). Most of our results were obtained for S=10 or S=20.

Empirical runtimes. In Table S11 we note the measured runtimes for some of the results reported in this paper. Those runtimes should be considered with care, as they depend on the selected hyperparameter configuration (including the number of training iterations), the underlying compute hardware and its occupation, as well as the implementation

efficiency of each individual method. For instance, the runtime difference between PR-BBB and PR-RADIAL in column 1D REGRESSION can in large part be explained by the fact that the chosen hyperparameter configuration for PR-RADIAL used 100 MC samples to estimate the NLL loss term as opposed to 10 used for the PR-BBB result. Yet, despite these caveats, the provided numbers give a general idea of the runtime differences between methods.

F.2. Continual learning regularization in distribution space

The goal of the CL regularization in the PR-CL framework is to ensure that found posterior approximations do not change when learning new tasks, as discussed in Sec. C.2. This desideratum can be directly enforced if, for the considered variational family, an analytic expression for a divergence measure is accessible (e.g., cf. Sec. C.3.1/ Eq. 10). Whenever such divergence measure is not available, we avoid sample-based regularization, and thus regularize at the level of the output of the TC system, resorting to an L2 regularization of the distributional parameters (cf. Eq. 1). In our experiments this L2 regularization is sufficient, as we do not observe that forgetting is a major problem. A potential reason for the success of this simple regularization could be the discovery of flat minima as speculated in Ehret et al. (2021). However, a sound application of the PR-CL framework should regularize towards closeness in distribution space, as the chosen parameterization of the variational

Table S10. Hyperparameter values scanned across methods in our basic search. Note that these values were subsequently further tuned for each method and experiment. BNNs refer to all probabilistic methods (i.e. all considered methods except PR-DIRAC). PR refers to all PR-CL methods, which therefore require a TC network. IMPLICIT refers to all methods using implicit posterior approximations, which therefore require a WG network.

Methods	Hyperparameter	Searched values
All	learning rate batch size N_{mb} clip gradient norm main network activation function optimizer number of iterations (1D-Regression) number of iterations (2D Mode Class.) number of iterations (SplitMNIST) number of iterations (PermutedMNIST) number of epochs (SplitCIFAR-10)	le-5, le-4, le-3, le-2 32, 64, 128 None, 100 ReLU Adam 5000, 10000 2000, 5000 2000, 5000 5000, 10000 20, 40, 60
BNNs	prior variance σ_{prior}^2 prior-matching term scaling factor	1 1e-6, 1e-5, 1e0 (1 for low-dim. experiments)
BNNs (except VCL and PR-BBB)	number of samples for $prior$ -matching $term$ estimation number of MC samples for NLL estimation K	1, 10, 20 1, 10, 20
PR-BBB and VCL	CL regularizer local reparametrization trick	MSE, fKL, rKL, W2 True (only for MLPs), False
EWC	regularization strength	1e-4, 1e-3,, 1e3, 1e4
All PR	CL regularizer strength β TC hidden layers TC activation function size of task embeddings $\mathbf{e}^{(t)}$ initial SD of task embeddings $\mathbf{e}^{(t)}$ size of TC chunk embeddings $\mathbf{c}^{(l)}$ initial SD of TC chunk embeddings $\mathbf{c}^{(l)}$	1e-3, 1e-2, 1e2, 1e3 None, 10-10, 50-50, 100-100 ReLU, sigmoid 16, 32, 64 0.1, 1 16, 32, 64 0.1, 1
All IMPLICIT	variance σ_{noise} of WG output perturbation dimensionality of the latent vector \mathbf{z} initial SD of the latent vector \mathbf{z} WG hidden layers WG activation function size of WG chunk embeddings $\mathbf{c}^{(l)}$ initial SD of WG chunk embeddings $\mathbf{c}^{(l)}$	None, 1e-2, 1e-1 8, 16, 32 0.1, 1 None, 10-10, 50-50, 100-100 ReLU, sigmoid 16, 32, 64 0.1, 1
AVB	batch size K for D training number of D training steps use batch statistics D hidden layers	1, 10 1, 5 False, True 10-10, 100-100
SSGE	kernel width use heuristic kernel width number of samples S for gradient estimation threshold τ for eigenvalue ratio of eigenvalues J	0.1, 1 True, Ralse 10, 20, 50 1, 5, All
PR-BBB-CS	number of iterations for fine-tuning stage method for OOD uncertainty increase prior-matching term scaling factor during fine-tuning	2000, 5000 random labels, high entropy targets 1e-6, , 1e0

family is arbitrary, and it is unclear how perturbations in parameter space affect the encoded distributions. Therefore, this section provides guidance for future work on how a simple regularization acting on the outputs of the TC system can be interpreted as enforcing closeness in distribution space. Our discussion on this topic is inspired by the derivation of the natural gradient (Pascanu & Bengio, 2013), that allows to cast parameter updates into distribution updates.

Recall that the goal of regularization is to ensure that (cf.

Table S11. Measured runtime (hh:mm:ss) of simulations that lead to the results reported in Tables S2, S5 and S9. Only the runtime of the first gathered random seed is reported.

	1D REGRESSION	SPLITMNIST	SPLITCIFAR-10
PR-DIRAC	00:04:59	00:08:26	02:27:24
PR-BBB	00:10:34	00:06:10	12:02:31
PR-RADIAL	01:50:57	00:10:21	07:18:40
PR-SSGE	00:28:24	02:12:32	02:18:29
PR-AVB	03:30:36	N/A	N/A
VCL	01:40:51	00:03:21	09:07:38

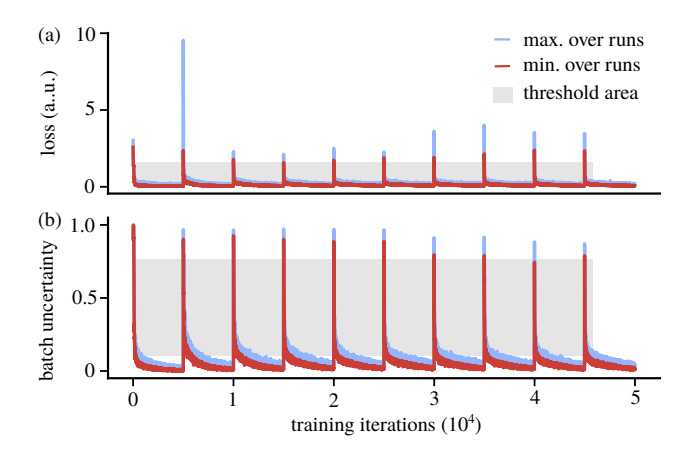


Figure S8. Task boundary detection in PermutedMNIST-10. Evolution of (a) the loss and (b) batch uncertainty when training tasks for 5000 iterations. The detection threshold of a potential task boundary detection system is bounded by the minimum (red) and maximum (black) values over 10 runs. The gray area indicates the range in which a threshold would successfully detect all task boundaries without causing false positives or false negatives.

SM Eq. 10):

$$\min_{\boldsymbol{\theta}^{(t)}} D(q_{\boldsymbol{\theta}^{(t,*)}}(\mathbf{W})||q_{\boldsymbol{\theta}^{(t)}}(\mathbf{W}))$$
 (48)

where $q_{\boldsymbol{\theta}^{(t,*)}}(\mathbf{W})$ denotes the approximate posterior of task t obtained from a checkpoint of the TC network before learning the current task, and D denotes some divergence measure. In particular, we consider the KL as a choice for the divergence measure, which for small parameter perturbations behaves like a metric in distribution space. Assuming the outputs $\boldsymbol{\theta}^{(t,*)}$ do not change much when learning task t (i.e. $\boldsymbol{\epsilon} = \boldsymbol{\theta}^{(t)} - \boldsymbol{\theta}^{(t,*)}$ is sufficiently small), we consider a Taylor approximation of Eq. 48 around $\boldsymbol{\theta}^{(t,*)}$, To compute this expression, we use the fact that the KL between identical distributions is zero, and we compute the first and second order terms of the approximation as follows. For the first order term we require the first derivative of the KL with

respect to $\boldsymbol{\theta}^{(t)}$ at $\boldsymbol{\theta}^{(t)} = \boldsymbol{\theta}^{(t,*)}$:

$$\begin{aligned}
& \left[\nabla_{\boldsymbol{\theta}^{(t)}} \text{KL} \left(q_{\boldsymbol{\theta}^{(t,*)}}(\mathbf{W}) || q_{\boldsymbol{\theta}^{(t)}}(\mathbf{W}) \right) \right] \Big|_{\boldsymbol{\theta}^{(t)} = \boldsymbol{\theta}^{(t,*)}} \\
&= - \int q_{\boldsymbol{\theta}^{(t,*)}}(\mathbf{W}) \left[\nabla_{\boldsymbol{\theta}^{(t)}} \log q_{\boldsymbol{\theta}^{(t)}}(\mathbf{W}) \right] \Big|_{\boldsymbol{\theta}^{(t)} = \boldsymbol{\theta}^{(t,*)}} d\mathbf{W} \\
&= 0
\end{aligned}$$

For the second order term we need the respective second derivative:

$$\begin{aligned}
&\left[\nabla_{\boldsymbol{\theta}^{(t)}}\nabla_{\boldsymbol{\theta}^{(t)}}^{T}KL\left(q_{\boldsymbol{\theta}^{(t,*)}}(\mathbf{W})||q_{\boldsymbol{\theta}^{(t)}}(\mathbf{W})\right)\right]\Big|_{\boldsymbol{\theta}^{(t)}=\boldsymbol{\theta}^{(t,*)}} \\
&=-\int q_{\boldsymbol{\theta}^{(t,*)}}(\mathbf{W}) \\
&\left[\nabla_{\boldsymbol{\theta}^{(t)}}\nabla_{\boldsymbol{\theta}^{(t)}}^{T}\log q_{\boldsymbol{\theta}^{(t)}}(\mathbf{W})\right]\Big|_{\boldsymbol{\theta}^{(t)}=\boldsymbol{\theta}^{(t,*)}} d\mathbf{W} \\
&=-\int q_{\boldsymbol{\theta}^{(t,*)}}(\mathbf{W})\left[\mathcal{H}_{\log q_{\boldsymbol{\theta}^{(t,*)}}(\mathbf{W})}\right]\Big|_{\boldsymbol{\theta}^{(t)}=\boldsymbol{\theta}^{(t,*)}} d\mathbf{W} \\
&=-\mathbb{E}_{q_{\boldsymbol{\theta}^{(t,*)}}(\mathbf{W})}\left[\mathcal{H}_{\log q_{\boldsymbol{\theta}^{(t,*)}}(\mathbf{W})}\right]
\end{aligned}$$

And we therefore obtain the following local approximation of the KL:

$$KL(q_{\boldsymbol{\theta}^{(t,*)}}(\mathbf{W})||q_{\boldsymbol{\theta}^{(t)}}(\mathbf{W}))$$

$$= KL(q_{\boldsymbol{\theta}^{(t,*)}}(\mathbf{W})||q_{\boldsymbol{\theta}^{(t,*)}+\boldsymbol{\epsilon}}(\mathbf{W}))$$

$$\approx -\frac{1}{2}\boldsymbol{\epsilon}^{T}\mathbb{E}_{q_{\boldsymbol{\theta}^{(t,*)}}(\mathbf{W})}[\mathcal{H}_{\log q_{\boldsymbol{\theta}^{(t,*)}}(\mathbf{W})}]\boldsymbol{\epsilon}$$

Thus, regularization in distribution space as demanded by Eq. 48 can be achieved for small ϵ using the quadratic form in Eq. 51. We denote the regularization matrix by $R^{(t)} \equiv \mathbb{E}_{q_{\boldsymbol{\theta}^{(t,*)}}(\mathbf{W})} \big[\mathcal{H}_{\log q_{\boldsymbol{\theta}^{(t,*)}}(\mathbf{W})} \big]$ to highlight the elegance and computational simplicity of the final CL regularizer:

$$\min_{\boldsymbol{\theta}^{(t)}} \frac{1}{2} (\boldsymbol{\theta}^{(t)} - \boldsymbol{\theta}^{(t,*)})^T R^{(t)} (\boldsymbol{\theta}^{(t)} - \boldsymbol{\theta}^{(t,*)})$$
 (52)

Note that $R^{(t)}$ has to be computed once after task t has been trained on, 8 and for $R^{(t)} = I$ we recover the isotropic regularization of Eq. 1.

⁷As we will see below, the KL divergence is for infinitesimal parameter perturbations approximately equal to the Rao distance (Nielsen, 2013).

⁸In the strict sense, $R^{(t)}$ is specific to the used checkpoint

When interpreting $q_{\boldsymbol{\theta}^{(t,*)}}(\mathbf{W})$ as a likelihood function, it can be seen that $R^{(t)}$ is the corresponding Fisher information matrix (cf. Eq. 30) and can be computed via:

$$R^{(t)} = \mathbb{E}_{q_{\boldsymbol{\theta}^{(t,*)}}(\mathbf{W})} \left[\left(\nabla_{\boldsymbol{\theta}^{(t,*)}} \log q_{\boldsymbol{\theta}^{(t,*)}}(\mathbf{W}) \right) \right]$$

$$\left(\nabla_{\boldsymbol{\theta}^{(t,*)}} \log q_{\boldsymbol{\theta}^{(t,*)}}(\mathbf{W}) \right)^{T}$$
(53)

Note, that the quantity estimated by algorithms such as SSGE (cf. Sec. C.4.2) is $\nabla_{\mathbf{W}} \log q_{\boldsymbol{\theta}^{(t)}}(\mathbf{W})$ and not the score function $\nabla_{\boldsymbol{\theta}^{(t)}} \log q_{\boldsymbol{\theta}^{(t)}}(\mathbf{W})$. It is therefore not straightforward to see how to approximate the Fisher information matrix and thus the regularization matrix $R^{(t)}$.

However, as deep learning often benefits from coarse approximations, we propose the following heuristic to estimate $R^{(t)}$ if the simple regularization of Eq. 1 is not sufficient. Assuming the training of each task is successful and the variational family contains the correct posterior, we have that $q_{\boldsymbol{\theta}^{(t,*)}}(\mathbf{W}) \approx \frac{1}{Z} p(\mathcal{D}^{(t)} \mid \mathbf{W}) p(\mathbf{W})$, where Z is some unknown normalization constant. We can therefore rewrite the Hessian as $\mathcal{H}_{\log q_{\boldsymbol{\theta}^{(t,*)}}(\mathbf{W})} \approx \mathcal{H}_{\log p(\mathcal{D}^{(t)}|\mathbf{W})} + \mathcal{H}_{\log p(\mathbf{W})}$. The term $\mathcal{H}_{\log p(\mathbf{W})}$ has a simple analytic expression for a Gaussian prior and $\mathcal{H}_{\log p(\mathcal{D}^{(t)}|\mathbf{W})}$ can be computed for a given variate **w** as long as the data $\mathcal{D}^{(t)}$ is available and the model is twice differentiable. If $R^{(t)}$ is computed right after a task has been learned, it can be safely assumed that $\mathcal{D}^{(t)}$ is still available (similar to the Fisher computation in EWC (cf. Sec. C.5.2)). Hence, $R^{(t)}$ can be approximated via an MC estimate since sampling from $q_{\boldsymbol{\theta}^{(t,*)}}(\mathbf{W})$ is always possible. Crucially, the actual CL regularization via Eq. 53 is efficient to compute and does not require sampling from $q_{\boldsymbol{\theta}^{(t,*)}}(\mathbf{W})$.

F.3. Deep Ensembles

A successful approach for OOD detection are deep ensembles (Snoek et al., 2019), which in the simplest case correspond to several deterministic networks trained independently, and whose predictions are aggregated during inference (Lakshminarayanan et al., 2017). Due to the nonconvexity of the loss landscape and the stochasticity innate to maximum-likelihood training, distinct solutions are obtained despite training with the same dataset. Although, to the best of our knowledge, such an ensemble of models cannot be interpreted as a sample from the Bayesian posterior, having access to a set of diverse predictions makes it possible to infer task identity based on model disagreement, which is not possible in the plain deterministic case. In addition, deep ensembles are just as easy to train as single deterministic solutions, but do require more training

resources. This is in contrast to the increased training difficulty of BNNs, where continuous weight distributions are sought. However, despite their attractiveness, ensembles lack some of the advantages that come with a Bayesian approach. These include the ability to drop i.i.d. assumptions within tasks or the ability to revisit and update existing knowledge.

Analogously to PR-DIRAC, our framework can also be adapted to work with ensembles. In this case, the TC system maintains multiple embeddings per task; one per ensemble member. Although not in the context of CL, this idea has already been explored by Oswald et al. (2021), who showed improved OOD detection compared to the single model baseline. To combine the advantages of BNNs and deep ensembles, Wilson & Izmailov (2020) proposed to train an ensemble of BNNs. This is an intriguing future direction for our framework, as the beneficial CL properties of BNNs are preserved. For instance, a simple and scalable approach such as PR-BBB could be turned into an ensemble of Gaussian posterior approximations by allowing the use of more than one embedding vector per task, which may allow to capture multiple modes of the posterior and ultimately lead to better task inference.

 $q_{\theta^{(t,*)}}$, which can change whenever a new checkpoint of the TC system is made and thus whenever a new task arrives. We ignore this detail for computational simplicity and due to the approximate nature of the proposed regularization.